KU LEUVEN

ARENBERG DOCTORAL SCHOOL
Faculty of Engineering Science



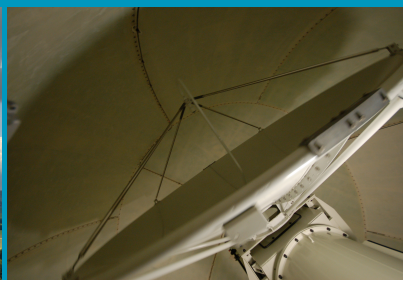

Precipitation estimation from weather radar measurements

statistical analysis of convective storms and extreme rainfall

Edouard Goudenhoofdt

Supervisors:
prof. dr. ir. Patrick Willems
dr. ir. Laurent Delobbe
(Royal Meteorological Institute)

Dissertation presented in partial fulfillment of the requirements for the degree of Doctor of Engineering Science (PhD): Civil Engineering

January 2018

Precipitation estimation from weather radar measurements

statistical analysis of convective storms and extreme rainfall

Edouard GOUDENHOOFDT

Examination committee:
prof. dr. ir. Omer Van der Biest, chair
prof. dr. ir. Patrick Willems, supervisor
dr. ir. Laurent Delobbe, supervisor
(Royal Meteorological Institute)
prof. dr. ir. Jaak Monbaliu
prof. dr. Nicole van Lipzig
prof. dr. ir. Remko Uijlenhoet
(Wageningen University & Research)
dr. Tanja Winterrath
(Deutscher Wetterdienst)

Dissertation presented in partial fulfillment of the requirements for the degree of Doctor of Engineering Science (PhD): Civil Engineering

January 2018

Uitgegeven in eigen beheer, Edouard Goudenhoofdt, Kasteelpark Arenberg 40 - box 2448, B-3001 Leuven (Belgium)

Preface

The Royal Meteorological Institute of Belgium is responsible for issuing weather forecasts and warnings. It also provides reference meteorological and climatological information. Since November 2007 I have been working at the Institute in the weather radar and lightning detection group of dr. Laurent Delobbe. For three successive projects founded by the Belgian Science Policy, I studied the combination of radar and rain gauge data, the characteristics of convective storms and the construction of a radar-based precipitation climatology. As engineer in applied mathematics I particularly enjoyed solving the problems associated with the processing of radar measurements.

During the PhD defense of my colleague dr. Emmanuel Roulin in June 2014, I had the opportunity to meet prof. Patrick Willems from the University of Leuven. We discussed about the potential of using radar precipitation observations for applications in urban and river hydrology. Soon after I applied for a PhD based on my research career considering that it constitutes a nice story. After one year of research, we decided to focus on the study of extreme local precipitation. I hope we can further investigate our ideas in future collaborations after this thesis.

An additional motivation for my work is the possibility to turn my research into practical use for the society. I am currently the coordinator of the cooperation between the Royal Meteorological Institute of Belgium and the hydrological service of the Walloon region. The main goal of the cooperation, which started in March 2016 thanks to the efforts of dr. Christian Tricot and ir. Philippe Dierickx, is to develop meteorological observations, forecasts and warnings products useful for hydrology. The first important achievement was obtained in September 2016 with the realtime production of the radar-based precipitation estimation.

Taking into account these particular circumstances, I would like to thank my

promoters, jury, colleagues, family and friends for their support during this thesis.

Abstract

This thesis aims to improve the measurement, observation and statistical analysis of precipitation which is generally defined as falling aqueous particles. A particular interest is dedicated to rainfall, which is defined as liquid precipitation on the ground. Weather phenomena associated with precipitation impacts human life and economies over a wide range of temporal and spatial scales. The study of precipitation in Belgium, which has been based on rain gauge measurements, can now benefit from more than 10 years of radar measurements. The high resolution observations provided by radars are needed to study convective storms and for the verification of weather and climate models. Accurate rainfall estimation is required for flood risk management, especially at the urban scale. Unfortunately radars are not yet widely used due to the many sources of error in their measurements and the uncertainties associated with the derived rainfall estimation.

The archived data of a C-band weather radar are used over the longest period available to improve the knowledge of precipitation in Belgium. Different methods combining a basic radar rainfall estimation with rain gauge measurements are evaluated. The characteristics of convective storms are analysed based on their identification and tracking in the volume reflectivity data. The reflectivity measurements are processed to control their quality and to obtain the best rainfall estimation. The radar-based rainfall estimation is verified by comparison with independent rain gauges and by looking at maps of descriptive statistics. Its potential for the study of local extreme rainfall is investigated by comparison with rain gauge analysis. For this purpose a new regional approach is proposed to fully exploit the radar information. The overall methodology is partly based on the refinement of existing approaches with simplicity and robustness in mind. Given the computational challenge, efforts have been made to ensure the high quality of the software implementation.

A simple gauge bias correction significantly improves the performance of radar rainfall estimation. A further increase in performance is obtained by using

spatial interpolation. Locally convective storms are observed 6 hours per year on average with no significant spatial variations. The distribution of convective activity indices (number of storms, area coverage and total mass) and individual storm properties (volume, mass, top, duration, speed) follows a power law with significant diurnal, monthly and annual variations. The main benefit for the rainfall estimation is obtained by taking into account the vertical profile of reflectivity. The new algorithm allows a 50 % increase in areal coverage compared to a basic algorithm. Radar artifacts are significantly reduced by the removal of non-meteorological echoes and the hail threshold. Estimation errors and sampling explain the few differences between radar-based and gauge 1 hour rainfall extremes. Using regression on a quantile-quantile plot, the fit of an exponential extreme value distribution model to both datasets are consistent thanks to the high uncertainty. The novel regional approach to the radar extremes allows to reproduce the results of long rain gauge records and to significantly reduce the model uncertainty.

The availability and quality of the precipitation observations are fundamental to obtain robust results. The statistical results can be easily extended by using other radars and longer periods. The precipitation datasets have been used for research applications mainly for weather model verification. The radar-based rainfall estimation has been implemented operationally for hydrological purposes. Information on estimation uncertainty is important for many applications but has not been addressed in this thesis. The study of areal rainfall extremes is a natural extension to the study of local rainfall extremes. The use of the radar-based rainfall estimation for flood risk management is promising. The statistical results obtained in this thesis could enrich the climatic information regarding precipitation in Belgium.

Beknopte samenvatting

Dit doctoraatsonderzoek had als doel om de waarnemingen en statistische analyse van neerslag verder te verbeteren. Het belang van goede neerslagdata kan niet onderschat worden, gezien het grote socio-economische belang die weersverschijnselen geassocieerd met neerslag hebben en dit over een breed scala van temporele en ruimtelijke schalen. De studie van neerslag in België, die op heden hoofdzakelijk gebaseerd is op pluviometer- en pluviograafmetingen, kunnen nu profiteren van meer dan 10 jaar weerradardata. Radars leveren waarnemingen met hoge resolutie. Deze zijn nodig om convectieve regenbuien te bestuderen en als basis voor de verificatie van weer- en klimaatmodellen. Nauwkeurige lokale neerslagschattingen zijn ook nodig voor overstromingsrisicoanalyse – en beheer, zowel op de stroomgebiedsschaal als voor toepassingen inzake stedelijke hydrologie. Helaas zijn neerslaggegevens op basis van radars nog niet veel gebruikt voor zulke toepassingen vanwege de radarmeetfouten en de onzekerheden geassocieerd met de afgeleide schatting van neerslagintensiteiten uit de radarsignalen.

Voor dit doctoraatsonderzoek werden de gearchiveerde waarnemingen van de C-band weerradar in Wideumont over de langst beschikbare meetperiode gebruikt om de kennis m.b.t. neerslag in België en vooral van de convectieve en extreme buien te verbeteren. Verschillende methodes voor het combineren van de radarneerslagschattingen met pluviograafmetingen werden geëvalueerd. De kenmerken van convectieve neerslagcellen werden geanalyseerd op basis van hun identificatie en tracking in de volumereflectiviteitsgegevens. De reflectiviteitsmetingen werden verwerkt om voldoende kwaliteit te garanderen en een beste kwantitatieve neerslagschatting te bekomen. De radargebaseerde schatting van de neerslag werd geverifieerd door vergelijking met onafhankelijke neerslagwaarnemingen van pluviografen en via ruimtelijke kaarten van beschrijvende statistieken. Verder werd het potentieel van de radarneerslagschattingen onderzocht voor het bestuderen van lokale extreme regenval en dit in vergelijking met een pluviograaf-gebaseerde analyse. Er werd een nieuwe regionale methode ontwikkeld die bovendien voldoende eenvoudig

en robuust kan toegepast worden. Bovendien zijn er inspanningen geleverd om de hoge kwaliteit van de software-implementatie te waarborgen.

Een eenvoudige correctie van de systematische afwijking t.o.v. pluviograafmetingen verhoogde de nauwkeurigheid van de radarneerslagschattingen al aanzienlijk. Een verdere toename van de kwaliteit werd bekomen door gebruik van ruimtelijke interpolatie. Er werd vastgesteld dat lokale convectieve buien zich gemiddeld 6 uur per jaar voordoen zonder significante ruimtelijke variaties. Voor bepaalde kenmerken van de convectie activiteit werden indices afgeleid zoals voor het aantal buien, de gebiedsdekking, de totale buimassa en individuele buieigenschappen zoals het volume, de massa, de tophoogte, de duur, de snelheid. Deze kansverdelingen van deze indices blijken typisch een machtsverband te vertonen met significante dagelijkse, maandelijkse en jaarlijkse variaties. De neerslagschatting kon aanzienlijk verbeterd worden door rekening te houden met het verticale profiel van de reflectiviteit. Het nieuwe algoritme zorgde voor een toename van 50 % in de ruimtelijke dekkingsgraad in vergelijking met een basisalgoritme. Radar-artefacten werden aanzienlijk verminderd door het verwijderen van niet-meteorologische echo's en hageldrempel. Schattingsfouten en de beschikbare set aan buien verklaren de kleine verschillen tussen de radar- en pluviograaf-gebaseerde neerslagschattingen voor de 1-uur extreme neerslagintensiteiten. Met behulp van regressie in kwantiel-kwantiel plots en het gebruik van een exponentieel model voor de extreme-waarden-verdeling bleken beide datasets redelijk consistent. De nieuwe regionale analyse op de radarextremen liet toe om extreme-waarden-schattingen van neerslagintensiteiten aanzienlijk te verbeteren t.o.v. deze afgeleid op basis van lange reeksen van pluviograafmetingen.

Zowel de beschikbaarheid als de kwaliteit van de neerslagobservaties zijn fundamenteel om tot robuuste schattingen te komen. De statistische resultaten kunnen eenvoudig worden uitgebreid met behulp van andere radars en voor langere meetperiodes. De kwantitatieve neerslagschattingen zoals afgeleid in dit onderzoek werden recent reeds gebruikt voor tal van toepassingen, zoals de verificatie van een weermodel en als invoer voor hydrologische toepassingen. Informatie m.b.t. de schattingsonzekerheden is belangrijk voor heel wat toepassingen, maar werd niet behandeld in dit proefschrift. Ook de studie van gebiedsneerslagextremen vormt een verdere uitbreiding van het onderzoek. Verder blijken de radar-gebaseerde neerslagschattingen veelbelovend om als basis te gebruiken voor overstromingsrisicobeheer en voor tal van andere toepassingen in het domein van het waterbeheer en de waterbouwkunde.

List of Abbreviations

BB bright band. 59, 67–72, 76, 81–83, 85, 86, 129

C-Band a radio frequency band from 4 to 8 GHz. 13, 15, 32, 33, 35, 36, 59, 61

CAP the basic algorithm used for comparison (same as QPE1). 101, 103, 107, 109, 111, 120

CAPPI Constant Altitude Plan Position Indicator. 16

DEM digital elevation model. 65

F20 the fraction of estimated values similar to the reference. 78–82, 85, 86

IDF intensity duration frequency. 98, 118, 131

KED kriging with external drift. 24–27, 30, 31, 59, 60, 73, 78–84, 86, 89–92, 125

MAD mean absolute difference or error between estimated and reference values (same as MAE). 78, 80–82, 85, 86

MAE mean absolute difference or error between estimated and reference values (same as MAD). 22–30

MAVPR mean apparent vertical profile of reflectivity. 69–72, 76

MB mean bias between estimated and reference values. 22, 25

MCS mesoscale convective system. 48, 52, 56, 126, 127

MFB mean field bias. 24, 25, 59, 73, 78–83, 89, 90, 101, 103, 107, 109–111, 121, 125

NEXRAD the US weather radar network. 36, 41, 61

NWP numerical weather prediction. 3, 130, 132

POT peaks over threshold. 9, 96, 97, 99

QPE quantitative precipitation estimation. 5, 8, 59–62, 76, 86, 87, 97, 98, 101, 103, 106, 108, 109, 111, 115–117, 127, 130, 131

QPE1 the basic QPE algorithm used for comparison (same as CAP). 61, 62, 74, 76–86, 88–93

QPE2 the new algorithm. 61, 62, 75–93

QQR distribution fitting method to extreme values based on a regression in quantile-quantile plots. 99, 105, 113

RFA regional frequency analysis. 96–98, 113, 114

RMIB the Royal Meteorological Institute of Belgium. 3, 15, 16, 22, 36, 38, 61, 63, 64, 67, 69, 74–76, 78–81, 83, 84, 87–89, 91, 98, 99, 132

SCS the scatter score : measures the multiplicative error spread. 22, 25–27, 78–82, 85, 86

SPW the hydrological service of the Walloon region of Belgium. 16, 22, 63, 74, 75, 77, 83, 91, 99–103, 109–111, 121

TITAN the thunderstorm identification, tracking, analysis and nowcasting system developed at the National Center for Atmospheric Research (US). 33, 35, 36, 38–41, 43, 46, 55, 57

VPR vertical profile of reflectivity. 8, 14, 15, 59, 61, 67–70, 72, 76, 77, 80, 82, 85, 86, 101, 111, 127

List of Symbols

C	Fractional areal coverage of the identified storms
G	Rain gauge measurement of rainfall accumulation [mm]
M	Equivalent water mass [g]
N	Number of identified storms
R	Radar rainfall rate [$\mathrm{mm\,h^{-1}}$] or rainfall accumulation [mm]
W	Total water mass of the identified storms [g]
Z	Radar reflectivity [$\mathrm{mm^6\,m^{-3}}$]
z	Radar reflectivity expressed on a decibel scale [dBZ]

Contents

Chapter 1

Introduction

1.1 Motivation

1.1.1 Meteorology

Precipitation is generally defined as "all liquid or solid phase aqueous particles that originate in the atmosphere and fall to the earth's surface" (Glickman and Zenk, 2000). It occurs when air is being forced to rise in meteorological situations such as weather fronts, thermal convection and orographic effect. Precipitation is also defined as the amount, usually expressed in millimeters or inches of liquid water depth, of the water substance that has fallen at a given point over a specified period of time (Glickman and Zenk, 2000). The term rainfall, which is widely used for any types of precipitation, is restricted to surface liquid precipitation in this work. The study of precipitation can be divided in three areas (Testik and Gebremichael, 2013) : microphysics, measurement and estimation, and statistical analyses. Although some knowledge of microphysics is necessary to measure precipitation, it will not be the focus of this research.

Human beings rely heavily on water resources for their basic needs (agricultural, domestic, industrial, environmental). This is why 600 years ago the first rain gauge network has been developed by King Sejong the Great in Korea. Nowadays rain gauge data from about 40 000 stations in the world have been collected by the "Global Precipitation Climatology Centre" for research purposes (Schneider et al., 2014). In Belgium, very dense rain gauge networks have been developed since the end of the nineteenth century (Demarée, 2013). Anyhow a rain gauge network is always limited when the rainfall field exhibits high temporal and

spatial variability (e.g., Beek et al., 2012). The use of amateur stations can improve rainfall estimation in urban areas (Vos et al., 2017).

Storms produced by cumulonimbus clouds are localised and cause severe rainfall, hail, wind gust and tornadoes which affect people. Soon after the U.S. air force started to track aircrafts, it became obvious that microwave radar would be an excellent tool for the observation of convective storms and for tracking balloons to measure wind (Atlas and Ulbrich, 1990). A weather radar transmits electromagnetic pulses in a given direction and its energy is partly reflected by the hydrometeors back to the radar (Fig. 1.1). The potential usefulness of radar in meteorology has been increased by using the Doppler functionality (Rogers, 1990) to measure radial winds. Additionally polarization techniques have been developed to identify the sizes and shapes of the hydrometeors (Metcalf, 1990). The reader interested to learn the principles of weather radars is referred to Rinehart (1991) for a basic introduction, to Doviak and Zrnić (2006) for an emphasis on the quantitative measurement of the meteorological parameters and to Fabry (2015) for a focus on practical applications.

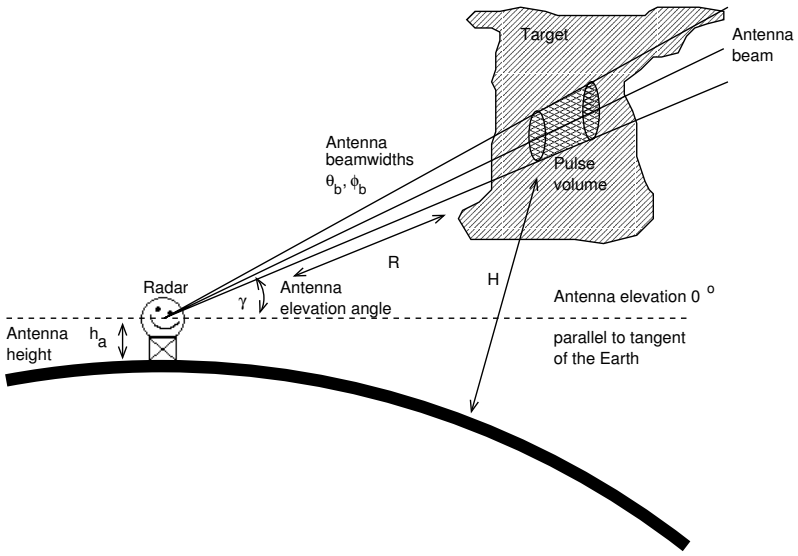

Figure 1.1: Propagation of electromagnetic waves through the atmosphere for a pulse weather radar. The radar beam travels in straight lines assuming a $\frac{4}{3}$ Earth radius standard beam refraction. From Michelson et al. (2005).

Weather radars are now widely used by meteorological services to monitor precipitation. In Europe, efforts are being made to improve harmonization of

the radar systems and their measurements (Huuskonen et al., 2014). Since 1952 in Belgium, several X-band radars have been operated by the army forces for the purpose of wind finding (Demarée, 2013). In 1975 a radar dedicated to storm monitoring was installed in Zaventem at Brussels airport by the civil aviation agency (now Belgocontrol). It was upgraded in 2003 with digital processing and a dedicated archiving system. In 2001 the Royal Meteorological Institute of Belgium (RMIB) installed its first radar in Wideumont, situated south-east of Belgium. In 2012 a dual-polarization radar was installed by RMIB in Jabbeke (north-west of Belgium) to allow a full coverage of the country. In 2016 the *Vlaamse Milieumaatschappij* installed a dual-pol radar in Helchteren (north-east of Belgium) for hydrological purposes. If you add radars from *Meteo-France*, the *Koninklijk Nederlands Meteorologisch Instituut* and the *Deutscher Wetterdienst*, Belgium has one of the best radar coverage in the World (see Fig. 1.2).

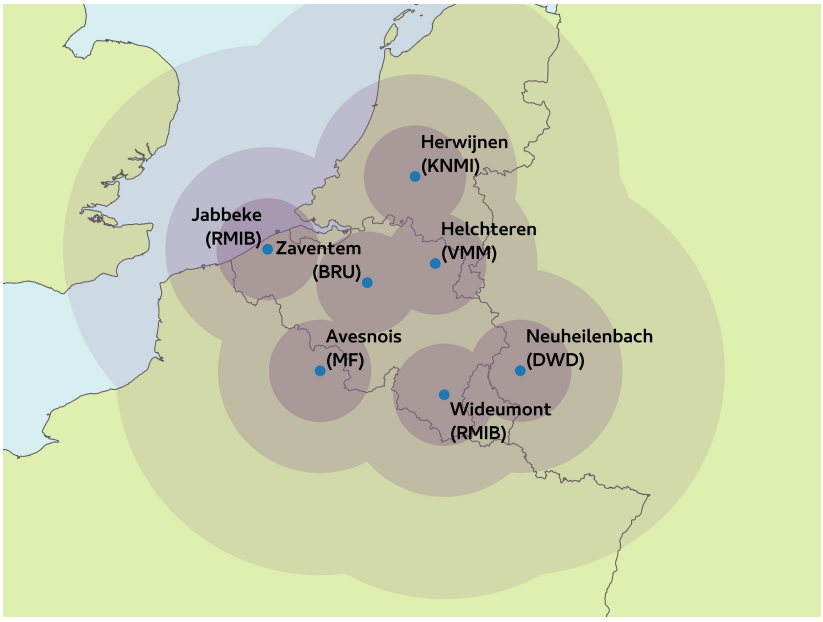

Figure 1.2: The weather radars covering Belgium : Avesnois (*Meteo-France*) Helchteren (*Vlaamse Milieumaatschappij*), Herwijnen (*Koninklijk Nederlands Meteorologisch Instituut*), Jabbeke (RMIB), Neuheilenbach (*Deutscher Wetterdienst*), Wideumont (RMIB) and Zaventem (Brussels airport). The circles have a radius of 50, 100 and 200 km.

Weather forecasting remains a big challenge for the scientific community due to the increasing number of atmospheric processes resolved, the nonlinear

complexity of the system and the imperfect observations that need to be assimilated by the models (Bauer et al., 2015). On one hand, volumetric precipitation observations of good quality are needed for data assimilation in numerical weather prediction (NWP) models (Wattrelot et al., 2014; Bick et al., 2016). For example in the US, a complex quality-controlled radar reflectivity mosaic has been developed (Liu et al., 2016). On the other hand, radar-based rainfall estimates are required to properly evaluate high resolution NWP precipitation forecasts (Ebert et al., 2013).

1.1.2 Hydrology and hydraulics

Rainfall is the main driven force in hydrology which is the study of the movement of water on the earth's surface. Over the past 30 years flooding killed more than 200 000 people and affected more than 2.8 billion others worldwide (Jakubicka et al., 2010). Water also impacts natural environment, agriculture, energy supply and tourism. In the last 15 years the interest has moved from water stream flow prediction at a limited number of locations to the prediction of all water balance components for a whole region (Delrieu et al., 2009). There is now a need for accurate and reliable remote sensing observations to calibrate, drive and constrain operational flood forecasting (Li et al., 2016). The Brussels, Flanders and Walloon regions of Belgium are responsible for issuing flood warnings. They are particularly interested by radar-based rainfall products.

There is a growing number of people living in cities. Hydrological processes in urban environment occur at very small temporal and spatial scales. Since rainfall also exhibits spatial variability at small scales high resolution rainfall data are needed in urban hydrology (Berne et al., 2004; Cristiano et al., 2017). Weather radars (especially X-Band) together with downscaling techniques have been proposed (Ochoa-Rodriguez et al., 2015). The use of radar data is quickly developing in this field (see Thorndahl et al., 2017, for a review).

Humans have been developing hydraulic structures like dams, dykes, flood control reservoirs, movable weirs and urban drainage systems to manage the flow of water. For their design, statistics of extreme rainfall are very important. Due to the long records available, rain gauge data are widely used to derive such statistics (e.g., Willems, 2011). It is unclear how those statistics should be adapted in the context of climate variations (Arnbjerg-Nielsen et al., 2013). The use of spatial rainfall (e.g., derived from radar data) has the potential to provide short duration extreme statistics with higher accuracy and higher spatial resolution while being representative of the current climate.

The many sources of errors in radar-based quantitative precipitation estimation (QPE) have, however, prevented its usage in hydrology. The challenges are

summarised by Berne and Krajewski, 2013 : the issue of data management, the understanding of the radar error structure in space and time, the development of small complementary research radar networks, the improvement of precipitation forecasting, the radar estimation of snowfall, and sub-kilometric hydrological modeling.

1.1.3 Regional climatology

The observed and projected climate change on earth is a world issue (Stocker et al., 2013). The world meteorological organisation (WMO) international programme CORDEX has been started in 2009 to collaborate on the study of regional climate change (Giorgi and Gutowski, 2015). In the recent years convective-permitting regional climate models have emerged (Prein et al., 2015). However the use of high resolution observations datasets (e.g., based on radar) for verification are still limited (Prein et al., 2013; Kendon et al., 2017).

In Belgium the CORDEX framework has been extended with a special partnership of different research institutes and universities. Simulations have been performed to reproduce the current climate (Van Weverberg et al., 2014; Giot et al., 2016; Wyard et al., 2017) or to predict future climate (Saeed et al., 2016). Some analysis are focusing on extreme rainfall (De Troch et al., 2013; Tabari et al., 2016; Hosseinzadehtalaei et al., 2017) but do not make use of radar data for verification. Using radar-based rainfall estimation instead of rain gauges should permit better evaluation of the modelled precipitation.

The WMO "Global Framework for Climate Services" vision is "To enable better management of the risks of climate variability and change and adaptation to climate change, through the development and incorporation of science-based climate information and prediction into planning, policy and practice on the global, regional and national scale". The goal are similar to the "Global Monitoring for Environment and Security" programme of the European Union. High resolution rainfall datasets are needed in this context. Satellites offer a global solution but their resolution and accuracy is limited compared to weather radars.

1.2 Goal

Until now the knowledge of precipitation has been mainly based on rain gauge measurements at surface stations. It is limited because precipitation exhibits variability at small spatial scales while a rain gauge has a very limited

interception area, typically 200 cm^2. In most developed countries, more than a decade of high resolution weather radar measurements are now available for the scientific community. Unfortunately the wealth of information contained in these volumetric measurements are yet to be unleashed. The scientific and computational challenges related to the processing of these measurements have prevented its full exploitation. In particular the quality of the radar measurements is affected by many sources of uncertainties and errors (see Fig. 1.3). In this thesis the challenges are tackled to improve the knowledge of precipitation. For this general purpose, four specific objectives with an increasing degree of difficulty are defined.

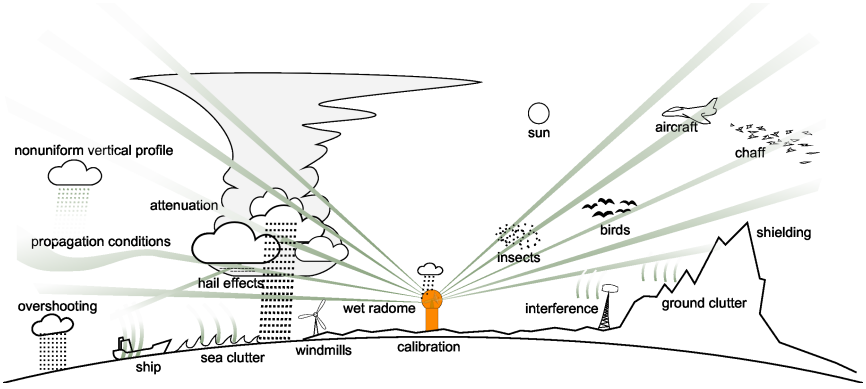

Figure 1.3: Phenomena affecting the radar data quality. From Holleman et al. (2006).

1.2.1 Evaluation of radar-gauge merging methods

To improve rainfall estimation it is recommended to combine radar rainfall estimates with rain gauge measurements. Plenty of methods have been proposed in the literature with various degrees of complexity (Gjertsen et al., 2003). Meanwhile only a few verification studies have been performed using several years of data (e.g., Young et al., 2000; Cole and Moore, 2008; Nelson et al., 2010; Berndt et al., 2014; Jewell and Gaussiat, 2015).

Previous verification studies do not combine all the strengths developed in this thesis :

- the implementation of several merging methods with various degrees of complexity ;

- the use of an independent rain gauge network as reference ;
- an extended assessment of the method's performance using a large variety of scores ;
- an analysis of the results in function of the month of the year or the distance from the radar ;
- a study of the effect of network density.

1.2.2 Statistical analysis of convective storm characteristics

Two different approaches for the analysis of convective storms from radar data can be found in the literature. The Eulerian approach is based on the temporal analysis of precipitation at a given point. It is generally used to derive long-term statistics at relatively large temporal (i.e. 1 hour) and spatial resolution (i.e. 4 km) from 2D data (e.g., Schumacher and Johnson, 2006; Carbone and Tuttle, 2008; Weusthoff and Hauf, 2008; Lombardo and Colle, 2010). The Lagrangian approach is based on the tracking of spatial features across successive radar images. It requires higher spatial and temporal resolution but can be used with 2D data (e.g., Weusthoff and Hauf, 2008; Davini et al., 2011; Kaltenboeck and Steinheimer, 2015). A limited number of studies make specific use of 3D data (e.g., López et al., 1984; Potts et al., 2000; Bellon and Zawadzki, 2003; May and Ballinger, 2007; Saxen et al., 2008; Mohee and Miller, 2010; Peter et al., 2015).

In this thesis the convective storm characteristics in and around Belgium are analysed using 10 years of volumetric radar data. To our knowledge, such a long dataset has never been used in Europe for this kind of study. While most studies are limited to a particular aspect of convective storms, an in-depth analysis using both Eulerian and Lagrangian approaches is performed. In particular the following characteristics of convective storms are studied :

- their mode of organisation;
- the temporal variations of the global activity in the study area : the number of storms, their intensity and their total mass;
- the spatial variations of the activity and its correlation with temporal variations;
- the spatial and temporal variations of the individual storm properties (volume, top, mass);
- their duration, speed and direction.

The definition of 3 indices to characterise the convective storm activity over a given area and the application of the theory of spatial point process to storm initiation are particularly original.

1.2.3 Generation and verification of rainfall estimation from volumetric radar measurements

Efforts to provide gridded rainfall datasets are important due to the increasing number of applications. Interpolated gauge measurements (Haylock et al., 2008, e.g.,) are used in many studies but their representativity for convective cells are limited. Weather model reanalyses offer estimations over the globe but are prone to large bias (Leeuw et al., 2014). Satellite-based precipitation estimation is available at the global scale from infrared imagers or passive microwave radiometers but their resolution and accuracy are still limited (Tang et al., 2014). Weather radars have the highest potential but provide only indirect measurements of precipitation with many sources of errors. In the last 10 years, the most important issues have been tackled in operational QPE algorithms (e.g., Tabary, 2007; Germann et al., 2006). However, they have not been verified on an extended period. Furthermore the period with consistent datasets are limited due to inherent updates of the QPE algorithms. Datasets based on a reprocessing of volumetric radar measurements are limited due to the unavailability of archive data, the lack of well-documented algorithms and the computation resources required (Krajewski et al., 2011). Existing datasets are limited by their temporal sampling (Wright et al., 2013b) or lack of vertical profile of reflectivity (VPR) correction (Overeem et al., 2009b; Thorndahl et al., 2014).

In this thesis a careful processing of the volumetric data is made including beam blockage correction, removal of non-meteorological echoes using several techniques, correction for the height of the measurement (i.e. VPR correction) and specific Z-R relationships for stratiform, convective and hail precipitation. The algorithms, based in part on the literature, are designed to be relatively simple and robust. The radar-based estimation is combined with dense hourly rain gauge measurements using both a simple and a complex method. The algorithms are tuned on a selection of cases and compared to a basic algorithm in order to evaluate the improvements. A verification for the period 2005-2014 is made against independent rain gauge measurements using different statistical scores. The visual improvement on maps of descriptive statistics are also presented. To the author's knowledge, such long-term, comprehensive and independent verification of radar-based precipitation estimates has not been done yet.

1.2.4 Regional frequency analysis of extreme rainfall from radar-based estimates

The analysis of sub-daily rainfall extremes is currently mainly based on rain gauge data. The peaks over threshold (POT) selection method is popular and can be combined with a regional approach (Roth et al., 2015, e.g.,) or a spatial model (Van de Vyver, 2012) to reduce the uncertainty. Meanwhile dealing with intersite dependence is a well known challenge (e.g., Hosking and Wallis, 1988). With some assumptions on the underlying precipitation process, the significantly higher amount of information contained in the radar data can be used to reduce the uncertainty of the frequency analysis. The radar pixel can be consider as representative for small-scale precipitation but the sub-pixel variability (from gauge to gauge) can be significant (Peleg et al., 2016). A few studies explored the potential of radar-based estimation (Overeem et al., 2009a; Wright et al., 2014b; Marra and Morin, 2015) but some overestimation for short durations was generally found.

New insights are provided in this thesis thanks to:

- high-quality radar-based estimates and rain gauge measurements;
- a detailed analysis of the differences for 1 and 24 h rainfall extremes between the radar and automatic rain gauges;
- the use of a fitting method which focuses on the tail of the distribution and finds the optimal rank (Willems et al., 2007);
- the application of a new regional method based on the spatially independent radar extremes in a circle of 20 km around the target location;
- the validation of the method against high resolution gauges with 40 years of records.

The method is applied for the whole of Belgium to study the large scale spatial variations.

1.3 Research strategy

1.3.1 Data

In Belgium, the full volumetric data of operational radars have been archived. Unfortunately the Jabbeke and Helchteren radars have too short period of

records and the exploitation of data from the Zaventem radar is difficult. Therefore only the data from the Wideumont radar (Fig. 1.4) is used in this research. To obtain the most robust results, the longest available period of data is used for each analysis. The different rain gauge networks available in the range of the Wideumont radar are used for rainfall estimation and verification. Particular attention is paid to the quality control of the radar and gauge data.

Figure 1.4: The radar of Wideumont is located in the Ardennes, situated in south-east of Belgium. The radar antenna is located at the top of a tower overhanging trees and is protected from rain by a radome

1.3.2 Algorithms

In the last decades, numerous algorithms have been proposed by the scientific community for the processing of the radar reflectivity measurements. It is important to note that they are often designed for specific technical and meteorological settings. In this thesis, an algorithm is either created or adapted from an existing one in order to meet certain criteria:

- it is suitable for the Wideumont scanning strategy.
- it can be used on other radars with no or very little adaptations.

- it is reliable in most weather situations occurring in Belgium.
- it is optimized to have a reasonable computation time.
- its complexity is limited as much as possible to make tuning and evaluation easier.

1.3.3 Software implementation

A good implementation of the algorithms is crucial for the validity of the results. The work done in this research rely as much as possible on open source softwares which are advocated in Heistermann et al., 2015. In particular, a library covering all aspects of radar data management and processing has been developed. The high-level programming language Python has been chosen for quick development and testing. Efforts have been made on the modularity and optimization of the code. A small fraction of the code has been integrated into an open source library for radar processing (Heistermann et al., 2013).

1.3.4 Statistical analyses

In this work different types of statistical analyses are performed on the precipitation data. Relatively simple descriptive statistics are used to analyse the precipitation field and the convective storms. Advanced statistical tools, sometimes inspired from other fields, are also used :

- geostatistics for the merging of radar and gauge data;
- spatial point process to study storm initiation;
- verification metrics to evaluate rainfall estimation against rain gauge measurement;
- regional frequency analysis and fitting methods for the study of radar extremes.

Statistical significance tests are performed for some results but deriving conclusions are difficult due to the rainfall estimation errors. While it is not the goal of the thesis, physical explanations for the obtained results are often proposed.

1.4 Outline

The motivation, goal and strategy of the research are presented in the introduction. It has been conducted on an extended time period from 2008 to 2017 and is presented in chronological order. Research questions related to the objectives defined above are investigated in the successive chapters of the dissertation :

- chapter 2 : how best to combine radar and rain gauge observations?
- chapter 3 : what are the characteristics of convective storms in Belgium?
- chapter 4 : how to obtain the best rainfall estimation from volumetric radar measurements?
- chapter 5 : what is the potential of radar rainfall estimates for extreme value analysis?

Each chapter corresponds to an article published in an international peer-reviewed journal. The main results of the thesis, their implications and prospects for future work are provided in the conclusions.

Chapter 2

Evaluation of radar-gauge merging methods for quantitative precipitation estimates[1]

Abstract

Accurate quantitative precipitation estimates are of crucial importance for hydrological studies and applications. When spatial precipitation fields are required, rain gauge measurements are often combined with weather radar observations. In this chapter, we evaluate several radar-gauge merging methods with various degrees of complexity: from mean field bias correction to geostatistical merging techniques. The study area is the Walloon region of Belgium, which is mostly located in the Meuse catchment. A basic estimation from a C-Band Doppler radar and measurements from a dense rain gauge network are used to estimate daily rainfall accumulations over this area. The relative performance of the different merging methods are assessed through a comparison against daily measurements from an independent gauge network. A 4-year verification is performed using several statistical quality parameters. It

[1] based on E. Goudenhoofdt and L. Delobbe (2009). "Evaluation of radar-gauge merging methods for quantitative precipitation estimates". In: *Hydrology and Earth System Sciences* 13.2, p. 195. DOI: 10.5194/hess-13-195-2009

appears that the geostatistical merging methods perform best with the mean absolute error decreasing by 40% with respect to the original data. A mean field bias correction still achieves a reduction of 25%. A seasonal analysis shows that the benefit of using radar observations is particularly significant during summer. The effect of the network density on the performance of the methods is also investigated. For this purpose, a simple approach to remove gauges from a network is proposed. The analysis reveals that the sensitivity is relatively high for the geostatistical methods but rather small for the simple methods. The geostatistical merging methods give the best results for all tested network densities and their relative benefit increases with the network density.

2.1 Introduction

Interest in quantitative estimation of rainfall based on weather radar has increased during the last years. Indeed new applications have risen in the field of distributed hydrological modelling or numerical weather prediction which require accurate precipitation estimates at high spatial resolution.

Weather radar is a remote sensing instrument that measures the reflectivity of precipitation at a given altitude. Those measurements can be used to estimate precipitation at ground level. Several sources of errors affect the accuracy of this estimation (e.g., Wilson and Brandes, 1979; Joss et al., 1990; Germann et al., 2006; Ciach et al., 2007). The measure of reflectivity itself can suffer from electronic miscalibration, contamination by non-meteorological echoes or range effect (attenuation, increase of the sample volume due to beam broadening). When retrieving the rainfall estimation at ground level, additional uncertainties arise. Those are due to the non-uniform vertical profile of reflectivity (VPR) and the conversion of radar reflectivity into rain rates (Z-R relationship). Nevertheless, a weather radar provides precipitation estimation at high spatial and temporal resolution over a large area. A network of rain gauges can provide more accurate point-wise measurements but the spatial representativity is limited. The two observation systems are generally seen as complementary and it is interesting to combine them.

Merging radar and gauge observations has been an intense topic of research since the beginning of the operational use of weather radars in the 70's. A review of gauge adjustment methods and operational use in Europe can be found in a COST 717 report (Gjertsen et al., 2004). More complex methods have been proposed such as co-kriging (Krajewski, 1987; Sun et al., 2000), statistical objective analysis (Pereira Fo. et al., 1998) or Kalman filtering approach (e.g., Todini, 2001; Seo and Breidenbach, 2002; Chumchean et al., 2006). Some of

those methods are very time consuming and are not well suited in an operational context. It is important to note that the merging methods are best applied after the full processing of radar data including ground echo elimination, VPR correction or attenuation correction (e.g., Germann et al., 2006; Tabary, 2007; Uijlenhoet and Berne, 2008). However the correction of radar errors and uncertainties is a relatively difficult task. The merging methods, which are often relatively simple, offer a practical solution to improve the basic radar estimation. The extra non-linearities that could be introduced by the corrections would make the comparison of the methods more difficult.

The aim of this study is to perform a long-term verification of different existing merging methods. Several methods of various degrees of complexity have been implemented and tested. All selected methods are appropriate for operational use. Verification of the merging methods faces the problem that the real precipitation field is unknown. A traditional approach is to compare precipitation estimates with rain gauges. Cross-validation (i.e. removing a gauge from the adjustment network to use it for verification) is a possible method but the drawback is that the network used for adjustment varies. In this study an independent verification network is used, more suitable to analyse the performance of the methods. Since the time sampling of this network is 24 h, the merging is made on daily accumulations. Several statistics are then computed to evaluate and compare the different methods. Similar long-term verification has been performed in recent studies but limited to one (e.g., Borga et al., 2002; Holleman, 2007) or a few methods (e.g., Cole and Moore, 2008; Heistermann et al., 2008; Salek and Novák, 2008). In Schuurmans et al. (2007), three different geostatistical methods have been compared based on 74 selected rainfall events.

The impact of the gauge network density on the merging methods performance has been little assessed in past studies (e.g., Sokol, 2003; Chumchean et al., 2006). One of the contributions of this work is to determine the best method for a given network density.

The characteristics of the radar and the rain gauge networks can be found in Sect. 2.2. The different methods used for merging are described in Sect. 2.3 and the results of a 4-year verification against rain gauges are presented in Sect. 2.4. In Sect. 2.5, a sensitivity analysis to the density of the network used for merging is carried out.

2.2 Radar and gauge observations

The Royal Meteorological Institute of Belgium (RMIB) operates a single-polarisation C-Band weather radar. It is located in Wideumont at 592 m above sea level. The radar observations are routinely used at RMIB for operational short-term precipitation forecast, detection of severe thunderstorms (Delobbe and Holleman, 2006) and a posteriori analysis in the case of severe weather events. The use of the Wideumont radar observations for hydrological studies and applications is also an important field of research and development (e.g., Berne et al., 2005; Delobbe et al., 2006; Leclercq et al., 2008).

The radar performs a 5-elevation scan every 5 min with reflectivity measurements up to 240 km. The beam width is 1 degree. The resolution of the radar polar data is 250 m in range and 1 degree in azimuth. A time-domain Doppler filtering is applied for ground clutter removal. An additional treatment, based on a static clutter map, is applied to the volume reflectivity file to eliminate residual permanent ground clutter caused by some surrounding hills. A pseudo-Constant Altitude Plan Position Indicator (CAPPI) at 1500 m above sea level is extracted from the 5-elevation scan (0.3°, 0.9°, 1.8°, 3.3°and 6°) on a Cartesian grid with a resolution of 600 m × 600 m. The height of the pseudo-CAPPI is chosen to limit the effect of ground clutter. Reflectivity factors are then converted into precipitation rates using the Marshall-Palmer relation $Z{=}aR^b$ with $a{=}200$ and $b{=}1.6$. The 5 min images are integrated in time to produce a 24 h rainfall accumulation starting at 08:00 LT.

The hydrological service of the Walloon region of Belgium (SPW) operates a dense (1 gauge per 135 km^2) and integrated network of 90 telemetric rain gauges. Most of them are tipping bucket systems providing hourly rainfall accumulations. The collected data are used for hydrological modelling and directly sent to RMIB. The rain gauges are controlled on site every three months and in a specialised workshop every year. Every day, a quality control of the data is performed by RMIB using a comparison with neighbouring stations. Radar data are also used in this quality control for the elimination of outliers.

RMIB maintains also a climatological network including 270 stations with daily measurements of precipitation accumulation between 8 and 8 local time (LT). These stations are manual and the data are generally available with a significant delay. The data undergo a drastic quality control. This network is routinely used for the long-term verification of radar precipitation estimates. It will be used here to evaluate the radar-gauge merging methods.

Since the estimation of precipitation can be very inaccurate at large distance from the radar, a maximum range of 120 km is used. The SPW network, used for adjustment, is then reduced to 74 gauges. Several stations of the RMIB

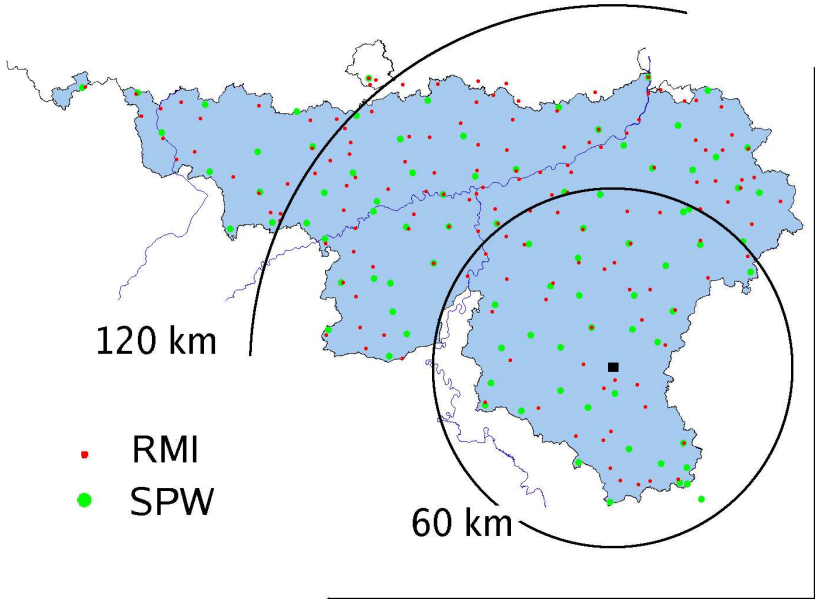

Figure 2.1: The Walloon Region of Belgium with the Wideumont radar coverage and the rain gauge networks of SPW and RMIB.

network are not always available during the 4-year verification period. Those stations are removed to ensure that the same network is used for the whole period. The remaining verification network includes 110 gauges. The positions of the radar and the two rain gauge networks can be seen in Fig. 2.1. The topography of the area of interest is shown in Fig. 2.2.

2.3 Description of the methods

Various methods combining radar and rain gauge data have been implemented to obtain the best estimation of precipitation. Several methods require the comparison between a rain gauge measurement G and a corresponding radar value R. The spatial sampling issue is of crucial importance when radar areal estimates are compared or combined with gauge point measurements (Villarini et al., 2008). In our study, the average over 9 radar pixels around the gauge location is used as the corresponding radar precipitation estimation. This allows

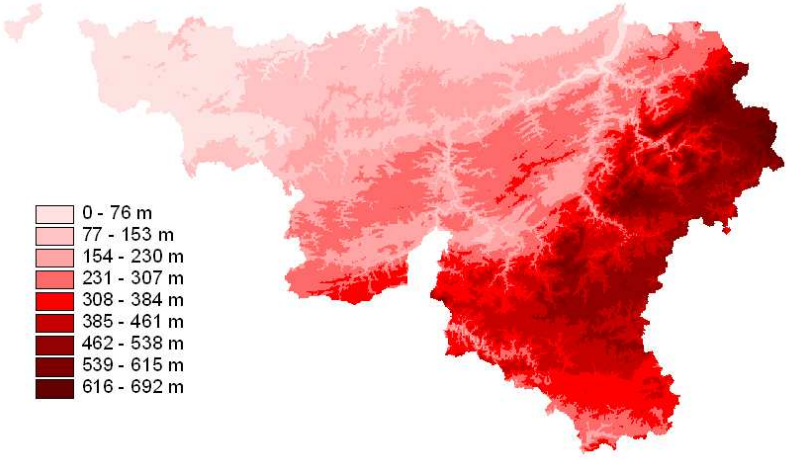

Figure 2.2: Topography map of the Walloon region

limiting the effect of wind drift which can be very significant (Lack and Fox, 2007). Spatial sampling error increases when the radar estimate is based on a larger number of pixels especially in convective situation. However this effect decreases with increasing accumulation time and is therefore relatively limited at a daily time scale. Besides, the use of a larger radar estimation area allows reducing the temporal sampling error.

Only the pairs for which both R and G exceed 1 mm are considered as valid. A day is valid if there are at least 10 valid pairs. The methods are applied on a square domain containing the Walloon region. It means that some areas fall outside the network convex hull (i.e. the boundary of the minimal convex set containing all the gauges). On those areas, adjusted values must be seen as extrapolation. The uncertainties associated with those values are then higher.

2.3.1 Mean field bias correction (MFB)

The assumption here is that the radar estimates are affected by a uniform multiplicative error. This error can be due for example to a bad electronic calibration or an erroneous coefficient a in the Z-R relationship. The adjustment

factor is estimated as a mean field bias:

$$C_{\mathrm{MFB}} = \frac{\sum_{i=1}^{N} G_i}{\sum_{i=1}^{N} R_i} \tag{2.1}$$

where N is the number of valid radar-gauge pairs, G_i and R_i are the gauge and radar values associated with gauge i.

2.3.2 Range-dependent adjustment (RDA)

This method assumes that the R/G ratio is a function of the distance from the radar. Range dependences are essentially produced by the increasing height of the measurements, beam broadening and attenuation effects. The range dependent adjustment is mainly based on the BALTEX adjustment method (Michelson et al., 2000). The relation between R/G expressed in log-scale and range is approximated by a second order polynomial whose coefficients are determined using a least squares fit.

$$\log C_{\mathrm{RDA}} = ar^2 + br + c \tag{2.2}$$

where r is the distance from the radar. The range dependent multiplicative factor C_{RDA} is derived from the polynomial fit.

2.3.3 Static local bias correction and range dependent adjustment (SRD)

The static local bias correction aims at correcting for visibility effects. The correction is calculated from a one-year data set using the climatological gauge network. The 24 h radar accumulations are first adjusted by a mean field bias correction. Then, for each gauge location, the averaged residual bias over 1 year is estimated. Finally a spatial interpolation based on kriging is performed to obtain the correction field. To simulate an operational context, the correction calculated over a given year is used for the next year. The fields obtained for 2004, 2005 (see Fig. 2.3), 2006 and 2007 are very similar. This correction is applied before a range dependent adjustment (Slb + RDa = SRD).

2.3.4 Brandes spatial adjustment (BRA)

This spatial method was proposed by Brandes (1975). A correction factor is calculated at each rain gauge site. All the factors are then interpolated on the

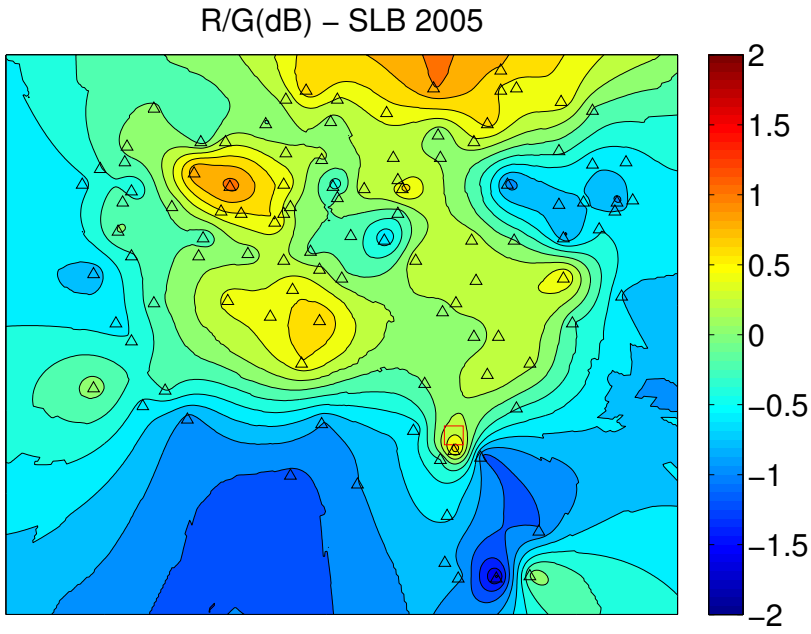

Figure 2.3: Static local bias correction field (in dB) for the year 2005 with gauges (triangles) and radar (square) locations.

whole radar field. This method follows the Barnes objective analysis scheme based on a negative exponential weighting to produce the calibration field:

$$C_{\mathrm{BRA}} = \frac{\sum_{i=1}^{N} w_i \left(G_i / R_i\right)}{\sum_{i=1}^{N} w_i} \qquad w_i = \exp \frac{-d_i^2}{k} \tag{2.3}$$

where d_i is the distance between the grid point and the gauge i. The parameter k controls the degree of smoothing in the Brandes method. It is assumed constant over the whole domain. The parameter k is computed as a function of the mean density δ of the network, given by the number of gauges divided by the total area. A simple inverse relation has been chosen :

$$k = (2\delta)^{-1} \tag{2.4}$$

The factor 2 was adjusted to get an optimal k for the full network. The optimal k was estimated by trial and error based on the verification for the year 2006. The same relation between k and δ is used for the reduced networks (see Sect. 2.5).

2.3.5 Ordinary kriging (KRI)

A geostatistical method like ordinary kriging deals with the spatial interpolation of a random field from observations at several locations. A general description is presented in Goovaerts (1997). This method requires the definition of a variogram characterising the spatial variability of the precipitation field. The estimation U_0 at a specific location is a linear combination of the gauge values G_i:

$$U_0 = \sum_{i=1}^{N} \lambda_i G_i \tag{2.5}$$

The weights λ_i are computed to obtain the best linear unbiased estimator assuming a constant unknown mean across the field. This involves solving a linear equation system whose size is equal to the number of gauges.

In this study, only the 20 nearest gauges are used. This allows reducing the computational cost with little loss of accuracy. The model variogram, assumed isotropic, is a first order linear function of the distance. More complex climatological variograms (i.e. Gaussian, exponential and spherical) have been tested but no significant improvements of the performance were observed. Those results are consistent with the study of Haberlandt (2007). The KRI method, based only on rain gauges, is used to evaluate the added value of radar observations in the other methods.

2.3.6 Kriging with radar-based error correction (KRE)

This method referenced as "conditional merging" in Sinclair and Pegram (2005) uses the radar field to estimate the error associated with the ordinary kriging method based on rain gauges and to correct it. First, radar values at each gauge site are used to produce a radar-based kriging field. This field is then subtracted from the original radar field to obtain an error field. Finally, the error field is added to the gauge-based kriging field. The KRE method is relatively simple and computationally efficient.

2.3.7 Kriging with external drift (KED)

This method is a non-stationary geostatistical method that uses the radar as auxiliary information. A general description is given in Wackernagel (2003). It follows the same scheme as the ordinary kriging except that the mean of the

estimated precipitation field is now considered as a linear function of the radar field. Additional constraints are then added to this scheme:

$$\sum_{i=1}^{N} \lambda_i R_i = R_0 \tag{2.6}$$

where R_i is the radar value at gauge location i, λ_i the corresponding weight and R_0 the radar value at the estimation location. The weights are given by solving the augmented system of linear equations. The variogram is also assumed linear and isotropic. This is the most complex and time consuming method. Note that an automatic method to compute a variogram model has been proposed recently by Velasco-Forero et al. (2009).

2.4 Long-term verification

2.4.1 Methodology

The performance of the radar-gauge merging methods has been evaluated by comparing the adjusted 24h precipitation accumulations R to the measurements of the climatological gauge network G. The testing period extends from 2005 to 2008, which includes 612 valid days. The gauge data used for the adjustment and for the verification are independent. Unfortunately the two networks have several locations in common or very close. The gauges of the RMIB network situated at a distance less than 2 km from a gauge of the SPW network are then removed. The remaining verification network includes 75 gauges.

Several quality parameters are found in the literature. The Root Mean Square Error :

$$RMSE = \sqrt{\frac{\sum_{i=1}^{N} (R_i - G_i)^2}{N}} \tag{2.7}$$

is the most common parameter used in verification studies. However, the Mean Absolute Error :

$$MAE = \frac{\sum_{i=1}^{N} |R_i - G_i|}{N} \tag{2.8}$$

is less sensitive to large errors and it is used here as first quality parameter. All pairs of gauge radar values are taken into account for these parameters.

A standard for objective judgement of radar performance is proposed in Germann et al. (2006). The mean bias (MB), the error distribution and the scatter score (SCS) as defined in that paper are also used in the present study. MB is the total

precipitation as seen by the radar divided by the total precipitation measured by the gauges. The error distribution is the cumulative contribution to total rainfall as a function of the R-G ratio expressed in dB. SCS is half the distance between the 16% and 84% percentiles of the error distribution. It is a robust measure of the spread of the multiplicative error, insensitive to outliers. The standard deviation of the multiplicative error (STD) and the root mean square factor :

$$RMSF(dB) = \sqrt{\frac{\sum_{i=1}^{N} \left(10 \log \frac{R_i}{G_i}\right)^2}{N}} \tag{2.9}$$

have also been calculated. Only pairs with both adjusted and gauge values larger than 1 mm for all the methods are taken into account. This ensures that the same data set is used for comparison between the different methods.

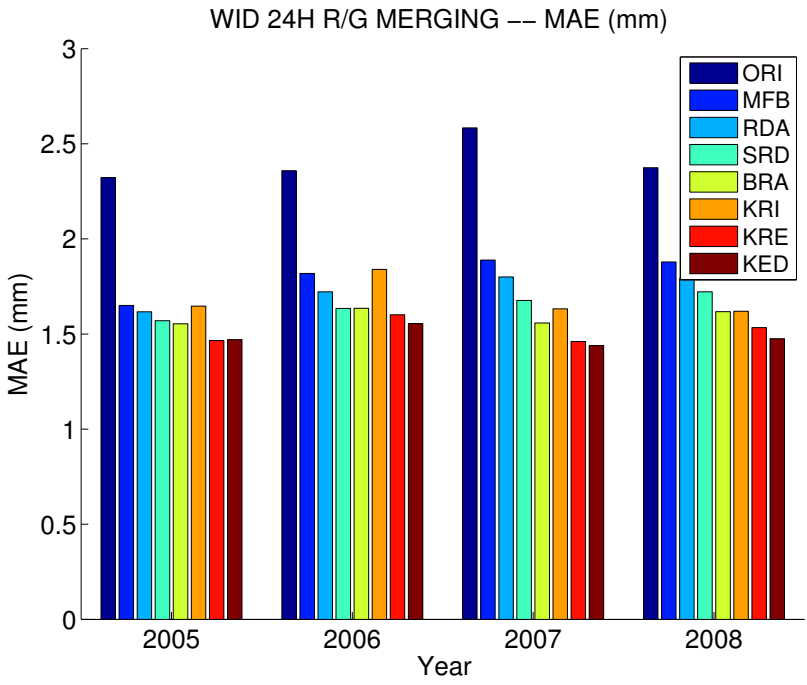

Figure 2.4: MAE of all radar-gauge merging methods.

2.4.2 Results

The verification methodology has been first applied for the four years separately. The goal is to verify the consistency of the results between the four datasets. As illustrated in Fig. 2.4, the relative performance of the different methods is similar for the four years. Nevertheless, the ordinary kriging method (KRI), using only rain gauges, exhibits some variability between the years. The 4 years taken as a whole will now be considered for the rest of the evaluation.

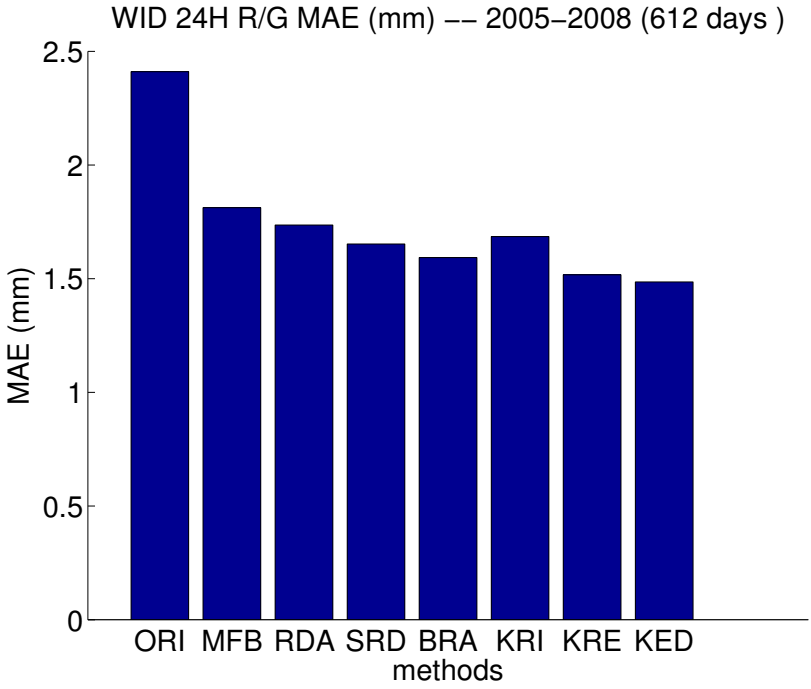

Figure 2.5: of all methods based on a 4-year verification.

As shown in Fig. 2.5, the MAE of all methods is significantly reduced compared to the MAE of the original radar data (ORI). A simple mean field bias (MFB) correction reduces the error by about 25%. Using the range dependent adjustment (RDA) allows a small additional improvement. A further improvement is obtained when a static local bias (SRD) correction is applied. The performance of the latter method is close to the Brandes one (BRA), which is also a spatial method. The ordinary kriging method (KRI), only based on rain gauge data, shows a result close to the RDA method. This good result

is due to the high density of the rain gauge network (see Sect. 2.5). The two geostatistical methods using both radar and rain gauge observations (KRE, kriging with external drift (KED)) perform best for this quality parameter. When the KED method is used, the error decreases by almost 40% with respect to the original data.

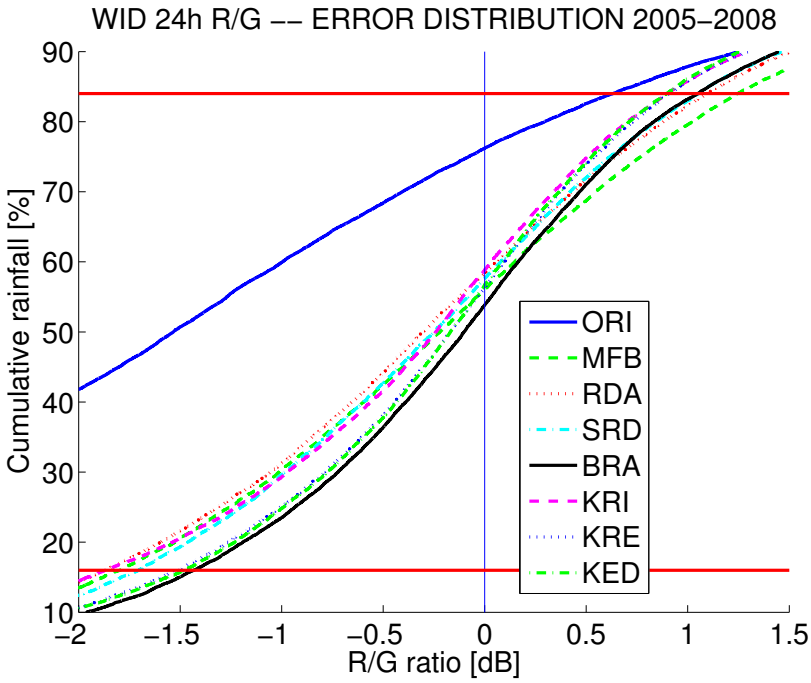

Figure 2.6: Error distribution based on a 4-year verification. The scatter score (SCS) for one method is half the distance between the 2 intersections of the curve with the 2 red lines.

Figure 2.6 shows the error distribution for the different methods. The vertical line divides the R/G ratios (in dB) in underestimation (left) and overestimation (right). A perfect match should give a step function, with a MB and SCS equal to zero. The original radar data (ORI) reveal a significant underestimation with a mean bias of −1.2 dB. The MFB correction succeeds in balancing the error distribution. The method combining a range-dependent adjustment and a static local bias correction (SRD) slightly reduces the spread of the error while the most sophisticated geostatistical method (KED) further tightens the error distribution. The ordinary kriging (KRI) shows a small underestimation.

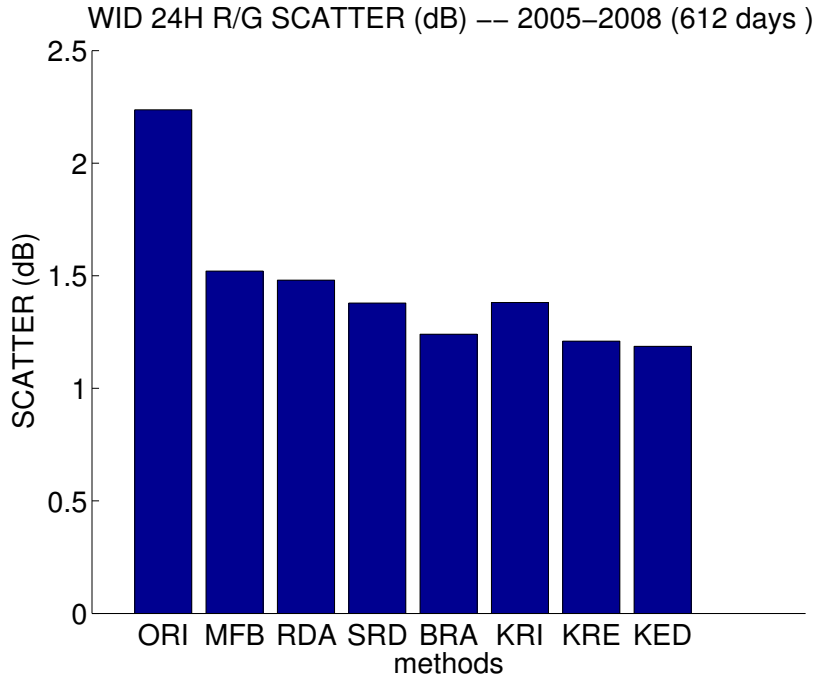

Figure 2.7: SCS for all methods based on a 4-year verification.

The results for the SCS (Fig. 2.7) are similar to the results for the MAE. It is worth pointing out that the relative performance of Brandes compared to the other methods is slightly better. Actually this method can sometimes lead to large errors that are taken into account for the MAE but not for the SCS. This figure also shows that methods with a daily spatial correction feature based on radar and gauges (BRA, KRE, KED) perform significantly better.

The values of the different statistics for all the methods can be found in table 2.1. It appears that the ranking of the methods is very similar for the different scores.

2.4.3 Seasonal variation

The spatial pattern of 24 h rainfall accumulation varies significantly along a year, from widespread precipitation during stratiform events in winter to very local precipitation cells during convective events in summer. Therefore the

Table 2.1: Several statistics (see Subsect. 2.4.1) for the 4-year verification of radar-gauge merging methods.

	MB (dB)	RMSE (mm)	RMSF (dB)	MAE (mm)	SCS (dB)	STD (dB)
ORI	−0.998	5.338	2.649	2.410	2.236	2.480
MFB	0.039	4.066	1.829	1.812	1.520	1.814
RDA	−0.070	4.129	1.741	1.735	1.480	1.738
SRD	−0.052	3.957	1.672	1.652	1.378	1.670
BRA	0.073	3.881	1.680	1.592	1.240	1.670
KRI	−0.153	3.958	1.833	1.685	1.380	1.833
KRE	−0.053	3.533	1.653	1.517	1.209	1.652
KED	−0.061	3.498	1.618	1.485	1.186	1.616

accuracy of radar precipitation estimates and the spatial representativity of gauge measurements depend on the season.

Figure 2.8 shows the value of the MAE (normalised by the MAE of the radar) with the data set sorted by month. The ranking of the methods slightly varies along the year. As expected, the estimation from the gauges only (KRI) is relatively inaccurate in the summer. It is outperformed by the mean field bias correction in this period. In the winter, the ordinary kriging (KRI) is better and very close to the KED, which is the best method for all months. This analysis points out that the additional information given by the radar is especially valuable during summer, when convective events prevail.

2.4.4 Range-dependence

The performance of the different algorithms as a function of range is analysed up to 120 km from the radar. The study area is divided into 6 range intervals of 20 km as shown in Fig. 2.9. The gap between the performance of the radar and that of the gauges is significant at short distance (<20 km) due to the bright band effect. This is also the case at long distance (>100 km) due to the decreasing accuracy of radar estimates. The small difference between KRI and KRE or KED at those ranges shows that the radar added value is very limited. The positive effect of the range dependent adjustment when compared to the mean field bias appears at distances further than 80 km. KED is the best method for all distances. Seasonal variation of the range dependence may exists and a preliminary analysis of this effect has been performed. A significant variability between the years has been found and no robust conclusions could be reached.

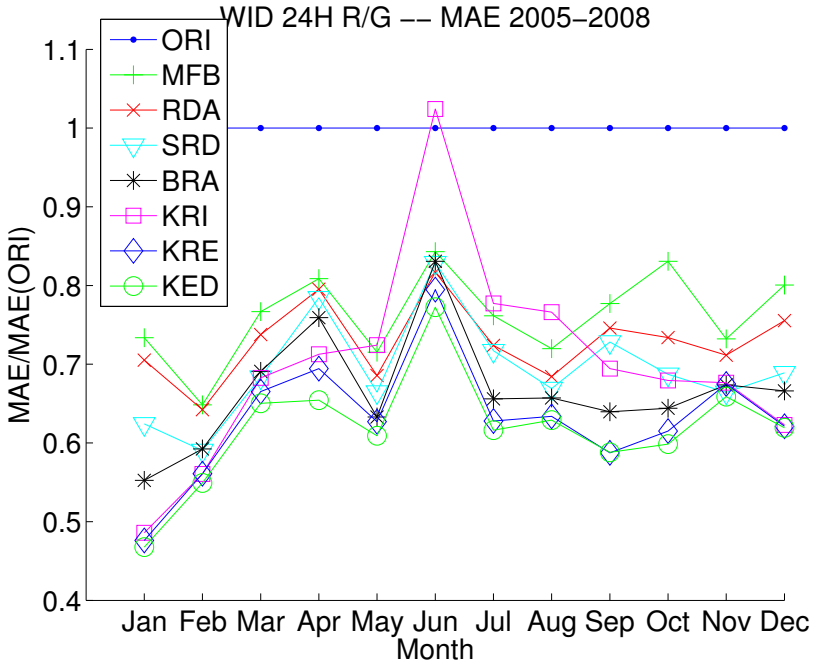

Figure 2.8: MAE of all methods computed for each month and normalised by the MAE of the original radar data.

2.5 Effect of the network density

The effect of gauge density on the performance of the different merging methods has been analysed. This is useful to select the most appropriate method for a given network density or to determine the minimum network density needed to achieve a given level of performance. None of the methods takes directly into account the density of the network except the Brandes method where an inverse relation is used to determine the smoothing factor k (see Sect. 2.3).

2.5.1 Removing gauges

As the region seen by the radar is characterised by low climatological variations, the assumption that the probability of precipitation is the same everywhere is valid. Consequently, a perfect network should be made of a regular grid of points considering a rectangular area. Actually the position of the gauges depends on

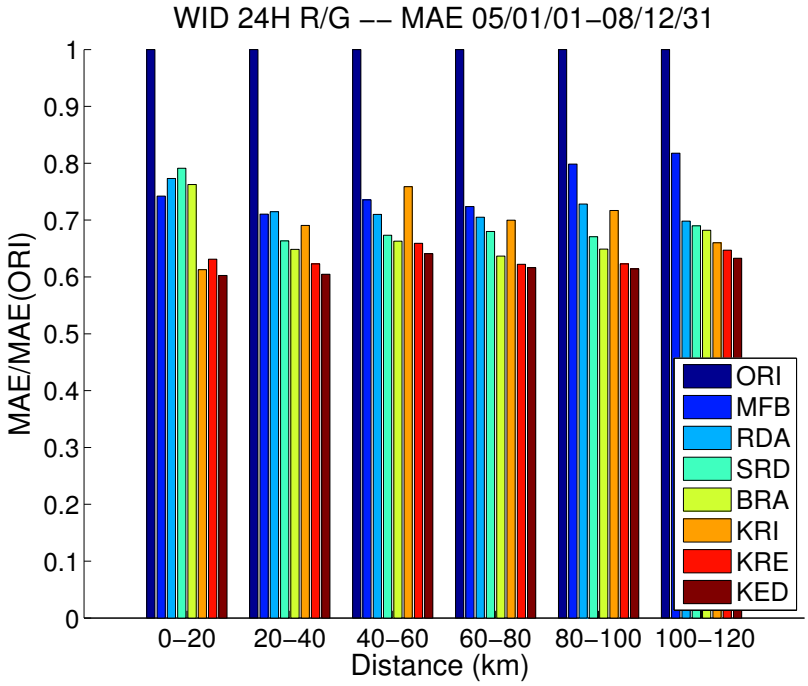

Figure 2.9: Effect of the distance from the radar on the MAE of all methods normalised by the MAE of the original radar data.

practical constraints and specific interest on catchment. The spatial distribution of gauges in a real network is then less uniform. It is obvious that gauges cannot be randomly removed from the network. Indeed, when the furthest gauge is removed, the coverage area decreases. Furthermore, a gauge that belongs to the convex hull (see Sect. 2.3) cannot be removed without decreasing the study area. A rain gauge must be removed from the network in such a way that the spatial distribution of the remaining gauges is as uniform as possible. A simple approach is proposed here, based on the distance between gauges. For each gauge, the sum of the inverse of the distance to the four nearest gauges is computed. Then the gauge with the maximum value (that is too close to its neighbours) is removed. The effect of the algorithm can be seen in Fig. 2.10 which shows the reduced networks of 50 and 20 gauges. Note that the convex hull is relatively well preserved while the number of gauges decreases.

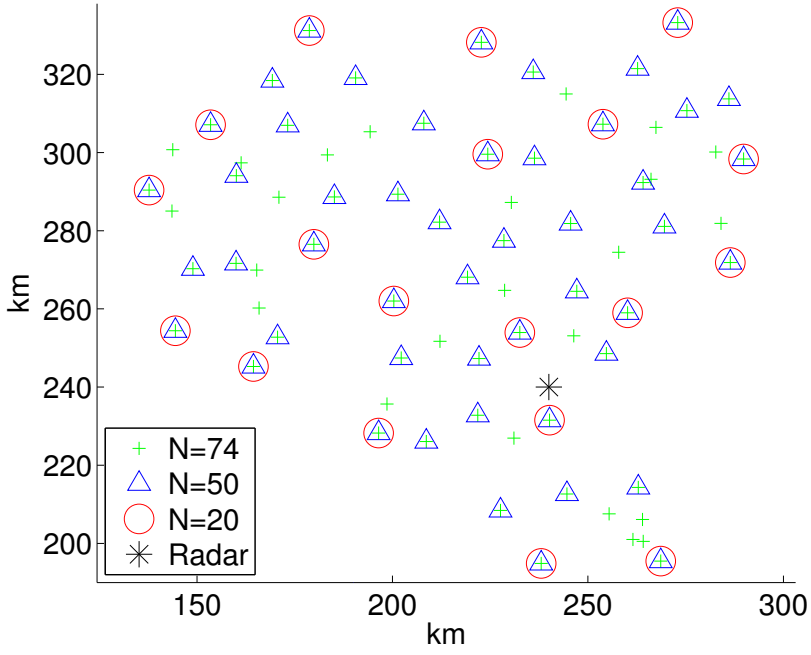

Figure 2.10: Gauge network of decreasing densities obtained by an algorithm for removing gauges.

2.5.2 Global statistics

A long term verification is performed with decreasing network densities. For the sake of consistency, the valid days for adjustment (see Sect. 2.3) at the lower density are taken as the common verification dataset for all densities.

Figure 2.11 shows that a mean field bias correction is not very sensitive to the gauge density and the performance remains acceptable even for a low density network. The performance of the range dependent adjustment, involving a second order polynomial fit, slightly increases with density but only for low densities. As expected, the ordinary kriging (KRI) is the most sensitive method to this parameter. Indeed, the error significantly grows when the density decreases. The MAEs of the Brandes (BRA) and the two geostatistical merging methods (KED, KRE) follow the same tendency but with a lower sensitivity. KED is the best method for all network densities. However, for the lowest tested density (1 gauge per 500 km^2), the static local bias followed by a range

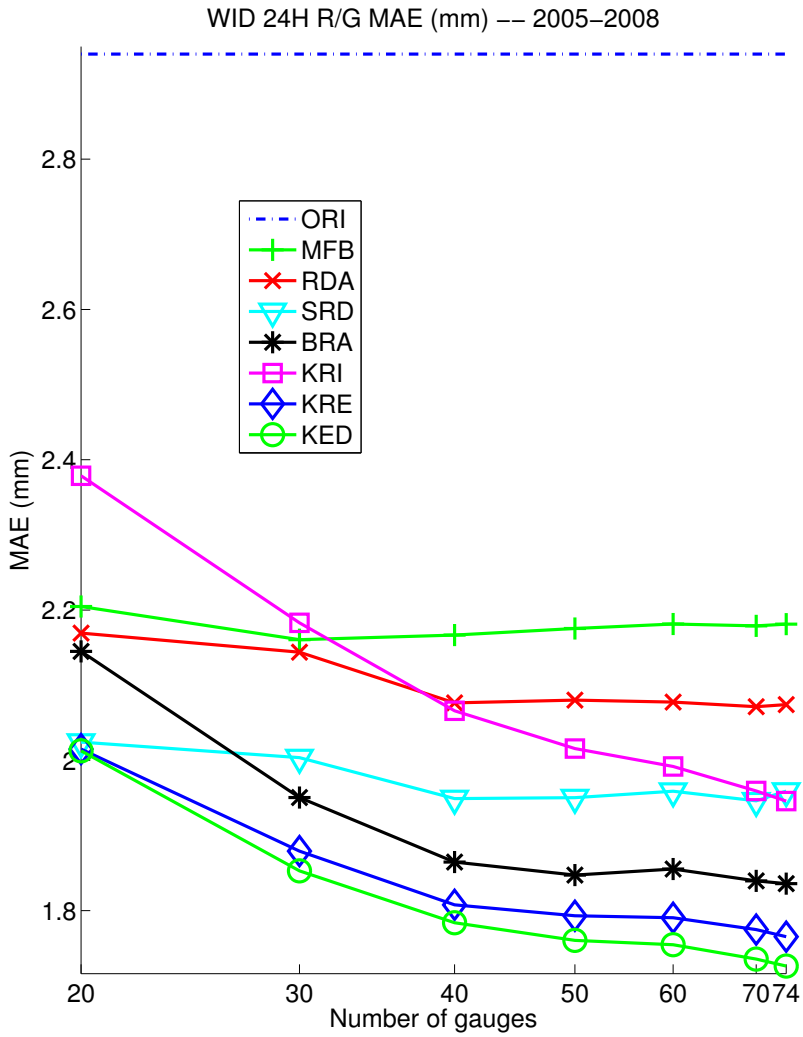

Figure 2.11: Mean absolute error of the merging methods for different network densities from 1 gauge per 500 km^2 (N=20) to 1 gauge per 135 km^2 (N=74).

dependent adjustment (SRD) performs as well as the most sophisticated methods (KRE and KED). Similar results have been obtained with the other quality parameters.

2.6 Conclusions

Various methods combining rainfall estimations from a C-Band weather radar and an automatic rain gauge network have been implemented. A 4-year verification up to 120 km range was carried out against an independent gauge network of daily measurements. Several statistics have been computed to evaluate the performance of the radar-gauge merging methods. The effect of the network density has also been tested.

The results point out that simple methods like mean field bias correction can significantly reduce the error of the radar estimation. Nevertheless, there is a clear benefit of using a spatial correction factor. Based upon our verification study, the best method is the kriging with external drift which makes use of the radar as secondary information to improve the spatial interpolation of gauges values. The kriging with radar-based error correction shows very similar performance while the computational cost is reduced. A seasonal verification shows interesting results. In the winter, when stratiform widespread precipitation prevails, the ordinary kriging based on gauges performs as well as the best radar-gauge merging method. In the summer, when convective events occur, the added value of radar observation is very clear. The sensitivity analysis to the gauge network density shows that the geostatistical merging methods perform best for all tested densities. Furthermore, their relative benefit increases with the density. A method combining a static local bias correction and a range dependent adjustment is less sensitive to the gauge density. For the lowest tested network density (1 gauge per 500 km^2), this method is as efficient as the most sophisticated merging methods.

Acknowledgements

The author would like to thank the four referees for their very valuable questions, comments and suggestions. The data from the automatic rain gauge network were kindly provided by the hydrological service of the Walloon Region of Belgium (Phillipe Dierickx and Marina Thunus). The contribution of Georges Bastin, Guillaume Leclercq and Luc Moens from the Centre for systems engineering and applied mechanics (Université catholique de Louvain) in the operational use of radar for hydrological applications is highly appreciated. Thanks to Maarten Reyniers for helpful comments and to Didier Dehem for providing the topography map. This study was carried out with the financial support of the Belgian Federal Science Policy Office.

Chapter 3

Statistical characteristics of convective storms in Belgium derived from volumetric weather radar observations[1]

Abstract

High resolution volumetric reflectivity measurements from a C-Band weather radar are used to study the characteristics of convective storms in Belgium. After clutter filtering, the data are processed by the storm tracking system TITAN using a 40 dBZ reflectivity threshold. The 10-year period of 5-min data includes more than 1 million identified storms, mostly organized in clusters. A storm is observed at a given point 6 hours per year on average. Regions of slightly higher probability are generally correlated with orographic variations. The probability of at least one storm in the study area is 15 % with a maximum of 35 % for July and August. The number of storms, their coverage and water mass is limited most of the time. The probablity to observe a high number of storms is maximum in June and in the early afternoon in phase with solar heating. The probability of large storm coverage and large water mass is highest

[1] based on E. Goudenhoofdt and L. Delobbe (2013). "Statistical Characteristics of Convective Storms in Belgium Derived from Volumetric Weather Radar Observations". In: *Journal of Applied Meteorology and Climatology* 52, p. 918. DOI: 10.1175/JAMC-D-12-079.1

in July and in the late afternoon. Convective storms are mostly small and weak. Deeper ones are found mainly in the afternoon while bigger and more intense ones also appear in the evening. The occurrence of the most intense storms does not vary along the day. Simple tracks have a mean duration of 25 minutes. Complex tracks, involving splitting or merging, last 70 minutes on average. Most convective storms move in the North-East direction with a median speed of $30\,\mathrm{kmh}^{-1}$. Their motion is slower in summer and in the afternoon. Regions with slightly higher convective initiation are related to orography.

3.1 Introduction

The goal of this chapter is to provide a comprehensive statistical analysis of convective storms in and around Belgium. The area of interest is characterized by a temperate climate, a nearby coastline and intermediate level of orography (maximum 694 m). Convective storms are common meteorological phenomena which involve complex processes at different temporal and spatial scales. Severe events cause flash floods, strong winds, hail falls and tornadoes which can significantly affect human activities. Due to its complexity, the nowcasting (i.e. very short-range forecasting) of convective storms initiation and development remains a challenging problem. In spite of major progress during last decades, current numerical weather prediction models are still not able to forecast convective storms with the spatial and temporal accuracy generally required by the end users. In order to improve the understanding of convective storms, several specific observational field campaigns have been performed (e.g., Wilson and Roberts, 2006; Browning et al., 2007; Wulfmeyer et al., 2011). Nevertheless, a better knowledge of convective storms behavior based on long-term observations is also required to develop nowcasting rules (Wilson et al., 2010). Such a knowledge is also beneficial for the verification of regional climate models, the design of hydraulic infrastructures (e.g., dam, sewer systems), and more generally for all activities that are affected by these storms.

Numerous studies on the statistical characteristics of convective storms in different regions of the world have been performed. They differ by the type of weather data used, the proposed methodologies and the final purpose of the study. Earlier works, which were based on weather station reports of heavy rain and thunder, suffer from bias due to the limited spatial representativity. Lightning detection network observations (Mäkelä et al., 2011) provide a good indication of the electrical activity of thunderstorms but miss convective storms when they do not produce lightning. Satellite observations provide valuable information about the characteristics of convective clouds for very large areas. Unfortunately large errors appear when deriving precipitation from infrared

brightness temperature (Tuttle et al., 2008). A higher accuracy can be obtained using a satellite precipitation radar like in the Tropical Rainfall Measuring Mission (Liu and Zipser, 2009), but mid-latitudes are only partially covered. Compared to satellite observations, the use of ground-based radar measurements can give better insight into the small scale spatial structure of convective systems. Indeed, weather radar provides volumetric reflectivity measurements at high spatial and temporal resolution. With a few minutes between each scan, it can well capture the precipitation activity of the convective storms from growth to decay. Radar reflectivity measurements are affected by various sources of error (Doviak and Zrnić, 2006). Calibration errors, side lobe effects, shielding, attenuation and ground clutter are the most important ones. Some of these errors tend to increase with distance from the radar. Furthermore, the atmospheric volume covered by the radar is limited by the cone-of-silence at short range and overshooting at long ranges. Attenuation can be particularly important in the presence of convective storms especially nearby the radar. Therefore a careful treatment of the radar data is required.

Two different approaches for the analysis of radar reflectivity data can be found in the literature. The Eulerian approach is based on the temporal analysis of the measured field at fixed points (typically each grid point), while the Lagrangian or object-oriented approach is based on the tracking of spatial features across successive images. The former approach is straightforward and is generally used to derive long-term statistics at larger time and spatial resolution using 2D radar data. For example, Weusthoff and Hauf (2008) developed a radar climatology of convective initiation and enhancements for the COPS region based on a 2D radar composite. In the Netherlands, Overeem et al. (2009b) derived a 10-year radar climatology of rainfall. Many studies can also be found in the US using the NOWRAD 2D radar composite (e.g., Schumacher and Johnson, 2006; Carbone and Tuttle, 2008; Lombardo and Colle, 2010). The Lagrangian approach is more complex since it requires specific feature identification and tracking techniques. The use of data with high spatial and temporal resolution is particularly suited for this approach. Popular convective storm tracking algorithms include TITAN (Dixon and Wiener, 1993) mainly developed by the National Center for Atmospheric Research and SCIT (Storm Cell Identification and Tracking) (Johnson et al., 1998) developed by the Storm Prediction Center. In Germany, Weusthoff and Hauf (2008) studied the life cycle of convective-shower cells using a specially adapted tracking algorithm on 5-min 2D radar composite data. A 6-year study of storm tracks over Northwestern Italy is proposed by Davini et al. (2011). A limited number of studies make specific use of volumetric data, mostly performed outside Europe. The size distribution of convective clouds is required for parametrization of its effects into general circulation models. An early comprehensive study of convective radar echoes can be found in López et al. (1984) for Florida using 2 years of

C-Band and S-band radar data and simple tracking techniques. Their results show the distribution of radar echo characteristics with a focus on individual cells, its temporal variability and life cycle dynamic. In a 2002-2006 study for North Dakota based on NEXRAD Level-III storm database (generated by SCIT), Mohee and Miller (2010) provide temporal statistics of convective storms and descriptive statistics of storm track properties (e.g., duration, intensity, mean speed). An extended nine-years analysis based on both reflectivity and velocity measurement of a S-band radar in Quebec can be found in Bellon and Zawadzki (2003). They provide results on the location, strength and frequency of occurrence of severe convective events. Saxen et al. (2008) provide a nine-year analysis of TITAN storm tracks (duration, size, speed, intensity, echo-top) for New Mexico. The same methodology was used in Australia with additional wind data by Potts et al. (2000) and with a focus on cell height by May and Ballinger (2007).

In this study, we analyze the convective storm frequency and characteristics in and around Belgium using high-resolution volumetric C-Band radar data over an observation period of 10 years. To our knowledge, such a long volumetric dataset has never been used in Europe for this kind of study. An objective methodology based on the TITAN storm tracker has been carried out to provide a robust and comprehensive analysis of those data. Both Eulerian and Lagrangian approaches are followed in the statistical analysis. The radar data, the clutter mitigation technique and the storm tracking system are presented in section 2. Section 3 describes the statistical methodology and the storm classification. In Section 4, the spatial and temporal characteristics of the convective storm activity are analyzed (Eulerian approach). The statistical characteristics of the convective storm tracks are analyzed in Section 5 (Lagrangian approach). Conclusions and perspectives are drawn in Section 6.

3.2 Radar data and storm tracking

3.2.1 C-band radar measurements

Since 2001, the Royal Meteorological Institute of Belgium (RMIB) operates a C-Band (5.62 GHz) weather radar located in Wideumont (49.9°N, 5.5°E), South-East of Belgium (Fig.3.1), at 592 m above sea level. The radar, which has a range of 240 km, covers Belgium and Luxembourg and also parts of France, The Netherlands and Germany. It is a single polarization radar with Doppler capability, used to filter ground echoes. A monitoring of the electronic calibration is performed using the mean ground clutter reflectivity at short range and the reflectivity produced by three towers in the vicinity of the radar.

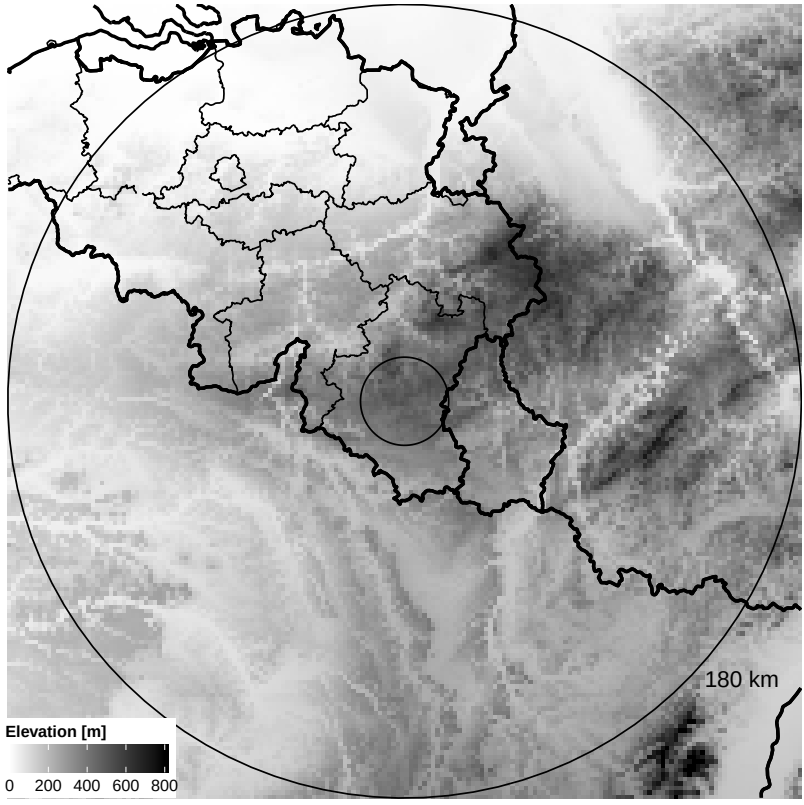

Figure 3.1: Elevation of the study area with location of the Wideumont radar, country borders and Belgian provinces.

These point targets also allow controlling range and azimuth assignments. The radar performs a dedicated reflectivity scan at 5 elevations (0.3°, 0.6°, 1.8°, 3.3°, 6.0°) every 5 minutes with a pulse repetition frequency of 600 Hz and pulse duration of 0.836 μs. The radar volume data have a resolution of 1° in azimuth (an average of 33 pulses) and 250 m in range (an average of 2 successive range bins). Every 15 minutes, the radar also performs a 10-elevation scan without Doppler filtering. A third scan, limited to 120 km, is used to retrieve radial velocity data. Thanks to the height of the radar tower and its position near the top of the Ardennes ridge beam blocking effects are extremely limited. More information regarding the radar characteristics and scanning strategy can be found in Delobbe and Holleman (2006). Only the data from the first scan of the Wideumont radar are used in this study. The vertical coverage of the second

scan is larger but the repetition cycle of 15 minutes is too long to properly track convective storms.

The volumetric data of the Wideumont radar have been archived at RMIB since 2002. No significant changes in the radar calibration have been encountered since 2002. The parameters of the Doppler filter have been changed in 2004 resulting in a stronger clutter filtering. No post processing corrections have been performed on the data. The radar data availability for the most active period (from April to September) is close to 97.5 %. If gaps of 15 minutes are tolerated, which is of the order of a storm duration, the availability reaches 98 %. We assume there is no convective activity for missing files in the least active period (from October to March).

3.2.2 Clutter mitigation technique

Weather radar measurements can be contaminated by non-meteorological echoes such as airplanes or insects. Nevertheless, the main source of clutter is due to the radar beam (including side lobes) reaching the ground. During normal beam propagation (NP clutter), it occurs mainly at elevated places such as hills surrounding the radar. It can also appear over larger areas during particular atmospheric conditions with abnormal propagation of the beam towards the ground (AP clutter). NP and AP clutter exhibit similar radar echoes that can be interpreted as precipitation echoes. If a contiguous contaminated area is sufficiently large, it can be mistaken as a convective storm by a cell tracker system. If such area is detected across successive radar images, it can be tracked as a convective storm. The resulting erroneous track is likely to have a very small mean speed. Since actual convective storms can be stationary, this characteristic can not be used as a selection criteria.

The identification and mitigation of ground clutter remains a challenging problem in radar meteorology mainly because it is not always easy to distinguish precipitation from clutter. A Doppler or statistical filter in the signal processor is typically used to remove near-zero velocity echoes. This kind of filter is not perfect and post processing of the radar data is needed for the remaining clutter. A summary of clutter mitigation techniques can be found in Hubbert et al. (2009), who recommend the fuzzy logic approach for its simplicity and practicability. This method, which is implemented in the TITAN system, uses a combination of several indicators to make a clutter elimination decision. In this study, the velocity field is not available for the first radar scan. Therefore two estimates of the reflectivity radar field spatial variation are used as indicators.

The texture feature is the mean squared difference of the reflectivity,

$$\mathrm{TDBZ} = \frac{1}{N}\sum_{i}^{N}\left(Z_i - Z_{i-1}\right)^2$$

where Z_i is the reflectivity at range gate i and N is the number of gates used along the radial beam. The so-called SPIN change (Steiner and Smith, 2002) feature measures the number of significant gradient changes along the radial beam which satisfy the conditions :

$$\mathrm{sign}\{Z_i - Z_{i-1}\} = -\mathrm{sign}\{Z_{i+1} - Z_i\}$$

$$\frac{\mid Z_i - Z_{i-1} \mid + \mid Z_{i+1} - Z_i \mid}{2} > 5\,\mathrm{dBZ}$$

For each indicator, an interest function is defined, which associates its value to the probability of being clutter. The interest functions used in this study are the same as in Kessinger and Andel (2003). If the final indicator exceeds 0.5, the gate is considered as clutter and its value set to zero.

3.2.3 Storm tracking

The storm tracker TITAN (Dixon and Wiener, 1993) has been developed for automatic identification, tracking and forecasting of convective storms based on radar reflectivity measurements. TITAN is in constant development by several contributors and it evolved in a large suite of software with many capabilities. It can ingest data from various types of weather radars and other observation systems while displaying them altogether. In a first step, the radar volume data in polar coordinates are transformed using a 8 points bi-linear interpolation into a 3D Cartesian grid of 0.5 km size. The storm identification algorithm defines a convective storm as a three-dimensional region with reflectivity values exceeding a given threshold. The volume of the region must be larger than a given threshold to be considered as a valid storm. The storm tracking algorithm matches storms across two successive radar scans using combinatorial optimization. It finds the set of storm paths that minimizes a cost function, which is the sum of volume and distance weighted differences for each path. Before the optimization step, it also uses an overlapping technique to match the storms. An example of storm identification and tracking is shown in Fig. 3.2. The algorithm can also deal with storms that exhibit some evolution, either by merging or splitting. Merging occurs when one identified storm is matched with several storms in the previous image. Splitting occurs when several identified storms are matched with one storm in the previous image. The whole path of the storm, from

genesis to decay including possible interactions is referred as a track, associated to a unique identification number. Tracks with or without interactions are labeled respectively as complex or simple tracks. Each individual track (i.e. component of a complex track between interactions) is associated to a second identification number. TITAN is also able to forecast storm evolution based on simple extrapolation using a linear or parabolic trend, but this feature is not the subject of this study.

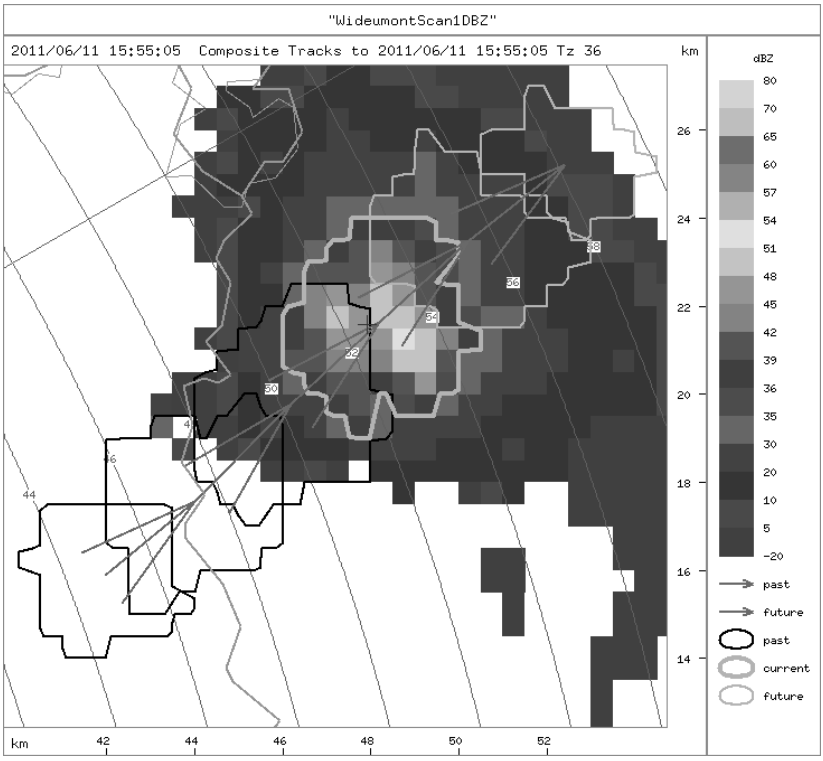

Figure 3.2: 2D visualization (maximum) of interpolated radar reflectivity data and tracking of a convective storm by TITAN.

3.2.4 Parameters tuning

The TITAN storm tracking system is based on several parameters influencing its performance. The grid size of the three-dimensional interpolation grid has been set to 0.5 km. This is consistent with the radar resolution and provides a sufficient

accuracy for storm detection. The basic and most important parameter is the reflectivity threshold used to identify a storm. The second important parameter is the volume threshold used to discard non significant identifications. These two parameters are strongly related. A high reflectivity threshold (typically 40 dBZ) leads to the identification of small convective cores. This choice allows easier tracking but both growth and decay stages of the storm can be missed. A low reflectivity threshold (typically 30 dBZ) leads to the identification of larges areas. The entire life cycle can be captured but the large storm areas may include several reflectivity peaks which are not identified individually. More generally, undesired behaviors of the tracking algorithm include : dropped association which breaks the storm track into several parts, permuted match between two storms close to each other and wrong match between a decaying cell and a newly born cell. A performance analysis of TITAN can be found in Han et al. (2009) with some suggestions for improvements. TITAN has been examined by eye for several distinct cases. To evaluate its performance over a long period an objective method is needed. Lakshmanan and Smith (2010) propose to compute bulk statistics on the track properties that reflect the good performance of the algorithm (i.e. mean duration of the tracks, linearity of the tracks and continuity of the storm attributes). For the Eulerian approach of this study, convective storms are identified using relatively high thresholds values of 40 dBZ (minimum volume of 10 km^3) and 45 dBZ (minimum volume of 5 km^3). This corresponds respectively to rain rates of 12 mmh^{-1} and 28 mmh^{-1} using the default NEXRAD relationship $Z = 300R^{1.4}$, which is valid for deep convection. Those reflectivity thresholds are used in many studies that follow the same approach. The 40 dBZ value is also proposed by Steiner et al. (1995) to identify convective precipitation. For the Lagrangian approach, the 40 dBZ threshold is used.

3.3 Statistical methodology

3.3.1 Storm properties

Ten years (from 2002 to 2011) of volumetric radar data have been processed by the TITAN storm tracking system. For each identified convective storm, different characteristics are computed by TITAN. These include morphological properties such as volume, precipitation area (i.e. the area of the storm close to the ground), and top (maximum height of the 18 dBZ region). Physical quantities such as water mass or precipitation rate are derived from the reflectivity values. The recording of all the grid points which make up the identified storm was not possible due to the huge amount of data. A two-dimensional representation

of the storm envelope (i.e. the area obtained from the 3D volume projection on the surface) is used as a good alternative. A fitted ellipse, which is defined by its center, orientation and minor/major radius is used as a first simple representation. This representation is not supposed to be realistic for a storm which exhibits a large extension in one direction. A more accurate representation is based on a convex polygon which is constructed by projecting 72 radials out of the storm envelope centroid (i.e. geometric center). Nonetheless, such polygon could fail to represent properly squall lines or bow echoes. Motion properties such as the speed and the direction are derived from successive tracked positions of the storm centroid. For the whole storm track, the mean and maximum of the storm properties are also computed. Additional properties have been computed such as the eccentricity of the fitted ellipse.

3.3.2 Storm types

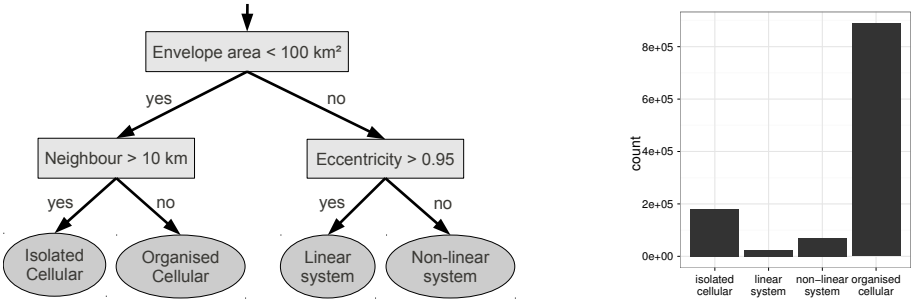

Figure 3.3: Classification of identified convective storms : (a) decision tree and (b) 10-year study period distribution.

It has been shown that severe weather produced by convective storms can be related to its morphological characteristics (e.g., Gallus et al., 2008). Various convective storm classifications have been proposed in the literature and a summary can be found in Schoen and Ashley (2011). Although storms exhibit a wide spectrum of morphologies and organizations, predominant modes of organization can be found in relation to synoptic and meso-scale forcing. Unorganized cellular convection is observed in weak shear environment while organized cellular convection (line or clusters) and supercells are associated with moderate to strong wind shear. A mesoscale convective system is defined as a contiguous convective precipitation area with a scale of more than 100 km in a given direction, which is often embedded in stratiform precipitation (Houze, 2004). Regarding the huge amount of data, it is necessary to use an automated

classification technique. While complex classification methods exist (e.g., neural network technique), a simple hierarchical technique based on a decision tree, is used in this study following Rigo and Llasat (2004) and Gagne et al. (2009). The classification is based on several morphological properties of the storm as shown in Fig.3.3a. The size of the envelope area is used to determine the general type (i.e. top of the decision tree) of identified storms. Storms that have a 40 dBZ envelope area smaller than 100 km^2 tend to have a single reflectivity peak and are given the cellular type. Storms which exhibit an envelope area bigger than 100 km^2 are usually made of contiguous reflectivity peaks and are labeled as convective systems. Since the TITAN algorithm lacks information about the organization of convective storms, an algorithm has been developed to compute the distance between the storms. Consequently, convective cells are further classified as isolated if no neighboring storms exist at a 10 km distance. Convective cells are considered as organized in the other case. Convective systems are classified as "linear" if the eccentricity of the fitted ellipse exceeds 0.95; "non-linear" otherwise. This classification is performed for each storm identified at a given time. It is clear that convective storm morphology and organization can evolve in time especially when splitting or merging occurs.

3.3.3 Storm selection

The performance of the storm identification and tracking algorithm is affected by the distance to the radar. At small distance, storms will not be identified due to the cone of silence while at large distance, only storms with large vertical development will be identified. Besides, the sample volume increases at larger distance due to beam broadening. Therefore the study area is limited to ranges from 20 km to 180 km and represents a total area size of about 10^5 km^2 (Fig.3.1). This selection criteria will be used for the Eulerian approach (based on the identified storms). For the Lagrangian approach (based on the tracked storms) a specific track selection is needed. To ensure that the complete path of the storms is captured, storm tracks that exist after or before a missing file are discarded. Furthermore, the whole storm track is limited to ranges from 20 km to 220 km. This ensures that a part of the track is not cut by the cone of silence or the border of the radar coverage. It is important to note that this spatial condition will discard long-living storms, typically mesoscale convective systems that can travel hundreds of kilometers.

3.4 Eulerian statistics

3.4.1 Sample description

During the whole 10-year period, more than 1 million storms have been identified at 40 dBZ by TITAN in the study area. Taking into account the 5 min timestep, it corresponds to a cumulative storm duration of 3500 days. If the 45 dBZ threshold is used, only half of these storms are identified. On Fig.3.3b one can see the distribution of convective storm types. The most frequent storm type observed is the cellular type. Organized cells are five times more frequent than isolated cells. Convective storm systems are relatively rare (about 5 %). Non-linear systems are more frequent than linear ones.

3.4.2 Local convective storm activity

Climate variations exist within the study area due to the coastal influence, the orography and the land cover. The probability of convective storm at a given location, $P_d(x, y)$ is calculated as the mean of the storm activity $i_d(x, y, t)$ over a given period. At a given time t, the storm activity $i_d(x, y, t)$ is equal to 1 if (x, y) is inside an identified convective storm (defined using reflectivity threshold d), 0 otherwise. Since the interpolated radar data have a resolution of $0.5\,\text{km} \times 0.5\,\text{km}$, the polygonal representation of the storm is back-transformed to this regular grid. Then the probability is computed for each pixel (I, J):

$$P_d(I, J) = \frac{1}{M} \sum_{T=1}^{M} i_d(I, J, T)$$

where M is the total number of measurement time step T during the period. Even though a temporal resolution of 5-min is small, a so-called jumping cell effect may occur for fast moving storms. Its impact is supposed to be very limited since the analysis is based on a long observation period.

Fig.3.4 shows the probability of convective storm in the study area. For the whole 10-year period (top panel), P_{40} (P_{45}) ranges mostly between 0.04 % (0.01 %) and 0.08 % (0.03 %). The average probability is around 0.07 % (0.02 %) which corresponds to about 6 (2) hours of convective activity per year. The standard deviation of the yearly P_{40} (top panel right figure) is 0.03 % on average, which highlights some interannual variability. This variability is higher for P_{45} (not shown) due to the smaller number of events. In North-East US, Murray and Colle (2011) found a probability ranging between 0.10 % and 0.30 % for P_{45} during April-September using a $2\,\text{km} \times 2\,\text{km}$ resolution. The probability of

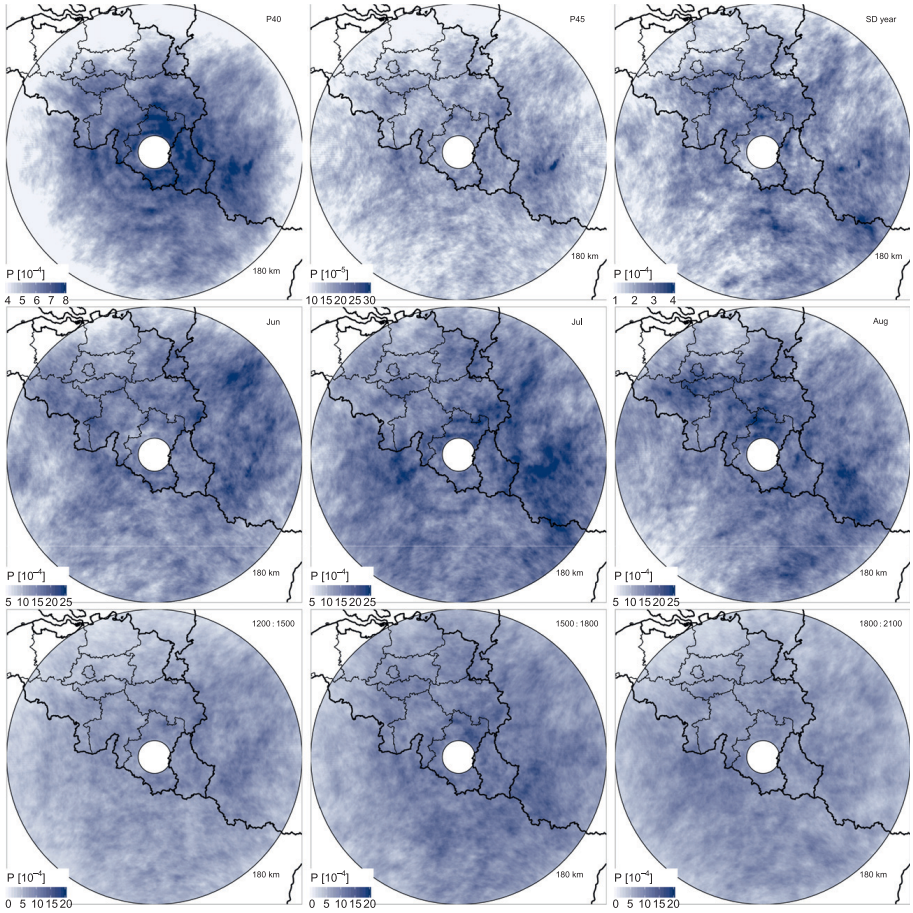

Figure 3.4: Probability of convective storm activity in the study area. Top panel : whole study period using 40 dBZ (P_{40}) or 45 dBZ (P_{45}) reflectivity threshold and standard deviation of yearly P_{40}. Middle panel : P_{40} for June, July and August. Bottom panel : P_{40} for 1200-1500 UTC, 1500-1800 UTC and 1800-2100 UTC

convective storm tends to decrease with distance to the radar. This is a combined effect of signal attenuation, beam broadening, and beam overshooting. Concentric circle patterns are slightly apparent on the image and are another radar artifact related to the 5-elevation scanning geometry. The probability of convective storm increases when going to the South-East of the study area.

This effect seems related to the general increase in orography. Localized areas with higher probability are also observed, especially on the North and East of the radar. These areas are correlated with the orographic features shown in Fig.3.1. It is unclear whether the observed spatial variations are caused by real climatic variations or by radar artifacts. The radar measurements are closer to the ground in high orography regions which could explain a higher detection rate of shallow convective storms. Besides, we cannot exclude that some ground echoes remain in the data even if a very careful ground clutter elimination has been performed. Ground echoes are more frequent in elevated places which could also contribute to correlate the radar-derived probability of convective storm with the orography.

The middle panel of Fig.3.4 shows the spatial variations of P_{40} for the months June, July and August. The probability reaches 0.25 % in July and August which corresponds to 2 hours per month. The relative probability tends to increase toward North-West between June and August. This might be related to the orography and the proximity of coast.

The bottom panel of Fig.3.4 shows the diurnal variations of P_{40} for the most active hours of the day. In the afternoon the probability increases toward East while in the evening the probability is slightly higher in the Western part of the study area.

3.4.3 Area-averaged convective storm activity

In this section we analyze the characteristics of the convective storm activity over the whole study area whose size is about $10^5 \mathrm{km}^2$. Different area-averaged indices are considered: the number of identified storms N, their fractional coverage C expressed in % and their total water mass W. If a storm lies on the border of the area, only a fraction of the storm is used to compute the indices. W is based on an empirical relationship between the reflectivity Z of the sample volume and its equivalent water mass M. In TITAN this relationship is $Z = 20645\, M^{1.75}$ for liquid water and $Z = 3.6683 \times 10^6\, M^{1.416}$ for solid water. The latter equation is used for reflectivity values exceeding 55 dBZ which are very likely associated with hail. The water mass M has a more physical meaning than the reflectivity Z but it must be kept in mind that it strongly depends on the $Z - M$ relationship.

Fig.3.5 shows the probability to exceed a given index value for different periods aggregated by years, months and hours. It is important to note that the results are shown using a logarithmic scale. Each probability is computed using all available 5-min data including dry periods. N and W are normalized to an area

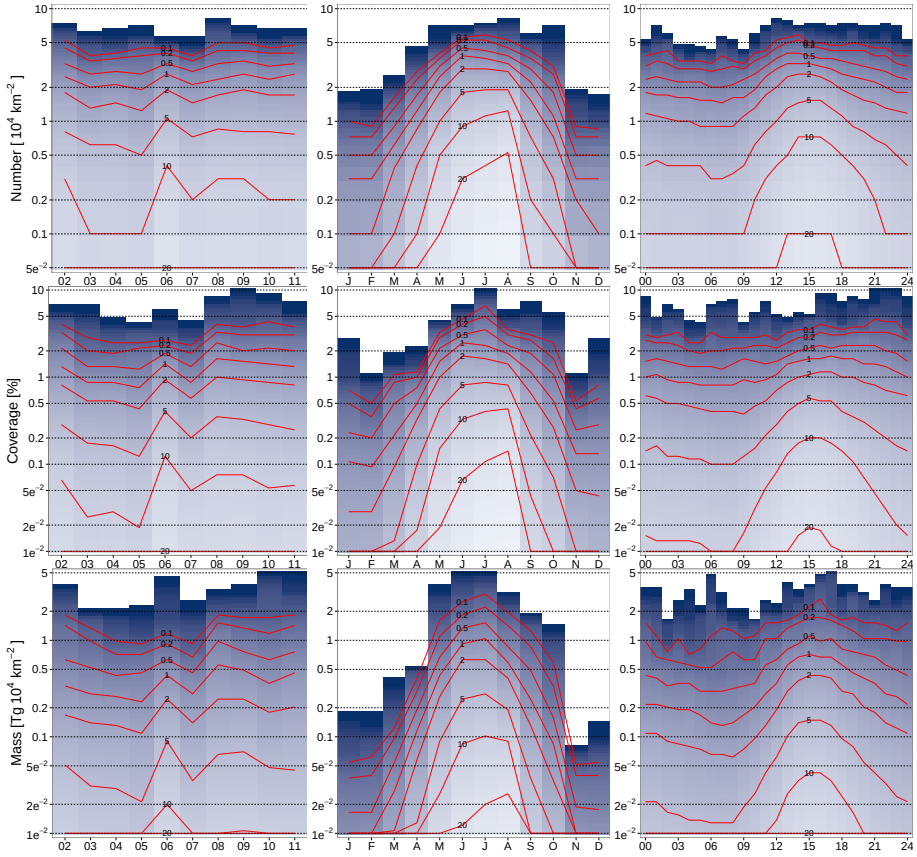

Figure 3.5: Absolute exceedance probability (in percentage) of convective storm activity indices (number of storms N, fractional coverage C and total water mass W) grouped by year (left), month (middle) and hour (right).

of $10^4\,\mathrm{km}^2$. Only the results for the 40 dBZ identification threshold are shown here.

The probability to observe at least one storm in the study area (which corresponds to 0.1 storm per $10^4\,\mathrm{km}^2$) ranges from 12 % to 20 % from year to year with an average of 15 %. This probability is above 20 % from May to August and reaches a maximum around 35 % in July-August. An important daily variation is observed with a lower probability during the night and the morning followed by a steep increase from 0900 UTC to 1500 UTC and a decrease in the evening. The diurnal maximum is the consequence of the solar heating

effect that helps triggering convection during the afternoon (local solar noon is around 1145 UTC). This well-known effect has been observed in many previous studies (e.g., Murray and Colle, 2011; Parker and Ahijevych, 2007). For the sake of comparison, the same probability has been computed over a reference area of $10^4\,\mathrm{km}^2$, which lies within the optimal range interval of the radar (70 km - 90 km). For this reference area, the probability is 6 % for the whole study period and reaches a maximum of 14 % in July-August.

The probability of exceedance decreases strongly for increasing number of storms. There is some interannual variability for the whole range of values. $P(N \geq 1)$, which is the probability to observe at least 1 storm per $10^4\,\mathrm{km}^2$, ranges from 2 % in 2005 to 5 % in 2006. It reaches a maximum in August with more than 10 %, slightly above July and June. For situations with more than 2 storms per $10^4\,\mathrm{km}^2$, the maximum probability is found in June. Additionally, the diurnal variation is more pronounced and reaches a maximum at 1300 UTC. Those results are related to the effect of surface heating which is maximum around 21 June and in the afternoon. Convective storms triggered by surface heating are mainly isolated cells which can develop everywhere in the domain. This kind of situation is likely to produce the highest number of storms.

Exceedance probabilities for the fractional storm coverage C exhibit a power law behavior. For a given index value, the probability is higher during the period 2008-2011 than the period 2003-2005. This effect tends to increase for increasing values of C. The rank of year 2006, which has the highest probability for C below 1%, significantly decreases for higher values. The maximum probability is found in August for C below 0.2 %, in June and July up to 2 % and July for higher values. By definition, mesoscale convective system (MCS)'s are likely to produce the largest storm coverage. Therefore the latest result suggests that MCS's were more frequent in July during the study period. There is a relative increase of probability in the evening when C increases. For $P(C > 2\,\%)$, the maximum probability is found between 1600 and 2000 UTC. The diurnal cycle is less clear for the highest values. Those effects might be related to the persistence of MCS's during the evening and sometimes in the night.

The distribution of the total water mass W is also skewed toward lower values. A similar yet higher interannual variability is found for this index. This effect is particularly important for situation with more than 1 teragram of water per $10^4\,\mathrm{km}^2$ with a probability much higher for the period 2008-2011 than the period 2003-2007. The seasonal variation is also clear for this index. An increase in the relative probability of July for increasing W values is observed. This effect can also be related to the prevalence of MCS's during this month and the fact that those events are the most severe. The diurnal variation of the probability is important for the whole range of values with a slight relative increase in the evening for increasing W. There is a second maximum of probability around

0600 UTC for extreme W values. Nevertheless, a much longer study period is required to confirm the latter result.

The interannual variability found in the analysis of the indices might be partially related to inter-annual variability of general circulation patterns. Allan and Zveryaev (2011) showed that summer precipitation variability over Europe is dominated by large-scale dynamics which are associated with the Summer North Atlantic Oscillation (SNAO). Especially, a positive SNAO is related to drier condition in North Europe (including Belgium) and wetter condition for South Europe. During the study period the SNAO was slightly positive on average during 2002-2007 while mostly negative from 2008 onward. The SNAO was extremely variable during summer 2006 which can be related to the contrasting results obtained for that year. A similar attempt to link convective activity with remote oceanic forcing can be found in Murray and Colle (2011). It is worth pointing out that our record is too short to derive any definitive conclusion.

Some extreme situations have been recorded during the study period. At 1255 UTC on 8 August 2008, almost 8 storms per $10^4\,\mathrm{km}^2$ have been observed in the study area. It was a typical case of isolated convective cells triggered by solar heating in the afternoon. During 14 July 2010 at 1755 UTC, the storm coverage exceeded 8 % of the study area. That day, a quasi-linear convective system caused strong winds and tornadoes (Hamid, 2012). The maximum total water mass was recorded during 28 June 2011 around 1700 UTC. Several mesoscale convective systems had developed in a very high CAPE (Convective available potential energy) environment. That day severe wind, heavy rain, large hail and a tornado were reported in the study area. It is interesting to note that those extreme events occurred during the 2008-2011 period when convective activity indices were higher on average.

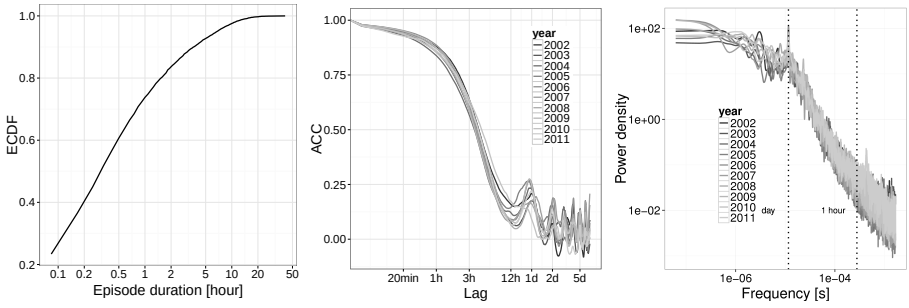

Figure 3.6: Time and frequency analysis of convective storm activity index (number of storms) : (a) distribution of convective episode duration, (b) autocorrelation function and (c) power spectrum.

The exceedance probability grouped by year, month or day does not characterize entirely the convective activity. It is also important to investigate its internal variability at all timescales. Convective storm activity is characterized by the succession of active and inactive periods. To analyze this intermittent behavior, a convective episode is defined as the interval of consecutive time steps with non-zero indices. It is worth pointing out that this definition strongly depends on the study area since convective storms can move out of it. Fig.3.6a shows the empirical cumulative distribution function of convective episode duration for each year. The distribution tends to be positively skewed with about 70 % of the episodes lasting less than 1 hour while only about 5 % exceed 5 hours. The longest episode inside the study area has been recorded during June 2008 and lasted 56 hours.

For the number of storms N, the autocorrelation of the time series is showed in Fig.3.6b. It measures the correlation of the index for a given time lag between two values of the time series. To ensure the stationarity of the time series, the analysis is performed for each year separately and focused on April-September months. It is shown that the correlation decreases strongly between 1 and 6 hours confirming that most of the convective episodes are short. The correlation is higher for 24 h lag than 12 h lag due to the diurnal cycle. On average, there is a slightly higher correlation for lag of 1 day than lag of 2 days or more. This implies there is a slightly higher probability of convective storm activity on a given day when the day before was active.

To better analyze the variability of the convective activity for all timescales involved, a spectral decomposition has been performed as seen in Fig.3.6c. The spectrum exhibits a power law behavior which is represented by a straight line on a logarithmic scale plot. This is a characteristic of a scale invariant process which means that the variability of the process at different time scales are related. Different scaling regimes (i.e. time scale ranges) can be observed. From lower frequency ($T = 6$ months) to intermediate frequency ($T = 1$ day), a relatively flat spectrum can be seen, which can be associated with the intra seasonal variability. A second scaling regime, ranging from intermediate to higher frequencies ($T = 1$ hour), can be associated with frontal disturbances. The scaling break around 1 day period may be due to the finite size of the study area. Those results are consistent with previous studies of precipitation time-series (e.g., Verrier et al., 2011). The peak at 1 day period is associated with the diurnal cycle.

For the sake of comparison, the temporal resolution of convective index timeseries has been reduced to 1 day using the mean (the results are not shown on the figures). A day is considered as a convective storm day if a cumulative storm duration of one hour is observed. For the part of the study area corresponding to Belgium, the yearly probability of convective storm days ranges from 24 %

to 33 % and is at a maximum in July and August around 56 %. From thunder reports in Belgium during 1971-1988, the probability of thunderstorm days is 22 % with a maximum at 38 % in May and June. The lower figures obtained with the stations are related to their limited spatial coverage and the fact that the reports are based on lightning only. From 11 synoptic stations in southwest Germany with coverage of about $10^4\,\mathrm{km}^2$, Kunz et al. (2009) found a probability of thunderstorm days ranging between 25.7 % and 44.3 % during April-September.

3.4.4 Storm properties

In this section the distribution of identified storms characteristics are analyzed. Since no large geographical variations of storm properties have been found (not shown) the analysis is based on all storms identified in the study area. Figure 3.7 shows the interannual, seasonal and diurnal variations of the time-averaged number of storms that exceed a given volume, echo-top or mass. This number, which is computed for the whole study area, is normalized to an area of $10^4\,\mathrm{km}^2$.

The distribution of storm volume follows a power law which implies that smaller storms are more often seen than bigger storms. The distribution is relatively similar from year to year for smaller storms. However, the average number of storm bigger than $1000\,\mathrm{km}^3$ is about 4 times higher for the years 2008-2011 than the years 2004 and 2005. The average number of storms exceeding a given volume is higher in June and July. This effect is much more marked for bigger storms. For volume increasing to about $2000\,\mathrm{km}^3$, a constant difference of average number is seen between the night minimum and the maximum. This maximum occurs 1 h later for biggest volumes than for small volumes. In the evening, there is an increase in the relative average number of storms for increasing volume. This result might also be related to the persistence of MCS's, which have bigger volumes by definition.

The storm echo-top is a good indication of the storm severity. It is calculated using the 18 dBZ reflectivity threshold. Obviously, the actual top of the cloud can be higher. Most of the identified storms have an echo top below 5 km. In July, the mean number of storms per $10^4\,\mathrm{km}^2$ area whose echo-top exceed 10 km is 0.01. The interannual variability of the probability slightly increases with increasing values. For echo-top above 5 km, the average number of storms is higher in June-July than in May and August. Contrarily to the volume, the diurnal variation becomes larger with increasing tops and no increase in the evening is observed.

The storm mass corresponds to the amount of water content inside the storm. The distribution of this characteristic also follows a power law with the most

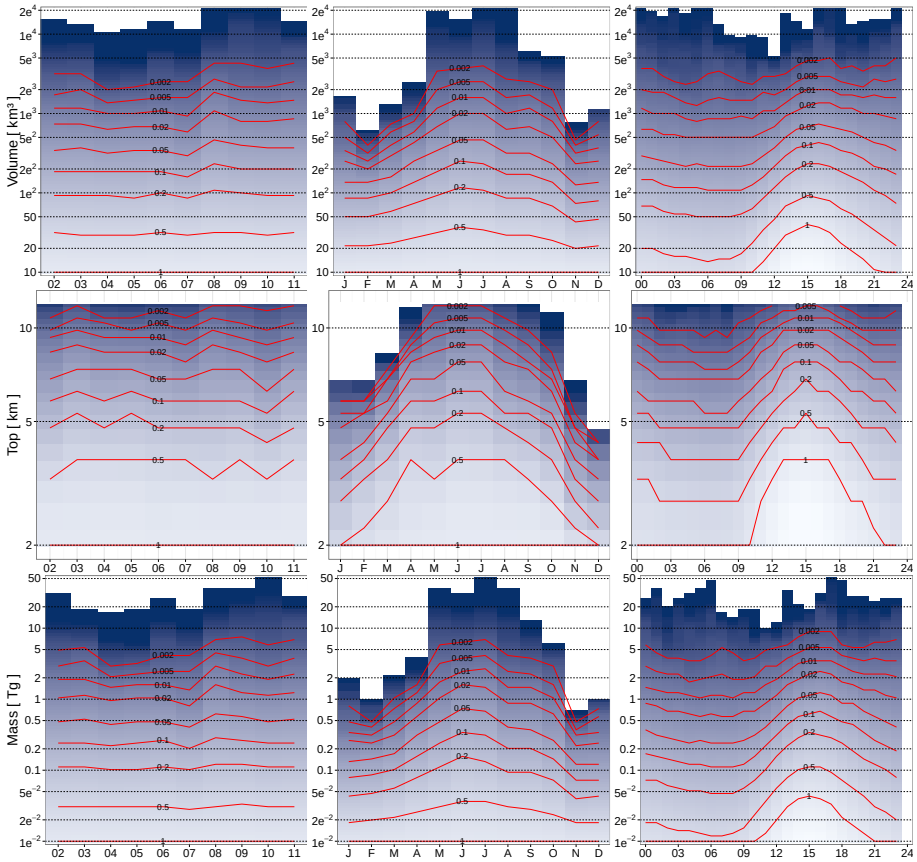

Figure 3.7: Time-averaged number of storms per $10^4\,\mathrm{km}^2$ exceeding a given storm characteristics (volume, echo-top and mass) grouped by year (left), month (middle) and hour (right).

intense storms being relatively rare. The interannual variability increases with increasing mass. For a given mass of 2 Tg, the mean number of storms is above 0.01 for the year 2008-2011 while it is close to 0.005 for year 2004 and 2005. For exceedance values above 0.2 Tg, the mean number of storms is 2 times higher in June-July than in May and August. However, for storms exceeding 10 Tg, it is also maximum May. The mean number of storms is highest during the afternoon for all values. Nevertheless, extreme values are observed at any time of the day.

The power law behavior of storm properties found in this study is consistent

with the results of previous studies (e.g., May and Ballinger, 2007; Saxen et al., 2008) and can be seen as a general characteristic of convective storms. The results obtained for higher values of storm characteristics should be taken with care since the sample of storms becomes relatively small.

3.5 Lagrangian statistics

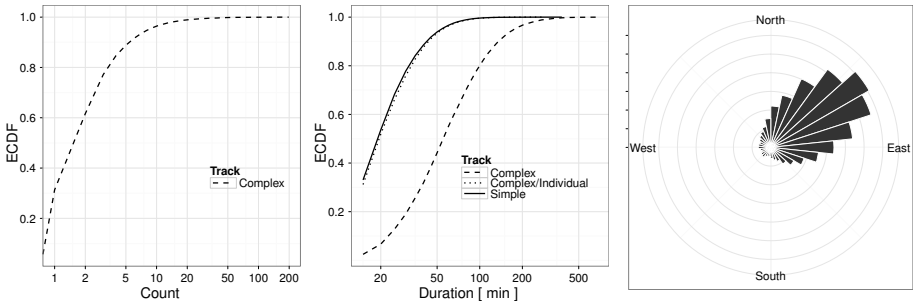

Figure 3.8: Distribution of storm tracks kinematic properties : (a) number of individual tracks per complex track, (b) duration and (c) mean direction.

3.5.1 Sample description

About 3 millions storm tracks have been recorded in the extended study area during the 10-year period. The percentage of those tracks impacted by missing files is 2 %. A few of them (10 %) reach the boundary of the study area. About 60 % of the tracks last less than 15 minutes and are discarded. After applying all selection criteria, the number of storm tracks is about 1 million, including 80 % of simple tracks. The 20 % of complex tracks (i.e. with merging or splitting) are mainly made of a few individuals tracks (Fig.3.8a).

3.5.2 Storm track kinematics

In this section we analyze the kinematic of storm tracks. The storm tracks are divided between simple and complex tracks. Furthermore, individual tracks within complex tracks are also analyzed. Individual tracks which last less than 15 minutes are discarded. On Fig.3.8b one can see the empirical cumulative distribution of storm track duration. The mean storm duration is 25 min for

simple tracks and 70 min for complex tracks. Simple storm tracks are mostly short lived with only 5 % lasting more than 50 minutes. Complex storm tracks, which are made of several individual tracks that interact, last more than 100 minutes with a probability of 20 %. Only 3 % of complex tracks exceed 200 minutes. It is interesting to note that the distribution of duration is similar for individual tracks and simple tracks. The tail of the distribution might be influenced by the limited size of the study area.

Fig.3.8c represents the distribution of the storm mean direction for both simple and complex tracks. It is computed using the successive positions of the storm volume centroid. It shows the prevalence of the North-East direction. This result is consistent with the distribution of surface wind direction prevailing during convective situations. A perfect match is not expected since the steering wind at given altitude can differ significantly from the surface wind.

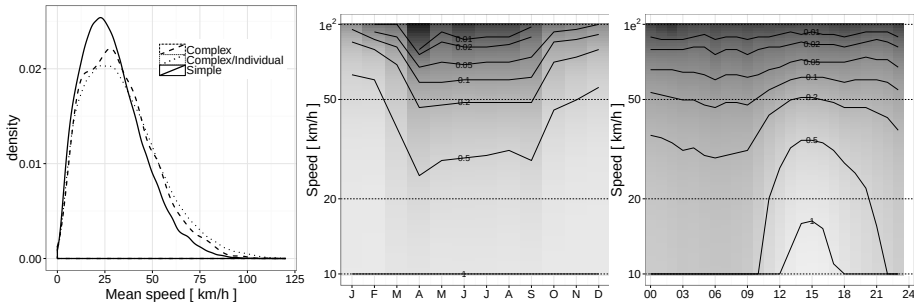

Figure 3.9: (a) Estimate density of storm tracks mean speed, (b) time-averaged number of identified storms exceeding a given speed grouped by month (b) and by hour (c).

The distribution of storm tracks mean speed (Fig.3.9a) follows a Weibull distribution. This is also the typical distribution of surface wind speed measurements. About half of the simple storm tracks exhibit a mean speed below 30 km h^{-1}. Their probability to exceed 60 km h^{-1} is only 5 %. The mean speed of individual tracks and complex tracks tend to be slightly higher. The analysis of the seasonal (Fig.3.9b) and diurnal (Fig.3.9c) variations shows that their motion is slower in the summer and in the afternoon.

3.5.3 Storm track initiation

We analyze here the spatial variations of convective storm initiation (e.g., Wulfmeyer et al., 2011) using both 40 dBZ and 45 dBZ thresholds. In Titan

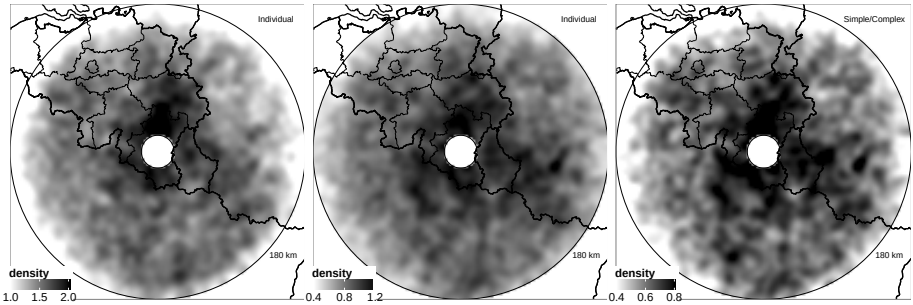

Figure 3.10: Density of storm initiation : individual tracks (including simple tracks) at (a) 40 dBZ and (b) 45 dBZ; (c) simple and complex tracks at 45 dBZ.

storm initiation corresponds to the position of the storm at the beginning of the track. The statistical framework of spatial point process (Diggle, 2003) is used. The storm volume centroid is used as a point representation of the 3D storm shape. This approximation is justified for convective cells but is less valid for bigger convective systems. A strong correlation between storm initiation locations is expected at short time scales given the predominance of organized convective storms. This effect is supposed to be very limited over a relatively long dataset. Fig.3.10 shows the density of convective storm initiation for the whole study period. It is obtained by using a kernel smoothing on the spatial point pattern. The analysis is performed using individual tracks (40 dBZ and 45 dBZ) and simple/complex tracks (45 dBZ). All tracks starting in the study area are taken into account. The 3 figures exhibits similar characteristics. Localized areas with higher or lower density are observed and correspond to orographic variations. The storm initiation spatial point pattern can be further analyzed using a test for complete spatial randomness (CSR). Our method is based on the distribution of nearest neighbor distance (not shown) which measures the dispersion or clustering of a spatial point pattern. This empirical distribution is compared to the Poisson distribution using the Clark-Evans statistical test. To mitigate the effect of the distance, the study area has been divided into range rings of 20 km width. For all rings, the results of the test of CSR is negative and the alternative hypothesis of clustering is retained. This suggests there exists preferred areas for initiation. Note however that the distribution is still very close to the Poisson distribution meaning that the clustering is limited.

3.6 Conclusions and perspectives

The characteristics of the convective storm activity in and around Belgium have been analyzed over a ten-year period (2002-2011). The analysis is based on high resolution volumetric radar observations which have been filtered by a fuzzy logic clutter mitigation technique. The TITAN algorithm has been used to identify and track convective storms on successive 5-min radar scans using a reflectivity threshold of 40 dBZ. In a study area limited between 20 km and 180 km distance from the radar, more than 1 million convective storms have been identified which represents a cumulative duration of 3500 days. A simple classification has been proposed which reveals that most storms are of the cellular type while convective systems are relatively rare. Convective cells tend to be organized rather than isolated.

The average probability of convective storm activity at a given location is 0.07 % which corresponds to 6 hours per year. Besides radar artifacts, the spatial variations of the probability is relatively limited. However some regions with slightly higher or lower activity can be identified and are related to the effect of orography. There is an inter-annual variability with an averaged standard deviation of 0.03 %. The relative probability tends to increase in the western part of the study area from May to August and from the afternoon to the evening.

The probability to observe at least one storm is 15 % for the whole study area whose size is 10^5 km^2. A 6 % probability is obtained for a 10^4 km^2 reference area. The probability is maximum in July and August with respectively 36 % and 14 % for the study area and the reference area. Most of the time during those active periods, the number of storms, their fractional coverage and their total water mass remain limited. The probability that one of this characteristics exceeds a certain level is higher for the year 2002 and the period 2008-2011 than for the period 2003-2007. This effect is more pronounced for severe events especially for the storm mass. It might be related to variations in general circulation patterns which are influenced by oceanic forcing such as the North Atlantic oscillation. During the year, high number of storms and large storm coverage are found preferably in June when surface heating is maximum. Events with very large storm coverage and with large total water mass are found mainly in July when most MCS's have been recorded. The probability to observe a high number of storms at the same time is highest in the early afternoon around 1300 UTC. The probability that storms cover large areas and have a huge mass of water is higher in the late afternoon and also in the evening. Due to the persistence of MCS's, the most severe situations in terms of total area and water mass can occur at any time of the day.

The occurrence of the activity in the study area is highly intermittent and its autocorrelation decreases quickly from 1 to 6 hours. There is a slightly higher probability of convective storm activity on a given day when the day before was active. The frequency analysis of the time series reveals a scaling behavior with two distinct regimes which can be related to the seasonal and synoptic variability.

No important variations in the storm characteristics have been found across the study area. Most of the identified convective storms have a relatively small volume, with a limited echo-top and generate a small amount of water. On average storms tend to be bigger, deeper and more intense in June and July. The diurnal variation increases when the echo-top increases while it is shifted toward the evening for increasing volume and water mass. The averaged number of severe storms does not vary substantially from May to August and along the day.

Storms tend to be short-lived with a mean duration of 25 min for simple tracks and 70 min for complex tracks. Individual tracks that are part of complex tracks follow the same distribution as simple tracks. Convective storms move preferably toward a North-East direction with a median speed of $30\,\mathrm{km\,h^{-1}}$ and tend to be slower in summer and in the afternoon. Regions with slightly more or slightly less storm initiations have been found and are related to orographic variations.

In spite of the limitations inherent to radar observations, this analysis gives an unprecedentedly view of the convective storm characteristics in the region covered by the radar. These characteristics are probably representative of a larger region including the North of France and Germany where the same methodology could be applied. This study, which was mainly observational, offers several perspectives for better understanding of the convective storm activity. First, additional observations from neighboring radars should be included in the analysis. In overlapping areas, the quality of the observations will be improved. Furthermore this will allow the discrimination between radar artifacts and true meteorological effects. It would be interesting to analyze the results obtained using other tracking methods (e.g. SCIT). The Lagrangian approach can be extended by studying the evolution of storm characteristics and their correlation. Additional storm properties could be analyzed by including other observations like lightning activity, cloud characteristics derived from satellite observations and water vapor fields derived from GPS. Finally, the relation between convective storm activity and weather regimes could be investigated.

Acknowledgment

The authors would like to thank the reviewers for their very constructive comments and suggestions which allowed a substantial improvement of the text. We would like to thank also Mike Dixon (UCAR, U.S.A.) for his support concerning the use of TITAN. The comments of Maryna Lukach, Dieter Poelman and Maarten Reyniers were highly appreciated. This research has been supported by the Belgian Federal Science Policy (Research project ACTION 1 MO/34/018).

Chapter 4

Generation and verification of rainfall estimates from 10-year volumetric weather radar measurements[1]

Abstract

Volumetric measurements from a C-Band weather radar in Belgium are reprocessed over the years 2005-2014 to improve the quantitative precipitation estimation (QPE). The data quality is controlled using static clutter and beam blockage maps and clutter identification based on vertical gradients, horizontal texture and satellite observations. A new QPE is obtained using stratiform-convective classification, a 40-min averaged vertical profile of reflectivity (VPR), a bright band (BB) identification and a specific transformation to rain rates for each precipitation regime. The rain rates are interpolated on a 500 m Cartesian grid, linearly accumulated and combined with hourly rain gauge measurements using mean field bias (MFB) or kriging with external drift (KED). The algorithms have been fine-tuned on 13 cases with various meteorological situations. A detailed validation against independent daily rain

[1]based on E. Goudenhoofdt and L. Delobbe (2016). "Generation and Verification of Rainfall Estimates from 10-Yr Volumetric Weather Radar Measurements". In: *Journal of Hydrometeorology* 17, p. 1223. DOI: 10.1175/JHM-D-15-0166.1

gauge measurements reveals the importance of the VPR correction. A 10-year verification shows a significant improvement of the new QPE, especially at short and long range, with roughly 50 % increase in coverage. Adding the KED allows averaged improvements of 38 %, 35 % and 80 % for the mean absolute difference, the multiplicative error spread and the fraction of good estimates, respectively. The benefit is higher in widespread situations and increases when considering higher rainfall amounts. The mitigation of radar artefacts is clearly visible on 10-year statistics including mean annual totals, probabilities to exceed 10 mm and maxima for hourly and daily accumulations. The correlation of mean totals with rain gauges increases from 0.54 to 0.66 with the new QPE and to 0.8 adding KED.

4.1 Introduction

Surface precipitation impacts human activities at a wide range of space and time scales. Therefore a detailed knowledge of its characteristics is needed for various applications. Predicting surface precipitation is one of the biggest challenge for numerical weather models and therefore the verification of forecast accuracy for this variable is important. Precipitation is also the main driving force in agriculture and hydrology. The interest of precipitation observations at high spatial and temporal resolution is particularly high in urban hydrology. For many applications, long time series of precipitation are needed. In hydrology, the estimation of areal rainfall extreme statistics is required for risk assessment. It is also useful for the verification of regional climate models. In a changing climate the evolution of the precipitation characteristics must be carefully monitored.

Various efforts to construct reference precipitation datasets have been reported in the literature. The most simple approach is the collection of gauge measurements which are interpolated on a gridded dataset. In Europe the reference 50-year daily dataset E-OBS (Haylock et al., 2008) is used in many studies. The main weakness remains the low spatial representativity of rain gauges which can miss small convective cells. Model reanalyses offer estimations over the globe but are prone to large bias (Leeuw et al., 2014). Their ever increasing resolutions are still not able to resolve convection properly. Satellite-based precipitation estimation is available at the global scale from infrared imagers or passive microwave radiometers but their resolution and accuracy are still limited (Tang et al., 2014). More reliable estimation is available from space-borne precipitation radar but only in the tropics (Yang and Nesbitt, 2014).

The potential of single-polarization ground-based weather radar to provide a reference precipitation dataset at very high temporal and spatial resolution with

good accuracy is large. Dual-polarization technology offers a greater potential but long time series are not available yet. Using merged radar-gauge products, Overeem et al. (2009b) derived annual maximum rainfall depths for durations of 15 min to 24 h and area sizes of 6 to 1.7×10^3 km^2 for the Netherlands. A reanalysis based on the French radar network demonstrated good results for streamflow simulation in some situations (Lobligeois et al., 2014). However, rainfall estimation from weather radar suffers from many sources of error and uncertainties which have been extensively discussed in the literature. The reader is referred to e.g., Uijlenhoet and Berne (2008) and Villarini and Krajewski (2010), for a detailed review. This has prevented the wide usage of radar observations in operational applications (e.g., hydrology). Recently the most important issues have been tackled for operational quantitative precipitation estimation (QPE) algorithms (e.g., Tabary, 2007; Germann et al., 2006). Since most weather services only archive 2D operational radar products (e.g., Nelson et al., 2010; Fairman et al., 2015), the quality of their dataset depends on the operational algorithm which was used to derive 2D product from the polar scans. Due to inherent updates of QPE algorithms, time periods with consistent data are limited. Improving the 2D radar product quality without 3D information is a difficult task (Wagner et al., 2012; Tabary, 2007). For example, it is not straightforward to correct for overestimation due to the melting layer in an interpolated 2D product. Archiving of volume radar data was not common a decade ago due to telecommunication and storage costs and the lack of interest in precipitation reanalysis. Therefore the number of long-term precipitation datasets making use of the full volumetric radar information is limited. Thorndahl et al. (2014) made a reanalysis of a relatively complete set of 10-year volume data in Denmark. It has been produced using a careful processing but without a correction for the vertical profile of reflectivity (VPR). Krajewski et al. (2011) developed a flexible framework for surface rainfall dataset generation from NEXRAD Level2 (volumetric) measurements which are available since 2002. The produced datasets have been used in several hydrological studies Smith et al. (2012).

At the Royal Meteorological Institute of Belgium (RMIB) the volumetric data from a single-pol C-Band Doppler radar are archived since 2002. Those data have already been used to derive convective storm track statistics in chapter 3. The operational QPE algorithm used since 2004 is an interpolation of reflectivity data from different elevation angles at a given height combined with a Marshall-Palmer relationship. This algorithm, which has been applied on the archived volume data using a height of 800 m above the radar level, is defined as QPE1. In this study a careful processing (defined as QPE2) of the volumetric data is made including beam blockage correction, application of a static clutter map, dynamical clutter identification, correction for the height of the measurement (i.e. VPR correction) and specific Z-R relationships. A

Figure 4.1: Flow chart of the new quantitative precipitation estimation (QPE2) : ellipses represent data and rectangles represent processing steps.

flowchart summarizing the processing steps and data flow of QPE2 is presented in Figure 4.1. The algorithms have been developed based on a literature review and with simplicity and robustness in mind for future operational use in realtime. A dense hourly rain gauge network with quality control available since 2005 is used in combination with the radar-based QPE using two methods. The new QPE algorithms are compared to QPE1 in order to evaluate the improvements. It is first validated on a selection of cases and then on the period 2005-2014 using an independent rain gauge network. To the author's knowledge, such long-term verification of radar-based precipitation estimates has not been done

yet. Several interesting statistics are derived from the 10-year dataset and compared to rain gauge statistics.

4.2 Weather Radar measurements

4.2.1 Radar reflectivity measurement

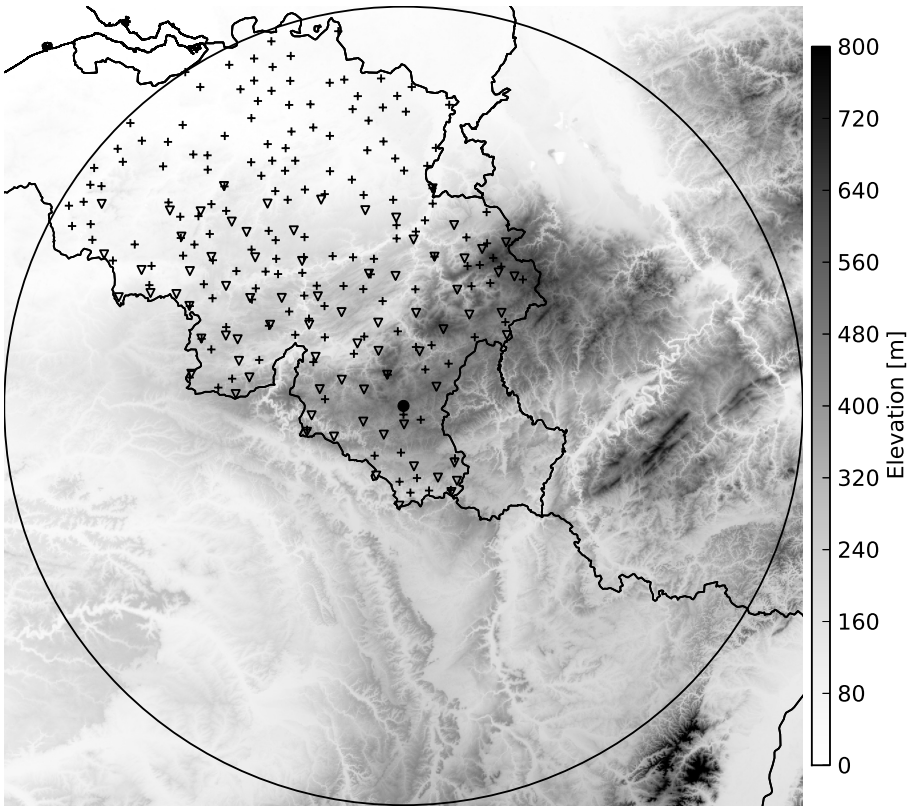

Figure 4.2: Elevation map centred at the Wideumont radar (black dot) up to 180 km range (circle) with SPW (triangle) and RMIB (cross) rain gauge networks (gauges removed due to clustering are not shown). Country borders with France, Luxembourg, Germany and the Netherlands are also displayed.

Since 2001, RMIB has been operating a C-Band (5.62 GHz) Doppler radar located in Wideumont (49.9°N, 5.5°E), South-East of Belgium at 592 m above

sea level (Fig. 4.2). With measurements up to 240 km, the radar covers Belgium, Luxembourg and also parts of France, The Netherlands and Germany. It is a single polarization radar with Doppler capability used to filter ground echoes. During the study period, the radar performed a dedicated reflectivity scan at 5 elevations (0.3°, 0.6°, 1.8°, 3.3°, 6.0°) every 5 minutes with a pulse repetition frequency of 600 Hz and pulse duration of 0.836 μs. The radar volume data have a resolution of 1° in azimuth (an average of 33 pulses) and 250 m in range (an average of 2 successive range bins). Thanks to the height of the radar tower and its position near the top of the Ardennes ridge, beam blockage effects are relatively limited. More information regarding the radar characteristics and scanning strategy can be found in Delobbe and Holleman (2006). The volumetric data of the Wideumont radar have been archived at RMIB since 2002. No significant changes in the radar calibration have been encountered except in April 2013 when a software and hardware updates occurred. During the update the radar constants have been reset to default resulting in a decrease of 1.3 dB. The Doppler filtering is active since April 2004 and is combined with a clutter to signal ratio (CSR) of 10 dB. The CSR has been reset to the default value of 15 dB during the 2013 update resulting in less values set to zero. No further post processing corrections have been performed on the volumetric data. The radar data availability is about 96 % for the 2005-2015 period. Since the data is coded with a resolution of 0.5 dBZ, a random uniform field (-0.25 dBZ, +0.25 dBZ) is added to simulate actual reflectivity values. This allows generating a smooth averaged empirical profile of reflectivity when the median is used as the averaging statistic.

4.2.2 Beam blockage correction

To compute beam blockage, we consider the trajectory of the beam in normal propagation conditions (i.e. using a 4/3 factor for the earth radius). The Shuttle Radar Topography Mission (SRTM) data (Farr et al., 2007) are used as digital elevation model (DEM) and have a resolution of 3 arcsecond (90 m). The beam blockage has been estimated using a formula proposed by Bech et al. (2007) which assumes a constant ground elevation across the beam. To simplify the computation the DEM is interpolated on a 300 meter grid, which is the resolution of the beam width at 10 km from the radar, where the first blockage occurs. If the blockage occurs close to the radar, a high accuracy of the height of the radar is required. It was found that using the Belgian reference for the radar height (592 m) results in a significant underestimation of the closest blockage. A correction of about 15 m was applied to this height to match the WGS84 system used by SRTM. Due to the relatively low elevation angle (0.3°) blockages up to 18 % were found for several narrow sectors (Fig. 4.3).

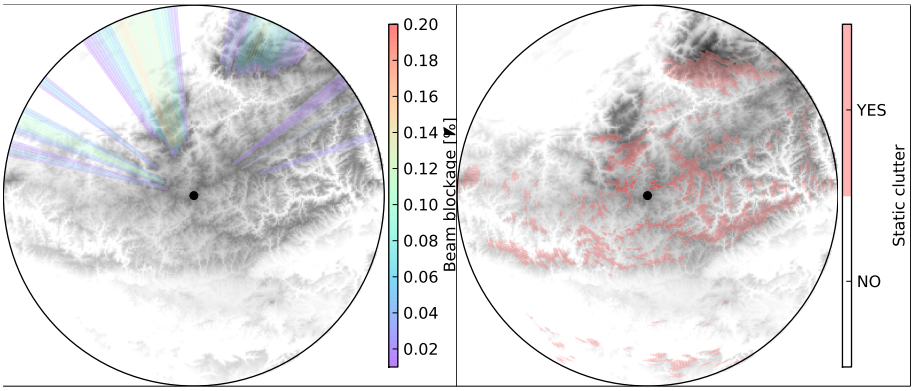

Figure 4.3: Static quality information for the lowest elevation (0.3°) scan up to 50 km : (left) beam blockage (right) clutter.

Uncertainties in elevation angles, beam propagation, DEM measurements and blockage computation method can lead to underestimation or overestimation of the actual beam blockage. The data are corrected for beam blockage using a 1-way correction. A smoothing of 1 degree is performed to take into account sample averaging in azimuth.

4.2.3 Clutter identification

Weather radar measurements can be contaminated by clutter (i.e. non-meteorological signals). In the atmosphere airplanes, birds and insects are a dynamical source of clutter. Nevertheless, the main source of clutter comes from the ground which is hit by the side lobes of the beam (or even its main lobe). Ground clutter occurs mainly at elevated places (e.g., hills) surrounding the radar. During abnormal propagation (AP) conditions, the lowest part of the beam can bend progressively towards the ground and clutter can be found at any distance from the radar. The identification and mitigation of clutter remains a challenging problem in radar meteorology because it can be difficult to distinguish from precipitation. Conventional radars use Doppler filtering to remove near-zero velocity pulse echoes. A statistical filter can also be used based on pulse to pulse fluctuations. However, those filters are not perfect and too aggressive settings can partly eliminate precipitation. Since pulse data are usually not sent to the data center, post processing of the radar moments (based on several pulses) is usually performed for remaining clutter. A summary of clutter mitigation techniques can be found in Hubbert et al. (2009), who

recommend the fuzzy logic approach for its simplicity and practicality. This technique uses a combination of features and probability functions to make a clutter identification decision. For example, Berenguer et al. (2006) combine 3 statistics from 3D data : shallow vertical extent, high spatial variability, and low radial velocities. In this study we combine satellite cloud-free echoes, strong vertical gradient and high spatial variability in a deterministic fashion. This corresponds to step probability functions in the fuzzy logic framework with a probability of one associated to clutter. Eventually a measurement is considered as clutter if at least one feature is equal to one.

Permanent clutter

Radar measurements are contaminated by static ground clutter even after Doppler filtering. Topographic features such as hills are permanent while others (e.g., trees, towers, building) might evolve in time due to human activities. Static clutter can be identified using detection probability maps over a given period. In an operational context this map should be updated regularly (i.e. each month) to take into account new sources of static clutter (e.g., wind farms). The bins whose measurements exceed 7 dBZ more than 50 % of the time are identified as static clutter. The threshold is chosen to match the threshold used for "no precipitation" in subsequent algorithms. This probability threshold is chosen to be significantly higher than the expected monthly maximum rainfall occurrence in Belgium. To compute this map, using unfiltered data is simple and robust. Using filtered (e.g., Doppler) data is more difficult but allows keeping meteorological information for the slightly contaminated bins. For the Wideumont radar no choice was possible since only filtered data have been archived. More problematic is the fact that bins exceeding a defined Clutter to Signal Ratio (CSR) have been set to "undetected" without flag and are therefore wrongly interpreted as zeros. To solve this problem radar data without CSR thresholding have been generated during one day without rain in 2013 and used to compute the static clutter map (Fig 4.3). In the lowest elevation, about 10 % of static clutter is found in the range 0-70 km. The static clutter map is applied before using the dynamical algorithms to improve their performance.

Satellite-based identification

Since 2005 a cloud type classification (Derrien and Le Gléau, 2005) with a resolution of 5 km is available each 15 min from SAFNWC (Satellite Application Facility for nowcasting) products based on MSG (Meteosat Second Generation) satellite measurements. Radar echoes in areas classified as "sea" or "ground" by the satellite are identified as clutter. Areas classified as snow or non-precipitating

clouds could also be identified as clutter. Since areas with actual rain can be misclassified in these classes, they are not used here. It is interesting to note that a parallax correction would have been required for non-precipitating cloud areas. The time lag between radar and satellite observations (up to 8 minutes) is taken into account. An upper bound on the steering wind, estimated from the ground wind, is used to reduce the potential cloud-free areas. The clutter identification based on satellite is very robust but limited to well defined cloud-free areas. It is particularly useful when clutter is difficult to distinguish from rainfall (e.g., in strong anomalous propagation conditions or at very large distance from the radar). Unfortunately the availability of derived satellite products at RMIB was limited to 90 % during the study period. Using a more complete dataset could help to remove even more clutter.

Vertical gradient

Algorithms based on the VPR have been proposed in several papers (Steiner and Smith, 2002; Berenguer et al., 2006). In case of precipitation, clutter can be identified by unrealistic vertical reflectivity gradients between two measurements at different elevations. A measurement at a given elevation is considered as clutter if the gradient between its value and the corresponding (horizontally) interpolated value on a higher (lower) elevation exceeds in magnitude $-20\,\mathrm{dBZ\,km^{-1}}$ ($+10\,\mathrm{dBZ\,km^{-1}}$). Due to variations from signal fluctuations a minimum absolute difference of 5 dBZ between two corresponding values at different elevations is required for clutter identification. For this particular algorithm, all measurements below 10 dBZ are set to 10 dBZ since gradients are not meaningful for low reflectivity values. Wrong clutter identification may occur in the bright band (BB) where high vertical gradient can be found. Therefore the BB is identified using the radar data or constructed from the estimated freezing level. The freezing level is estimated based on the extrapolation (1°C per 150 m) of the mean surface temperature measured by nearby automatic weather stations. Extra (e.g., model) information on the freezing level is not used due to technical limitations. In the BB, a safety margin is applied with higher thresholds ($-60\,\mathrm{dBZ\,km^{-1}}$ and $40\,\mathrm{dBZ\,km^{-1}}$ respectively) for clutter identification. Since measurements from different elevations are not simultaneous (there is a lag of 30 seconds between successive elevations), a smoothing distance is computed based on the estimated steering wind and applied to the data. An upper bound for the steering wind is computed as three times the wind measurements at 10 m averaged over 10 stations. This algorithm is useful for clutter inside precipitation regions which can not be easily identified by looking at the reflectivity texture.

Texture

We use a simple and fast texture-based technique originally developed by Gabella and Notarpietro (2002) for Cartesian data. It consists of a two-part identification algorithm using (1) echo continuity and (2) minimum echo area. The algorithm has been improved and made applicable to polar data. For the first part, each bin is compared with a neighbourhood which is selected based on a maximum distance. Since finding a circular neighbourhood is computationally intensive, it is approximated by a square window. If the proportion of neighbours with similar values is too small, the bin is considered as clutter. In this study, two bins are similar if their difference is less than 7 dBZ. The proportion of similar bins in the pre-defined neighborhood has to exceed 30 % for the bin to be identified as non-clutter. The maximum distance defining the square window is the most important parameter of the algorithm. It should be chosen close to the smallest precipitation scale. The default value of 1 km used in this study should be interpreted as a lower bound for convective storm size. This corresponds to a window of 27 bins for a range of 100 km and 9 bins for a range of 200 km, where only the radial information is used. Using the proportion of similar values instead of counting their total number allows dealing with bins which have no values (e.g, after the application of the static clutter map). For the second part (echo area), too thin contiguous echo areas (with values above 0 dBZ) are considered as clutter. An echo area is too thin if more than 90 % of its bins belong to its border. This second part is not applied when the bin azimuthal resolution is larger than the precipitation scale (within the range of 70 km). This texture-based technique can identify many different kinds of clutter. It is particularly useful for AP clutter in the lowest elevation and at distances where vertical information is limited.

4.3 Surface rainfall estimation

4.3.1 Radar-based estimation

The estimation of rainfall rate at the ground can be derived from radar reflectivity measurements. Due to the earth curvature and the positive elevation angles these measurements are obtained at heights increasing with range. It is well known that the VPR depends on the variations of hydrometeors phase and size distribution. The most striking effect is the BB which is an increase of reflectivity caused by melting snow in a layer under the freezing level. Another important effect is the increasing underestimation with range due to the lower reflectivity of snow and partial overshooting. Correction for the VPR has been

an active topic in radar meteorology for decades. Parameterized models can be fitted to observations using inverse methods (Vignal et al., 2003) but the most straightforward approach is to derive averaged empirical profiles. The profile is best estimated using data at close range of the radar to limit beam broadening effect. Germann and Joss (2002) compute the unconditional mean rainrate up to 70 km while Bellon et al. (2007) compute a reflectivity average over 20 km range intervals. Some authors stress the importance of distinguishing different type of precipitation (Kirstetter et al., 2010). For some cases a local VPR correction should be preferred (Kirstetter et al., 2010; Zhang and Qi, 2010; Hazenberg et al., 2013) but this has a computational cost. A hybrid approach combining empirical and modeled profiles has been recently proposed by Koistinen and Pohjola (2014). At the RMIB, a VPR correction has been proposed (Goudenhoofdt and Delobbe, 2012) based on a global average of normalized local profiles from data in the 0-70 km range. This study presents a new version of the algorithm with a focus on robustness.

Convective rainfall identification

For convective precipitation a uniform VPR is assumed and no correction is applied. Since their VPR are different, we first distinguish between stratiform and convective precipitation. Following the Steiner algorithm discussed in Vignal et al. (2003), a reflectivity value is considered as convective if it exceeds 40 dBZ or if it is significantly higher than its local background (defined by a search radius of 11 km). In a last step, convective areas are expanded by range-dependent smoothing. Values below 10 dBZ are set to 10 dBZ for proper background computation (only for this specific task). The original algorithm has been adapted to be applied on polar data with possible missing data. Another limitation was the false detection of the BB as convective precipitation. To consider a point as convective we require that the value from the lowest elevation angle and the corresponding interpolated value at 3000 m above the radar level are both identified as convective. No convective identification is made before the highest elevation angle reaches 1500 m, which corresponds to a range of 15 km.

Average profile estimation

Assuming that the VPR does not vary in space, the mean apparent vertical profile of reflectivity (MAVPR) is computed for each height interval as the median of reflectivity values considered as stratiform (i.e. not convective and exceeding 10 dBZ). Only data at close range are used to limit the beam broadening effect. A maximum distance of 45 km, which corresponds already to

a 800 m beam width, seems reasonable. A minimum distance of 5 km is chosen to avoid computing the lowest part of the VPR on a limited area. A minimum vertical resolution of 50 m is chosen to match the vertical resolution of the beam at 5 km from the radar. Even if the probability of residual ground clutter is low, we prefer not to use the lowest elevation in the computation of the MAVPR to make our reanalysis robust. To support this choice one notes that the vertical coverage of the lowest elevation is limited and that more useful data can be obtained from higher elevations. Using an unconditional average of reflectivity can be problematic in case of localised precipitation areas. The robustness of the profile depends on the amount of available measurements. As in Bellon et al. (2007), we impose a minimal number (i.e. 10000) of measurements for each vertical intervals. This is unfortunately not enough since it does not take into account the increasing sampling area per bin with range. Therefore we use an additional criterion based on the total sampled area (which is set to 1000 km^2) for each vertical interval. To be representative, the MAVPR should also cover a sufficient vertical extent. The MAVPR is considered as valid if it is available between 500 m and 2 km above the radar. If the mean 7 dBZ echotop in the selected area is lower than 2 km, it is taken as the upper limit required for a valid VPR. To increase the availability of a valid MAVPR, we use successive radar scans as in Hazenberg et al. (2013). The underlying assumption of VPR stationarity seems reasonable for an interval of 20 min. This corresponds to 9 radar volumes using both previous and next data. One notes that in realtime conditions, data from the future are not available and then only 5 radar volumes can be used. The MAVPR (noted $\mathbf{z_m}$) is checked for abnormal curvature by computing the 2nd order discrete difference $\mathrm{dd2}_i$ for each vertical interval i :

$$\mathbf{dd}(i) = \mathbf{z_m}(i+1) - \mathbf{z_m}(i) \tag{4.1}$$

$$\mathbf{dd2}(i) = \mathbf{dd}(i+1) - \mathbf{dd}(i) \tag{4.2}$$

The MAVPR is not valid if the maximum $\mathrm{dd2}_i$ (expected at the BB peak) exceeds 10 dBZ or if the number of $\mathrm{dd2}_i$ higher than 1 dBZ exceeds 5. If the MAVPR is not valid, the vertical resolution is increased by 50 m and the thresholds for $\mathrm{dd2}_i$ adapted. This procedure is applied to a resolution not higher than 200 m to ensure that the BB is properly resolved. If no valid MAVPR can be obtained, the closest one (up to 20 min) is used. In the worst case, a climatological profile with a constant slope ($-2\,\mathrm{dBZ\,km}^{-1}$) above the freezing level is used. The climatological profile is uniform below the freezing level.

An example of profile estimation is depicted in Fig. 4.4. The MAVPR obtained using a 50 m step is not valid because less than 10000 values have been used for some steps between 400 m and 2 km. This is solved by using a 100 m step since only the part above 2700 km is not valid. The valid part of the MAVPR has no abnormal curvature and is therefore selected for further processing.

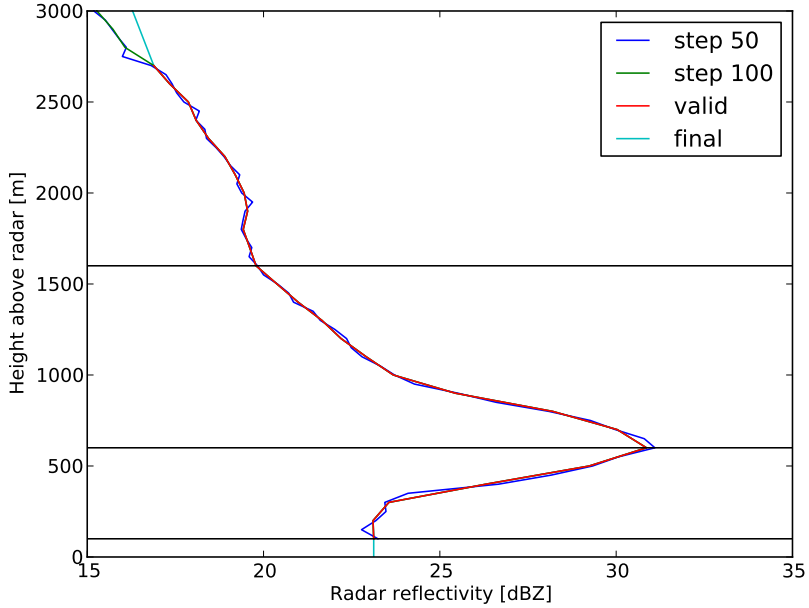

Figure 4.4: Estimation and extrapolation of the MAVPR : empirical profiles with a vertical step of 50 m and 100 m, the valid part of the latter and the final extrapolated profile. The identified bright band top, peak and bottom are represented by vertical lines.

Bright band identification

The identification of the BB is important for the extrapolation of the MAVPR. Due to beam broadening with increasing range, the BB depth increases and the BB peak decreases. The peak of the BB is identified by the maximum of the MAVPR. It is checked that the peak is not a spike, that a strong gradient exists below, a very strong negative gradient exists above and that the peak value is 3 dBZ larger than the values at + and - 500 m (at least one value is needed). Starting from the peak, the bottom of the BB is identified by the first gradient lower than $3\,\mathrm{dBZ\,km^{-1}}$ and at least 300 m below. Similarly, the top of the BB is identified by the first gradient exceeding $-5\,\mathrm{dBZ\,km^{-1}}$ and at least 300 m above. If no lower or upper bound for the BB can be found (i.e. when no profile value is available), the MAVPR is extrapolated linearly to - and + 500 m by -5 and -8 dBZ, respectively. If no BB can be identified, the freezing level is estimated as in the clutter identification. If the top of the MAVPR is above the freezing level, its value is extrapolated aloft using a constant gradient of

$-2\,\mathrm{dBZ\,km^{-1}}$. The MAVPR is finally extrapolated (uniformly) to the ground using the value at the lowest height.

An example of BB identification is depicted in Fig. 4.4. The maximum of the MAVPR at 600 m is clearly identified as the peak of the BB. The bottom and top of the BB are identified from the peak when both ends reach the vertical at 100 m and 1600 m, respectively. Since it is above the freezing level, the MAVPR is extrapolated aloft with a slightly decreasing slope. The lowest part of the MAVPR is then extrapolated to the ground.

MAVPR application

The ratio between the median profile $Z_m(h)$ and the apparent profile at a given range $Z_a(r,h)$ is applied to the measured equivalent reflectivity factor $Z_e(h)$ to obtain the surface reflectivity $Z_e(h=0)$:

$$Z_e(h=0) = Z_e(h)\frac{Z_m(h=0)}{Z_a(r,h)} \tag{4.3}$$

$$z = 10\log_{10}(Z) \tag{4.4}$$

$$z_e(h=0) = z_e(h) + z_m(h=0) - z_a(r,h) \tag{4.5}$$

where h is the height above the radar and r is the distance to the radar. The quantities Z_e, Z_m and Z_a are in the unit of $\mathrm{mm^6\,m^{-3}}$ and the corresponding z_e, z_m and z_a are expressed on a decibel scale with unit in dBZ. The quantity $z_m(h)$ is estimated at any height from the discrete profile $\mathbf{z_m}(i)$ (MAVPR) using linear interpolation (decibel scale). The quantity $Z_a(r,h)$ is obtained by the convolution of the median profile $Z_m(h)$ with the two-way normalised power-gain of the beam at distance r. Since $Z_m(h)$ is based on data at a given range interval the convolution is started in the middle of this interval. A more accurate but costly computation of the convolution Kirstetter et al. (2010) is not expected to significantly improve the results. According to Joss and Lee (1995), the correction factor should be limited to avoid instability. Therefore after a sensitivity test a maximum correction factor of 10 dBZ has been chosen. The height of the radar is taken as the ground reference for the extrapolation of the VPR. The case when the radar is in the BB is problematic since finding a good ZR relationship for melting snow can be complicated. We solve this problem by using a theoretical VPR profile in order to obtain a reflectivity value corresponding to rain. In practice we use the extrapolation procedure described above to find the corresponding value at the artificial lower limit of the BB. The estimation of reflectivity at the ground reference is applied for each elevation. Using a weighted (e.g, based on distance) average of several elevations

to mitigate residual errors and reflectivity measurement uncertainty is common. However, we think that after quality control the estimation from the lowest elevation is much better than from higher elevation. Therefore estimation from higher elevations are only used to fill gaps caused by the clutter removal. For this purpose, the data from higher elevations are bi-linearly interpolated in range to match the lowest elevation. Remaining gaps (i.e. when no precipitation information is found in the higher elevation) in the grid are interpolated using a nearest neighbour technique up to a 2 km maximum distance.

ZR relationship

The Marshall-Palmer relationship ($Z = 200R^{1.6}$) has been used operationally since the beginning of the radar measurements. For the reanalysis a more refined relationship from the RADOLAN product Wagner et al. (2012) of the German weather service has been considered :

$$Z = 200\,R^{1.6} \qquad if \quad dBZ \leq 44 \tag{4.6}$$

$$Z = 77\,R^{1.9} \qquad if \quad dBZ > 44 \tag{4.7}$$

For high reflectivity, the rainrate obtained with the latter is a bit lower. To deal with hail, a maximum reflectivity of 55 dBZ is used, which corresponds to $88\,\mathrm{mm\,h^{-1}}$. To avoid remaining artefacts (e.g., insects), reflectivity values below 7 dBZ (i.e. $0.1\,\mathrm{mm\,h^{-1}}$) are considered as no precipitation.

4.3.2 Radar-gauge merging

In a final stage, radar estimates can be combined with rain gauge measurements. A large variety of radar-gauge merging methods have been tested in chapter 2 at the daily scale. The results showed that a simple mean field bias (MFB) reduces the mean absolute error significantly and that a kriging with external drift (KED) performs best. Co-Kriging Krajewski (1987) is an attractive alternative method but its computational cost is too high to be considered in this study. Sideris et al. (2013) proposed to add temporal information to KED via co-Kriging. Due to the added complexity, this method is also not used here. The benefit of using hourly over daily adjustment has been showed by Thorndahl et al. (2014) and Berndt et al. (2014). In this chapter both MFB and KED methods are used on hourly Cartesian data. For a given gauge, the corresponding radar-based estimate is the one of the pixel where the gauge is located. Averaging over several pixels does not improve the correlation in most cases.

Rain gauge measurements

SPW operates a dense (1 gauge per 135 km^2) and integrated network of 90 telemetric rain gauges (Fig. 4.2). Most of them are tipping bucket systems providing hourly rainfall accumulations. The collected data are used for hydrological modelling and directly sent to RMIB. The rain gauges are controlled on site every three months and in a specialised workshop every year. Every day, a quality control of the data is performed by RMIB using a comparison with neighbouring stations. Radar data are also used in this quality control for the elimination of outliers. The classification of gauge data for the period 2005-2015 are 94.5% validated, 2.7% corrected, 2.3% classified as dry snow and 0.5% unclassified. Only validated data are used for combination with radar data. However the quality control is not perfect since errors in classification have been found in dry snow and convective situations by comparison with the climatological network. To make the merging methods more robust, the clustering of the rain gauge network is reduced by removing a few gauges.

Radar rainfall rate accumulation

Before accumulation, rainfall rate values from the polar grid are interpolated on a Cartesian grid of 500 m resolution. The interpolation is done using a uniform 500 m square window filter on the polar data followed by a nearest neighbour interpolation. This method is more accurate than an interpolation of points since it takes into account the actual areas of the polar bins and the Cartesian pixels. Rainfall accumulation over a given period is obtained by linear interpolation of the radar rainrates. No correction of temporal sampling errors (e.g., using optical flow) is performed since their occurrence is relatively low with a time step of 5 minutes. Indeed, small convective storms moving at a high speed are relatively rare (see chapter 3). Using Cartesian instead of polar data allows a better correlation between gauge and radar estimation by reducing time and space sampling differences, especially at close range.

Mean field bias correction

The assumption here is that the radar estimates are affected by a uniform multiplicative error. This error can be due to a bad electronic calibration or an erroneous coefficient a in $Z = aR^b$ relationship. For each time interval, the adjustment factor is computed as the median of the ratios of gauge and radar values. The adjustment is valid if there are at least 11 pairs with both values exceeding 0.2 mm. Due to a potential decrease (at least for QPE1) of radar

rainfall estimates caused by partial overshooting further than a certain distance, only gauges up to 100 km are used.

Kriging with external drift

This is a geostatistical method which combines the rain gauge values linearly and uses the radar as auxiliary information. It follows the same scheme as the ordinary Kriging except that the expected value of the estimated precipitation field is now considered as a linear function of the radar field (the drift). The weights are obtained by minimizing the estimation error which depends on the spatial correlation between radar and gauge values and their residuals. As proposed by Erdin et al. (2012), a square-root transformation is applied to precipitation values to approach gaussianity which is an underlying assumption in Kriging. Determining a suitable variogram for the residuals between the estimated value and the drift is challenging. The underlying assumption is that the residuals are correlated in space. A robust method is proposed by Schiemann et al. (2011) while Delrieu et al. (2014) suggest to derive event-based variograms. For the sake of simplicity, we use an exponential climatological variogram with a nugget of 0.1 and a range of 10 km. It is not easy to determine the decorrelation distance of the residuals. We prefer not to make assumptions on the correlation between the residuals beyond 10 km, since QPE2 might have removed the large scale errors. The stability of the method depends on the validity of rain gauge measurements and also the collocated radar estimates. Therefore no gauge location are used beyond 160 km due to potentially severe underestimation by the radar. Additionally a minimum correlation (Pearson coefficient) of 0.5 is required between the two estimates. The performance of this method decreases significantly with the distance to the raingauge network.

4.4 Evaluation

4.4.1 Rain gauge measurements

RMIB maintains a climatological network including 270 stations with daily measurements of precipitation accumulation between 8 and 8 local time (LT). From Fig.4.2 one notes that the coverage of the RMIB network is larger than the SPW network and that only a few locations belong to both networks. Most of these stations are manual and the data are generally available with some delay. The data are manually inspected on a monthly basis by well-trained operators. By arraying geographically in time sequence observers records, pattern analysis

performed by the trained staff allows revealing inconsistencies or anomalies. It will be used here to evaluate and compare the performance of the QPE methods. As for the merging network, a declustering is applied to reduce the influence of areas with high rain gauges density on the results. The hourly accumulations obtained by the merging methods are summed to match the 24 h accumulation of the RMIB network.

4.4.2 Examples

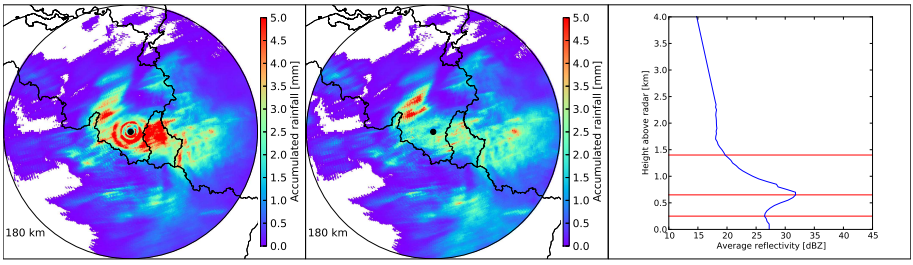

Figure 4.5: Stratiform case of 12 April 2013 : hourly accumulation from 0000 UTC to 0100 UTC based on QPE1 (left) or QPE2 (center); median averaged VPR based on 9 polar volumes (right), the BB peak and limits are identified by lines.

In Fig. 4.5, a typical winter case with stratiform precipitation is shown. A BB appears in the MAVPR between 600 m and 1600 m. If we compare QPE2 (new) with QPE1, we see that the rings due to the BB have been significantly reduced. The underestimation at long range is also reduced.

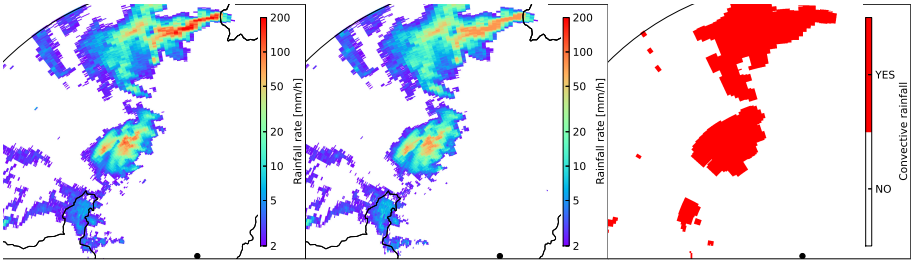

Figure 4.6: Convective case of 19 June 2013 : rainfall rate estimation at 1905 UTC for QPE1 (left) and QPE2 (center) and corresponding identified convective area (right).

Table 4.1: Probability of Detection (POD), False Alarm Ratio (FAR) and Critical Success Index (CSI) for hourly accumulations exceeding 0.1 mm against the SPW network. The scores are computed for all hours of the cases and then averaged.

	POD	FAR	CSI
QPE1	0.601	0.550	0.322
QPE2	0.632	0.512	0.363

In summer (Fig. 4.6), the distinction between convective and stratiform precipitation plays an important role. Indeed for the identified convective precipitation on each volume, no profile correction is performed. Furthermore, due to the limited area covered by stratiform precipitation, a climatological profile is used. There is a slight effect of decreasing the rainfall rate by using a specific Z-R relationship for convective precipitation in QPE2. But the main effect in this case is a significant decrease of the rainfall rates with QPE2 due to the maximum (hail) threshold (55 dBZ).

4.4.3 Case validation

In the first semester of 2013, 13 days with different rainfall situations have been chosen and sorted by chronological order. Stratiform precipitation (cases 1,4,6,9,10), a mix of rain and snow precipitation (cases 2,3,5,7 and 8), and convective precipitation (cases 11, 12 and 13) were observed. The various algorithms of QPE2 (and especially the VPR correction) have been fine-tuned on those cases. A categorical verification (Wilks, 1995) that hourly values exceed 0.1 mm against the SPW network is reported in Table 4.1. The scores are averaged over the 13 cases plus a few cases with little or no rain. It shows a decrease of the False Alarm Ratio (FAR) and an increase of the Probability of Detection (POD) with QPE2. This highlights the effect of the mitigation of clutter and correction of underestimation at long range, respectively. The high values of FAR are due to some cases with gauges covered by dry snow but not flagged by the quality control. A lower FAR and higher POD both increase the Critical Success Index (CSI), which measures the global performance. The quantitative performance of the algorithms are analysed using three different scores. The mean absolute difference measures the average additive error between the radar estimate R and the gauge measurement G :

$$\mathrm{MAD} = \mathrm{mean}|R_i - G_i| \tag{4.8}$$

This score is strongly influenced by heavy rainfall and outliers. It is therefore a good indicator of the robustness of the method. The Scatter score (Germann et

al., 2006) measures the multiplicative error spread :

$$\mathrm{SCS} = r_b - r_a \tag{4.9}$$

$$r_i = \frac{R_i}{G_i} \qquad r_i \geq r_{i-1} \tag{4.10}$$

$$c_i = \sum_{1}^{i} G_i / \sum_{1}^{n} G_i \qquad c_a \approx 0.16 \qquad c_b \approx 0.84 \tag{4.11}$$

where n is the number of radar-gauge pairs and r_i are the ratios between radar and gauge estimates sorted in increasing order. The ratios are expressed on a decibel scale and set to $-20\,\mathrm{dB}$ if the radar estimation is zero. The indices a and b correspond to the normalized cumulative sum of gauge values (defined as c_i) closest to 0.16 and 0.84. The fraction of radar estimates with less than 20 % of error measures the number of good estimates :

$$\mathrm{F20} = \frac{\sum_0^n \delta_i}{n} \tag{4.12}$$

$$\delta_i = 1 \quad if \quad 0.8 \leq r_i \leq 1.25 \tag{4.13}$$

$$\delta_i = 0 \quad otherwise \tag{4.14}$$

where n and r_i are defined above. This score allows a tolerance for the sampling difference between the radar and the gauge. It is worth pointing out that the SCS and F20 scores are both immune to outliers.

In Figure 4.7 one can see the relative performance of the quantitative precipitation estimates (QPE1 and QPE2) without merging (ORI) or with a merging method (MFB, KED) against the 24 h RMIB network up to 180 km. The scores are computed for each case on a set of gauge-radar pairs and then averaged. We do not compute the scores using all gauge-radar pairs at once since it would favor cases with widespread precipitation. As in the merging process, the corresponding radar-based estimate is chosen at the pixel where the gauge is located. To properly compare the methods, we use a fixed set of gauge values exceeding 1 mm. One first notes that the MAD is lower for QPE2 than QPE1 for all cases and merging methods. This is also true for SCS and F20 in most cases. The benefit of QPE2 is higher for the stratiform cases than for convective or snow/rain mix cases. The benefit of QPE2 is reduced after merging for most cases especially with KED. It could be explained by the fact that the merging is able to mitigate part of the error corrected by QPE2. The MFB method has little effect on SCS since only the bias is corrected. The score F20 is clearly improved using QPE2 and the merging methods for most cases and especially for stratiform cases.

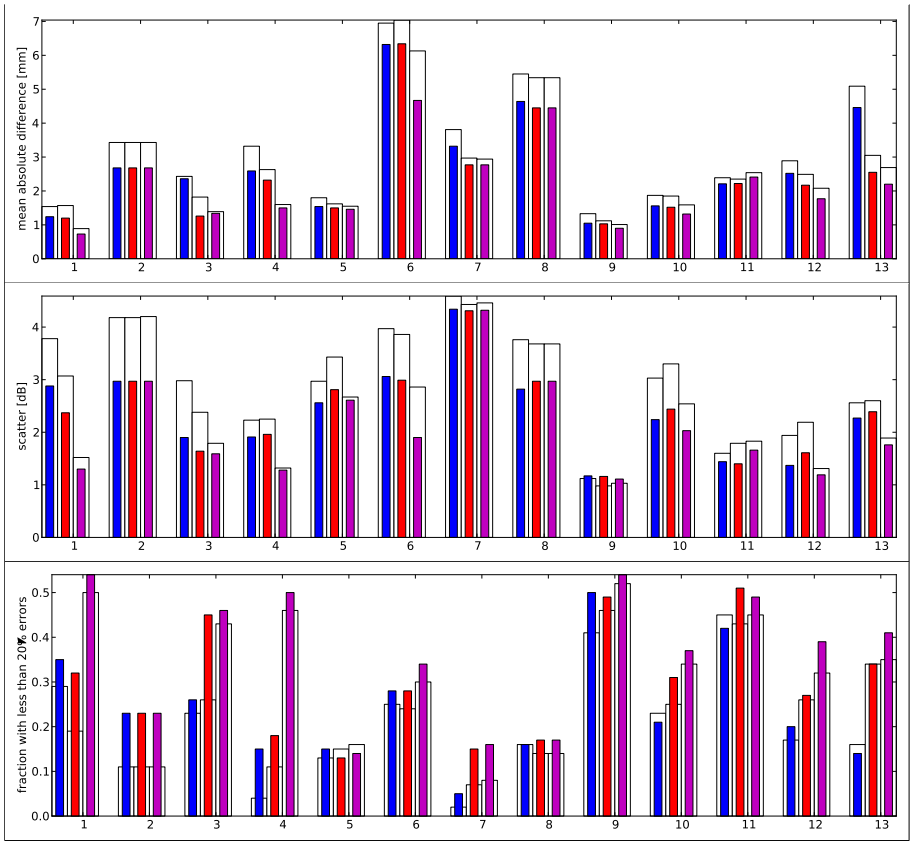

Figure 4.7: Validation of daily accumulation against the RMIB network for the 13 cases : Mean absolute difference (top), Scatter score (middle) and fraction of radar estimates with less than 20 % of error (bottom). For each numeroted case the bars corresponds from left to right to ORI (blue), MFB (red) and KED (magenta) merging methods. The white and coloured bars correspond to QPE1 and QPE2 respectively.

Table 4.2 reports the averaged statistics over all cases for QPE1 and QPE2 and 4 additional estimates to study the effect of the processing :

- PPI1 : the uncorrected lowest elevation angle (PPI)
- PPI2 : the lowest PPI where identified clutter have been replaced by values from higher elevations

Table 4.2: Verification of daily accummulations against RMIB network for gauges up to 180 km and values above 1 mm. The results of QPE1, QPE2 and four intermediate steps in combination of the merging methods are showed. The scores are averaged over 13 cases with more than 5 valid pairs.

Mean Absolute Difference (mm)

	QPE1	PPI1	PPI2	PPI3	$QPE2_{mp}$	QPE2
ORI	3.272	3.325	3.143	3.171	2.821	2.808
MFB	2.872	3.040	2.857	2.864	2.478	2.465
KED	2.546	2.793	2.485	2.488	2.176	2.170

Scatter score (dB)

	QPE1	PPI1	PPI2	PPI3	$QPE2_{mp}$	QPE2
ORI	2.980	3.196	3.173	3.180	2.409	2.391
MFB	2.938	3.113	3.137	3.109	2.441	2.426
KED	2.406	2.712	2.488	2.497	2.056	2.056

Fraction of estimates with less than 20 % of error

	QPE1	PPI1	PPI2	PPI3	$QPE2_{mp}$	QPE2
ORI	0.199	0.205	0.209	0.208	0.244	0.242
MFB	0.234	0.214	0.220	0.225	0.293	0.293
KED	0.323	0.280	0.311	0.317	0.364	0.364

- PPI3 : PPI2 with beam blockage correction
- $QPE2_{mp}$: QPE2 using Marshall-Palmer ZR relationship

As expected PPI1 performs the worst for all scores and merging methods. For all merging methods PPI2 performs slightly better than QPE1 for the MAD score but slightly worse for SCS and F20. A slight benefit of the beam blockage (PPI3) is obtained after merging for SCS and F20 scores. The significant improvement of QPE2 compared to PPI3 demonstrates the benefit of the VPR correction. The replacement of the Marshall-Palmer ZR relationship with an adapated ZR relationship has only a small positive impact on the averaged results. On average QPE2 without merging (ORI) performs better than QPE1+MFB especially for SCS. QPE1 with KED gives a similar performance as QPE2 with MFB.

Table 4.3: Probability of Detection (POD), False Alarm Ratio (FAR) and Critical Success Index (CSI) for daily accumulations exceeding 1 mm against RMIB network. The scores are computed for all days and then averaged over the 10 years.

	POD		FAR		CSI	
	QPE1	QPE2	QPE1	QPE2	QPE1	QPE2
ORI	0.663	0.704	0.365	0.323	0.466	0.517
MFB	0.671	0.710	0.364	0.322	0.475	0.525
KED	0.713	0.739	0.362	0.318	0.510	0.554

4.4.4 10-year verification

The precipitation estimates have been verified using the RMIB network for the 2005-2015 period. The results of the categorical verification (values exceeding 1 mm) are showed in Table 4.3. There is a positive impact of QPE2 with respect to QPE1 on POD due to the correction of underestimation at long range. The reduction of FAR suggests that clutter mitigation has played a role. The merging methods allow improving the POD but using KED reduces slightly the benefit of QPE2.

Figure 4.8 shows the scores computed at each rain gauge for values exceeding 1 mm. It is displayed as a function of the distance between the radar and the gauge. It is important to note that a perfect match with the gauge measurements is impossible since precipitation is estimated by the radar on a much bigger area (500 m $\times$ 500 m). It must be noted that a gauge with a very high MAD for QPE1 (due to ground clutter) has been removed to obtain a smooth average curve. The main result is that with QPE2 the MAD, SCS and F20 scores are improved respectively for 98 %, 92 % and 86 % of the gauges compared to QPE1. The general behavior for QPE1 and QPE2 is a decrease of performance further than a certain distance due to partial and complete overshooting, respectively. The benefit of QPE2 with respect to QPE1 is particularly apparent at short range and long range. It results from the correction of the BB effect and the correction of partial overshooting, respectively. The former result is more pronounced for the SCS and F20 scores. It can be explained by the fact that the BB error is highly variable. Another observation is that QPE2 has a relatively linear decrease of performance along the range for SCS and F20 scores. This could be explained by the increasing probability of attenuation by intense rainfall and hail, which is not corrected. There is little effect at long range for SCS when comparing QPE1 and QPE2 because the VPR correction (i.e. linear profile

Table 4.4: Verification of daily accumulation against the RMIB network (up to 150 km). The scores are computed for all days with more than 5 valid pairs and then averaged over the 10 years. Valid pairs are those with a gauge value exceeding a threshold given in the first row of the table.

Mean Absolute Difference (mm)

	0 mm		1 mm		5 mm		10 mm	
	QPE1	QPE2	QPE1	QPE2	QPE1	QPE2	QPE1	QPE2
ORI	1.263	1.170	2.437	2.274	4.100	3.731	6.170	5.574
MFB	1.104	1.038	2.107	2.002	3.513	3.252	5.157	4.751
KED	0.920	0.875	1.736	1.660	2.886	2.690	4.257	3.924

Scatter score (dB)

	0 mm		1 mm		5 mm		10 mm	
	QPE1	QPE2	QPE1	QPE2	QPE1	QPE2	QPE1	QPE2
ORI	2.963	2.770	2.255	2.211	1.622	1.538	1.397	1.312
MFB	2.977	2.782	2.271	2.223	1.635	1.550	1.401	1.333
KED	2.922	2.661	2.011	1.953	1.397	1.331	1.205	1.138

Fraction of estimates with less than 20 % error

	0 mm		1 mm		5 mm		10 mm	
	QPE1	QPE2	QPE1	QPE2	QPE1	QPE2	QPE1	QPE2
ORI	0.371	0.441	0.216	0.243	0.266	0.305	0.278	0.317
MFB	0.392	0.460	0.264	0.288	0.339	0.374	0.369	0.404
KED	0.405	0.481	0.351	0.370	0.451	0.479	0.496	0.526

above the BB) does not decrease the spread of the error. The effective range (i.e. where the MAD stays relatively constant) increases approximatively from 100 to 125 km which corresponds to a 50 % increase in areal coverage.

On Figure 4.9, one can see the mean absolute error for the merging methods. The MFB allows to improve both QPE1 and QPE2 significantly except at long range. The relative benefit of QPE2 is slightly smaller in the middle range. The KED method allows to further improve the performance of QPE1 and QPE2 but reduces the additional benefit of QPE2 at long range. The benefit of QPE2 at short range is enhanced after merging and is mainly due to the VPR correction. The results (not shown) are similar for the other scores. The averaged improvements from QPE1 to QPE2+KED for gauges up to 150 km are 38 %, 35 %, and 80 % respectively for the MAD, SCS and F20 scores.

The scores averaged over all days with at least 5 gauge values exceeding a given

threshold can be found in Table 4.4. Since the same weight is given for each day, the results are slightly different than the gauge-averaged statistics, which favor widespread situations. The range has been limited to 150 km, where the performance starts to drop significantly. Looking at gauge values exceeding 1 mm, QPE2+KED reduces the MAD from 2.44 to 1.66 mm and the SCS from 2.26 to 1.95 dB while F20 is increased from 0.22 to 0.37. The added value of the new processing increases with higher thresholds. At 10 mm the MAD decreases from 6.17 mm to 3.92 mm, the SCS from 1.40 to 1.14 dB and F20 increases from 0.28 to 0.53. It should be noted that part of the performance of the KED method could be due to smoothing effects.

4.4.5 Statistics

The global and local benefit of QPE2 and the merging methods can be seen by looking at Fig 4.10, which shows the mean annual total for the 10-year period. The full radar coverage is shown mainly to highlight the mitigation of radar artefacts. It is important to note that the estimates outside Belgium have not been verified, since it is not the purpose of the study. We can however expect good results given the relatively similar meteorological conditions within the radar coverage. The results of QPE2+KED have little value outside Belgium but are presented for the sake of consistency with the other figures. It can be seen that the impact of clutter has been significantly reduced. In particular the small lines due to airplanes (mainly South-West of the radar from 200 km range) and the interference line (South of the radar) have been removed. However there are still some limited areas contaminated by ground clutter which are slightly amplified by the merging methods. It is important to note that only a few gauges are located in areas with a higher probability of clutter. The underestimation due to beam blockage is reduced but still visible. This can be at least partially explained by varations in propagation conditions. The effect of the BB (i.e. concentric circles) on QPE1 is not very pronounced since it depends on the height of the freezing level and it is therefore spread over the range. The smoothed circles are properly removed by the usage of the lowest elevation in QPE2. The underestimation at long ranges is reduced using QPE2 and even more using QPE2+KED.

A comparison with mean annual totals of the SPW and RMIB network (up to 180 km) is showed on Figure 4.11. Compared to the SPW network, the correlation (Pearson coefficient) increases from 0.70 (QPE1) to 0.85 (QPE2). There is underestimation of radar estimates, even with QPE2, for values exceeding 1100 mm, which are located over the hills nearby the radar. This can be at least partially explained by the higher height of valid measurements in that region and the effect of orographic enhancement. The correlation

with the RMIB network increases from 0.54 (QPE1) to 0.66 (QPE2) and 0.80 (QPE2+KED). The lower correlation with the RMIB network can be explained by the greater proportion of gauges located far from the radar. However, a lower quality of some manual measurements can not be ruled out. In the study region it appears that the mean annual totals ranges between 600 mm and 1300 mm. There is a general correlation of the mean rainfall with topography (Fig. 4.2) and the maximum is found in the Belgian Ardennes. One notes though a significant decrease of precipitation in the region with the highest topography when crossing the border towards Germany. This might be due to the positive and negative orographic effects on precipitation associated with the dominant South-Westerly wind. The actual effect of topography is more difficult to interpret beyond 150 km due to systematic radar underestimation, as seen in the gauge verification. Those results are in good agreement with the precipitation maps for the period 1981-2010 obtained by Journée et al. (2015) using interpolated data from the RMIB network. Using 8 years of operational radar data in the UK, Fairman et al. (2015) also suggest that overshooting and orographic enhancement are the two main sources of difference with the gauges.

In figure 4.12, one can see the probability of hourly and daily accumulations to exceed 10 mm. For both statistics, using QPE2+KED allows to remove most radar artifacts appearing when using QPE1. The correlation with daily gauge values from the RMIB network (not shown) increases from 0.42 to 0.72. The probability of daily rainfall to exceed 10 mm ranges between 4 % and 12 % of the time and it is correlated with the mean annual total. The probability to exceed 10 mm in one hour is a less frequent event and exhibits higher variations. It is larger in the South East of the domain where it reaches a probability of about 0.1 %. This area is known for higher probability of convective storms (Weckwerth et al., 2011).

Fig 4.13 shows the maximum values of hourly and daily accumulations with QPE1 and QPE2 without merging. The effect of merging on the extremes is limited given the fact that convective cells are poorly resolved by rain gauge networks and it is therefore not shown. It is known that precipitation maxima on a 500 m square are lower than rain gauge maxima due to rainfall small scale variability. However, for QPE1, one finds values higher than expected from extreme precipitation models for Belgium based on rain gauges (Van de Vyver, 2012). Those unrealistic extremes, which are caused by clutter or by a wrong Z-R relationship applied to hail, are mitigated in QPE2. The radar maxima become slightly lower than rain gauge maxima (not shown) as expected due to the averaging over a much bigger area. The hourly accumulation maximum exhibits high small-scale variations but no large scale trend. The daily accumulation maximum also shows variations but at larger spatial scales. A region with higher values is still present in the South-East.

4.5 Conclusions

The polar volumetric data from a single-pol weather radar (Wideumont, Belgium) have been reanalyzed from 2005 to 2015 using a new processing chain (i.e. QPE2) to generate rainfall rates. A static clutter map and a beam blockage map are used to characterise the quality of the data. Clutter are identified dynamically using 3 different techniques : a comparison with a cloudtype product from satellite observations, the identification of unrealistic vertical gradient of reflectivity and the identification of abnormal horizontal reflectivity texture. A robust VPR correction has been applied to mitigate the effect of the BB and the underestimation at long ranges. A distinction between stratiform and convective precipitation is made using an enhanced version of the Steiner algorithm. Different VPR corrections and ZR relationships are applied for the two precipitation regimes. The maximum reflectivity is set to 55 dBZ for mitigating contamination by hail. Using a dense hourly rain gauge network, linearly accumulated radar rainfall rates are adjusted by mean field bias. A Kriging with external drift using a climatological exponential variogram with 10 km range and a square-root transformation is also applied to radar and rain gauge hourly rainfall estimates.

All algorithms have been fine-tuned on a selection of 13 cases with various meteorological situations. A validation of the cases is performed using an independent daily rain gauge network. The results for three different scores (MAD, SCS and F20) reveal a small to high benefit of QPE2 and the merging methods when compared to interpolated elevations at 800 m above radar level (QPE1). The VPR correction is responsible for most of the benefit while beam blockage correction and the alternative ZR relationships hardly improved the results. It is interesting to note that the quality-controlled lowest elevation exhibits similar performance as QPE1.

A 10-year verification of daily precipitation amounts has been performed against the independent daily network using the same scores. A categorical verification of values exceeding 1 mm shows that the false alarm ratio is reduced and the probability of detection is increased with QPE2, which are mainly due to clutter mitigation and VPR profile correction, respectively. Computing three different scores at each gauge location for values exceeding 1 mm reveals a clear benefit of QPE2 versus QPE1 especially at short and long range. In addition, QPE2 allows to increase the range with good quality estimate from 100 to 125 km or roughly 50 % more coverage. Using the merging methods allows further improvements but reduces the benefit of QPE2, except at short range. The average improvements from QPE1 to QPE2+KED for gauges up to 150 km are 38 %, 35 %, and 80 % respectively for the mean absolute difference (MAD), the multiplicative error spread (SCS) and the fraction of estimates with less than

20 % of error (F20). The average of daily statistics exhibits smaller improvements with 32 %, 14 % and 52 % obtained for the three scores with QPE2+KED. This suggests that larger benefits are obtained for widespread situations. The benefit increases when considering higher rainfall thresholds and with 10 mm daily amounts the improvements are 36 %, 18 % and 89 %, respectively.

The 10-year mean annual total clearly shows the mitigation of radar artefacts by QPE2, especially the clutter and the underestimation at long range. The correlation with rain gauge values increases from 0.54 for QPE1 to 0.80 for QPE2+KED. The probability to exceed 10 mm for hourly and daily accumulations further highlights the improvements made by QPE2 and the merging methods with mitigation of artefacts and increased correlation with rain gauge values. Looking at the 10-year maximum of hourly and daily accumulations reveals unrealistic high values for QPE1 compared to gauges due to clutter and hail. Using QPE2 mitigates those artefacts with more realistic hourly values slightly lower than rain gauge maxima as expected due to the bigger area of the radar estimate.

We would like to stress that finding parameters (e.g., reflectivity thresholds) which perform well in all conditions is particularly difficult. This task represents a significant part of the time spent on this study. For some situations with strong horizontal temperature gradients, the global VPR correction might not work properly, but this effect is limited by using data from a 40 minutes time window. While the most important errors have been mitigated, the processing of radar volume data could be further improved. One thinks of using dynamic beam blockage correction, using other radars to deal with attenuation, taking into account precipitation advection (e.g., using optical flow) when computing accumulation and refining the Kriging with external drift (e.g., with a real-time variogram estimation). The use of model output like temperature could also help in the validation of the BB identification. The verification of the precipitation dataset against rain gauge values gives a lower bound on the quality of the estimates. Therefore quantifying the uncertainty of the new estimates remains a challenge. A new dual-pol radar has been installed in Belgium since 2013 and volume data are archived. It will be interesting to see if the recently developed QPE algorithms making use of polarimetric information can significantly improve the scores of QPE2.

Given the good results obtained by the new radar processing chain, it is going to be implemented in realtime. Since the radar now performs a 15-elevation scan every 5 minutes, further improvements are expected. The enhanced operational QPE will propose a better input for the nowcasting systems running at RMIB, INCA-BE and STEPS (Foresti et al., 2016). The validated 10-year dataset produced here, which will be extended each year, can be used as basis for further studies, especially in hydrology. A direct application is to generate a rainfall

climatology and compare the results with conventional climatology based on rain gauges. One of the main benefit of using radar observations is the ability to compute areal rainfall extreme statistics for different area sizes.

Acknowledgments

This research was founded by the Belgian Federal Science Policy Office (BELSPO). The comments given by the three reviewers and Loris Foresti were highly appreciated.

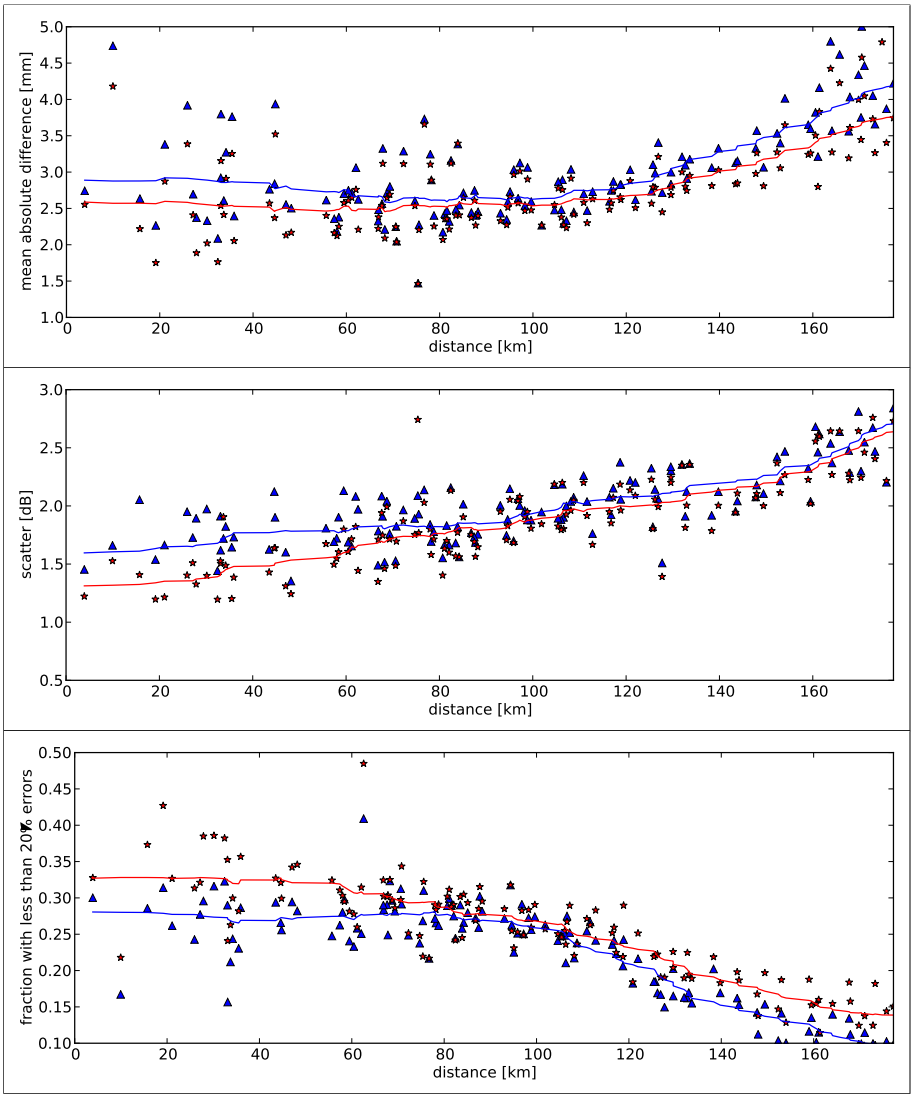

Figure 4.8: 2005-2015 verification of daily accumulation against RMIB network for QPE1 (blue, triangle) and QPE2 (red, stars) without merging. Only radar-gauge pairs with gauge value exceeding 1 mm are selected. The figures correpond to the Mean absolute difference (top), the Scatter score (middle) and the fraction of radar estimates with less than 20 % of error (bottom).

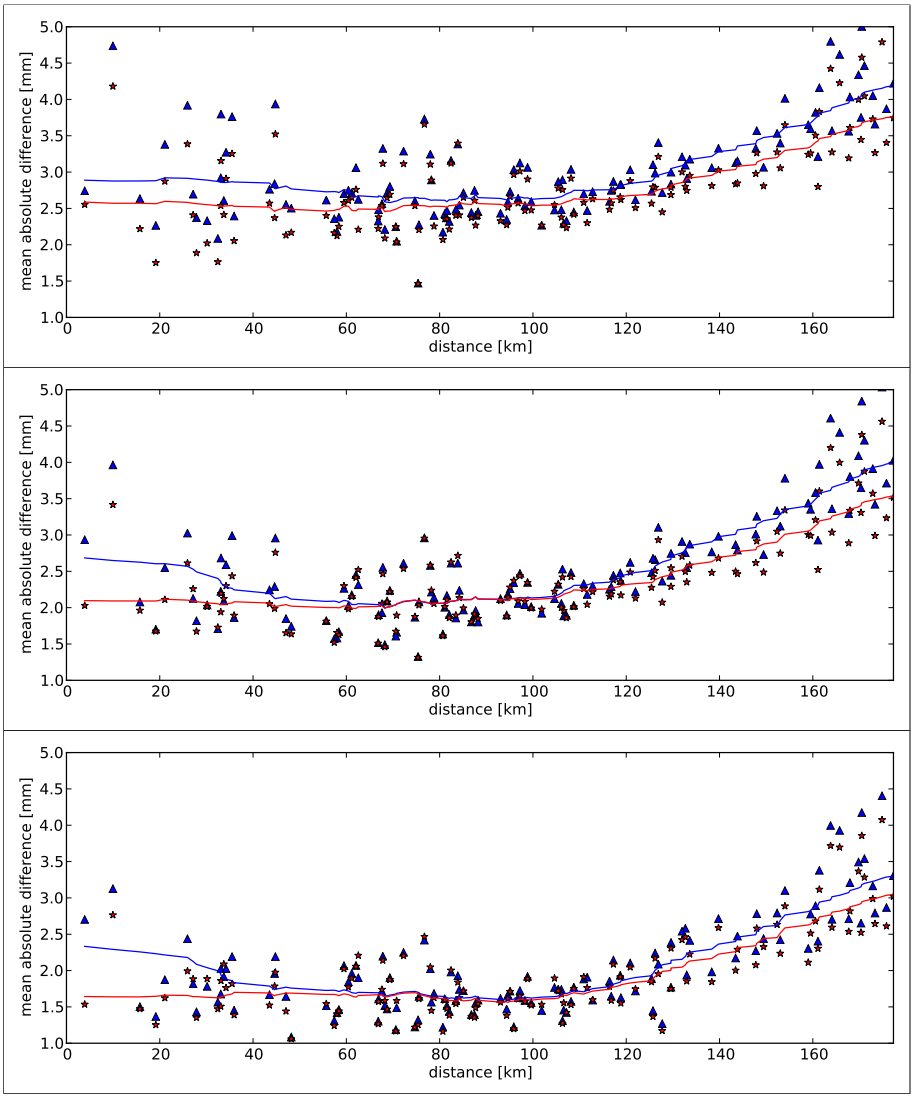

Figure 4.9: 2005-2015 verification of daily accumulation (Mean absolute difference) against RMIB network for QPE1 (blue, triangle) and QPE2 (red, stars). Only radar-gauge pairs with gauge values exceeding 1 mm are selected. The figures correspond to the merging methods ORI (top), MFB (middle) and KED (bottom).

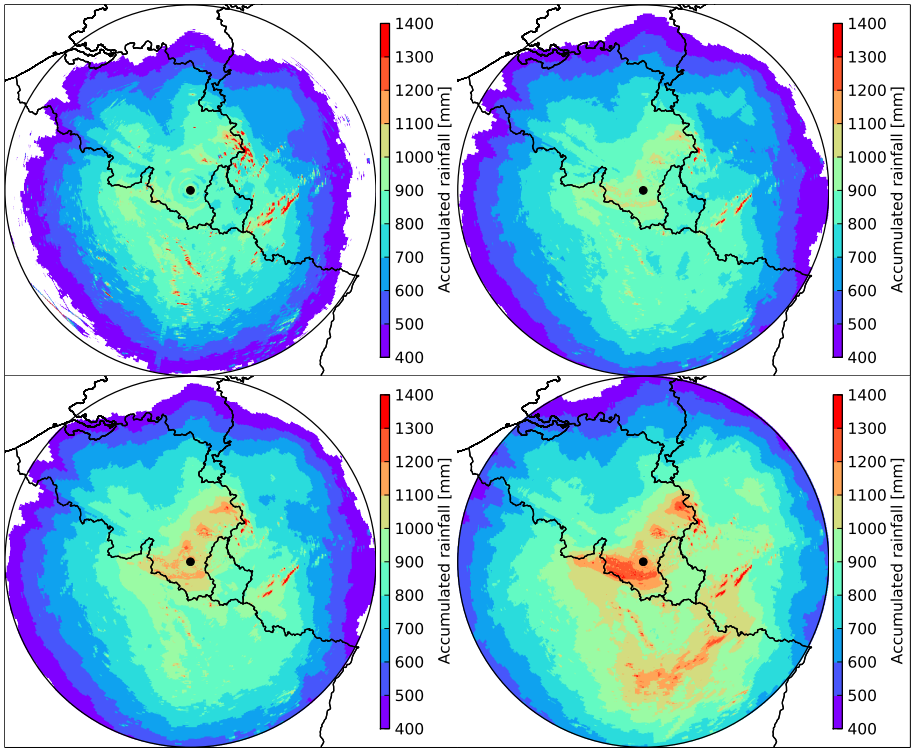

Figure 4.10: Annual total mean for the 2005-2015 period up to 220 km range based on QPE1 (top left), QPE2 (top right), QPE2+MFB (bottom left) and QPE2+KED (bottom right).

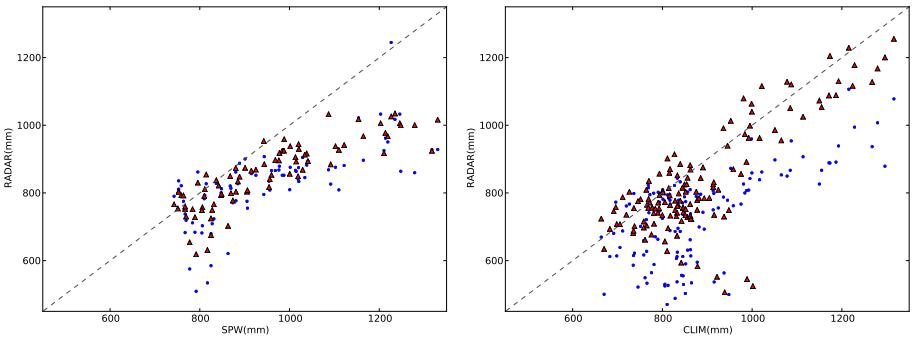

Figure 4.11: Scatter plots of mean annual total (mm) from QPE1 (blue, point) and QPE2 (red, triangle) against the SPW network (left) and from QPE1 (blue, point) and QPE2+KED (red, triangle) against the RMIB network (right).

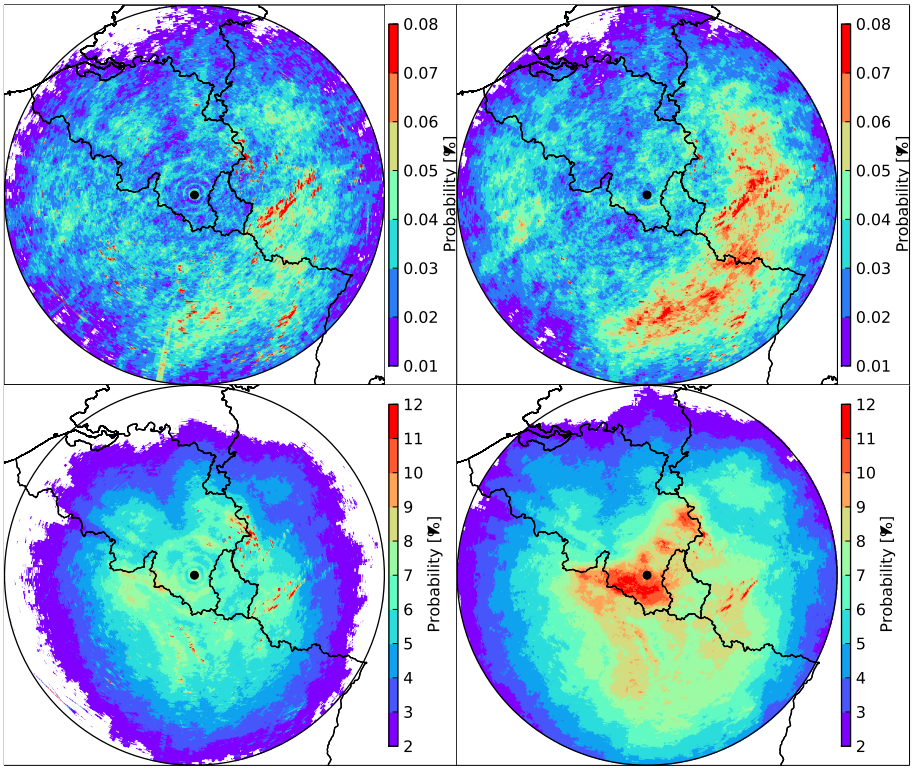

Figure 4.12: Probability of hourly (top) and daily (bottom) accumulation to exceed 10 mm for 2005-2015 based on QPE1 (left) up to 240 km range and QPE2+KED (right) up to 220 km range.

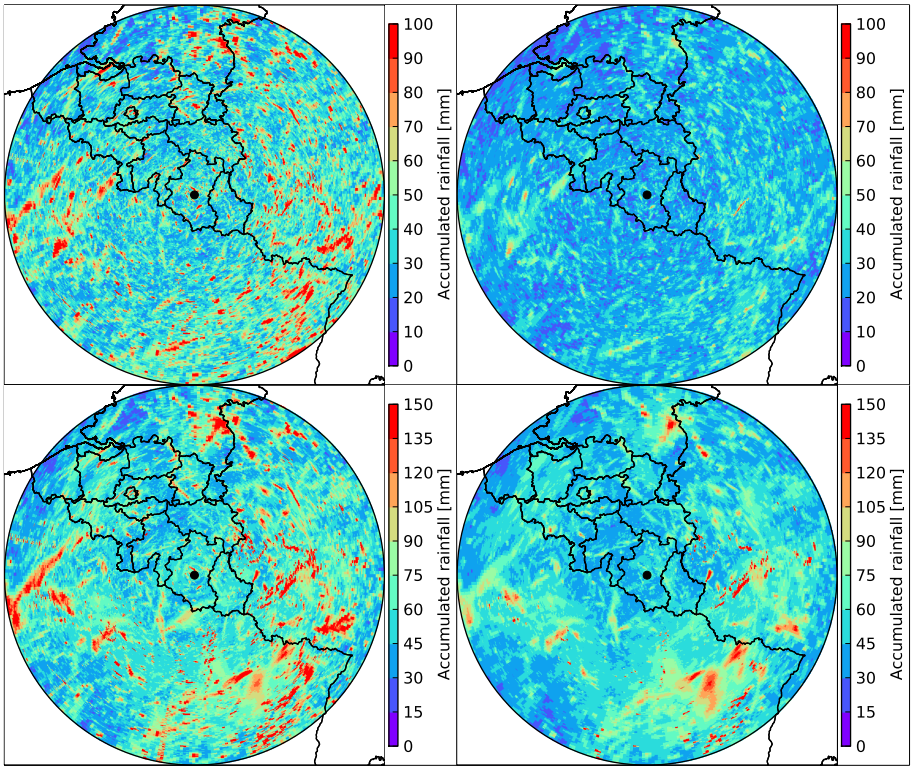

Figure 4.13: Maximum hourly (top) and daily (bottom) accumulation for 2005-2015 based on QPE1 (left) and QPE2 (right) up to 240 km range.

Chapter 5

Regional frequency analysis of extreme rainfall in Belgium based on radar estimates[1]

Abstract

In Belgium, only rain gauge time-series have been used so far to study extreme rainfall at a given location. In this chapter, the potential of a 12-year quantitative precipitation estimation (QPE) from a single weather radar is evaluated. For the period 2005-2016, 1 h and 24 h rainfall extremes from automatic rain gauges and collocated radar estimates are compared. The peak intensities are fitted to the exponential distribution using regression in quantile-quantile plots with a threshold rank which minimises the mean squared error. A basic radar product used as reference exhibits unrealistic high extremes and is not suitable for extreme value analysis. For 24 h rainfall extremes, which occur partly in winter, the radar-based QPE needs a bias correction. A few missing events are caused by the wind drift associated with convective cells and strong radar signal attenuation. Differences between radar and gauge rainfall values are caused by spatial and temporal sampling, gauge underestimations and radar errors. Nonetheless the fit to the QPE data is within the confidence interval of the gauge fit, which remains large due to the short study period. A regional

[1] based on E. Goudenhoofdt et al. (2017). "Regional frequency analysis of extreme rainfall in Belgium based on radar estimates". In: *Hydrology and Earth System Sciences* 21.10, pp. 5385–5399. DOI: 10.5194/hess-2017-150

frequency analysis for 1 h duration is performed at the locations of 4 gauges with 1965-2008 records using the spatially independent QPE data in a circle of 20 km. The confidence interval of the radar fit, which is small due to the sample size, contains the gauge fit for the two closest stations from the radar. In Brussels, the radar extremes are significantly higher than the gauge rainfall extremes; but similar to these observed by an automatic gauge during the same period. The extreme statistics exhibit slight variations related to topography. The radar-based extreme value analysis can be extended to other durations.

5.1 Introduction

Localised rainfall extremes can have a strong impact on human activities especially in urban areas (Ootegem et al., 2016). For flood management applications (e.g., sewer system and dam design) it is needed to know the probability that rainfall exceeds a given amount. This probability is often expressed as the rainfall level which, on average, will be exceeded once over a given period of T years, which is defined as the return period. For infrastructure design application, one is interested in return periods from 50 to 100 years. Such long return periods often exceeds the available observation period and a model is needed.

Extreme values are often extracted from a time series using block maxima, typically over one year (AM) for meteorological data. The performance of the statistical modelling applied to AM data is limited by the number of years available. The peaks over threshold (POT) method, where values exceeding a given threshold are kept, allows to increase the number of samples. The extreme value theory showed that under some hypotheses - including independence - of the random variables, the AM and POT series can asymptotically converge only to the 3-parameters distributions known as GEV and GPD, respectively.

Different fitting methods to the extreme value distributions have been developed in the literature. The maximum likelihood estimator (MLE) is the most widely used fitting method but for small samples it can lead to unrealistic parameter estimates. This problem is partially addressed with the generalised MLE proposed by Martins and Stedinger (2000) or the L-moments method (Overeem et al., 2009a). The above methods do not focus on the tail of the distribution, which is the most relevant for risk analysis. For this goal, Willems et al. (2007) proposed a method based on regression in Q-Q plots.

To reduce the uncertainty associated with the limited number of data at a single site, regional frequency analysis (RFA) methods have been proposed (Svensson and Jones, 2010). The RFA is characterised by the selection of the regions and

the parameter estimation approach applied to each region (Buishand, 1991). There are numerous studies of RFA for rainfall extremes based on rain gauge datasets. The index flood approach, which considers that only the location parameter varies in the region, is very popular (Gellens, 2000; Sveinsson et al., 2001; Rulfova et al., 2014). Uboldi et al. (2014) used a bootstrap technique to randomly select data from neighbouring locations with a probability depending on the distance and altitude difference with the target location. The combined use of POT and RFA methods is recommended by Roth et al. (2015).

One of the challenges in RFA is the intersite dependence (e.g., Hosking and Wallis, 1988). Even for 1 h duration, rainfall maxima exhibit spatial correlation (Vannitsem and Naveau, 2007). Using the sum of the length of all sites is common but causes underestimation of the extremes (e.g., Bardet et al., 2011). Several approaches have been proposed to deal with this problem (e.g., Castellarin, 2007; Weiss et al., 2014).

To obtain the rainfall statistics at any given point, spatial models have been developed using geographical and climatological covariates (e.g., Cooley et al., 2007). In Belgium, Van de Vyver (2012) derived a spatial GEV model depending linearly on the altitude. Rulfova et al. (2014) found for 6 h rainfall in the Czech Republic that the assumption of a linear model might be too restrictive, especially for convective precipitation.

The rain gauge network can capture rainfall extremes for widespread situations. However, they can only catch a small part of rainfall extremes caused by convective storms, which exhibit strong spatial variations over short distances. The use of high resolution gridded rainfall datasets to study rainfall extremes is still in its infancy. This can be explained by their unavailability, their processing requirements and their limited quality. Precipitation estimations from satellite offer global and relatively long records suitable for extreme value analysis (Marra et al., 2017) but still suffer from large uncertainties (Sapiano and Arkin, 2009). The best potential is currently provided by radar-based quantitative precipitation estimation (QPE) products. It should be noted that the radar estimates represent the averaged precipitation over a given area (typically a square of 1 km). While this area is much bigger than the gauge area, we will consider it as representative for small scale precipitation. It has been shown that the sub-pixel variability of rainfall extremes is significant, especially for short durations (Peleg et al., 2016). The relatively short record of radar datasets is an issue if the extreme statistics depend only on time (i.e. are completely dependent spatially). While this is a reasonable assumption for larger duration (e.g. 1 day), it is difficult to prove for short duration (e.g. 1 h). In case of significant climatic variations, a short record will be more representative of the extreme statistics.

In a pioneer work, Overeem et al. (2009a) showed that a 11-year radar data set is suitable to derive intensity duration frequency (IDF) curves for the Netherlands. But some differences with rain gauge results were found for short durations. Based on a unique 23-year radar data set in Israel, Marra and Morin (2015) found that the IDF curves were generally overestimated but 60 % of them lay within the raingauge IDF confidence intervals. In Ontario (Canada), Paixao et al. (2015) demonstrate the potential to integrate radar (Digital Precipitation Array product) to rain gauge analysis, especially to identify homogeneous regions of extreme rainfall. Saito and Matsuyama (2015) used a 26-year radar-gauge dataset (without RFA) to study the spatial variation of hourly rainfall extremes in Japan. They found significant spatial patterns but also large uncertainties in the radar datasets. Different index flood approaches were tested by Eldardiry et al. (2015) in Louisiana, who defined a region as a square window of 44 km size. They found for Louisiana (USA) that the relatively short period (13 years) explains the high uncertainty of the analysis, that the index flood method is recommended and that a systematic underestimation is associated with the radar products (its spatial resolution is $4 \times 4\,km$). Haberlandt and Berndt (2016) found that the operational DWD product is only suitable for studies on longer durations after bias correction. Using a 10-year high resolution radar rainfall dataset, Wright et al. (2014b) performed a regional frequency analysis using stochastic storm transposition. They found that the radar-based IDF estimates generally reproduce conventional gauge-based IDF estimates but overestimate these for longer return periods and shorter durations.

The potential of the radar data can be fully exploited by studying the extremes of the mean (or maximum) rainfall over areas. With the goal of deriving alert thresholds for 159 regions in Switserland, Panziera et al. (2016) studied the areal rainfall maxima (with sizes from the pixel to the region). Using RFA on squares, Overeem et al. (2010) derived areal rainfall depth-duration-frequency curves for the Netherlands. Wright et al. (2014b) applied a similar methodology but on different catchments in Louisiana.

In this study, we want to demonstrate the potential of high-resolution radar-based QPE to derive rainfall extreme statistics at a given location. To our knowledge none of the previous studies combine a high quality radar-based QPE with a high quality reference rain gauge measurements. At the Royal Meteorological Institute of Belgium (RMIB), a QPE has been derived from the reprocessing of raw volumetric radar measurements. This dataset has been used for various applications such as case studies and model verification. The methodology to derive this dataset has been verified for the period 2005-2014 against an independent rain gauge network (see chapter 4). RMIB also has a unique 40 year dataset of 10-min rain gauge measurements which has been used in extreme value studies (Vannitsem and Naveau, 2007; Van de Vyver, 2012).

Unlike existing radar studies, we select our data using the POT approach and use a fitting method based on a regression in quantile-quantile plots (QQR) proposed by Willems et al. (2007). Radar-based extreme statistics for 1 h and 24 h duration are compared with the ones derived from rain gauge data covering the same period. We propose a new regional frequency analysis which makes use of independent radar data in a predefined neighborhood. The results are compared with those obtained using the long-term rain gauge network. Finally, the regional approach is applied at each radar pixel on the whole of Belgium to study the spatial variations of the rainfall extremes.

5.2 Rainfall data

5.2.1 Raingauge measurements

Over the years, Belgium (Fig. 5.1) has been covered by several raingauge networks for different purposes.

Since the end of the 19th century, RMIB maintains a network (CLIM) of non-recording rain gauges from which rainfall measurements are taken at 8 am LT. The data are carefully controlled and used for climate applications (Journée et al., 2015).

A Hellmann-Fuess pluviograph has been in operation in Uccle (RMIB) from 1898 to 2008 and has enabled the compilation of a continuous time series of 10 min rainfall (Demarée, Gaston R., 2003). The 10 min rainfall values had to be manually extracted from line graphs on papers. Starting from the fifties, additional rain gauges were installed to constitute a network (BUL) for hydrological research. Since the rain gauges underestimate the rainfall by 5-10% due to its mechanism, its records have been calibrated using a collocated gauge from the CLIM network.

For weather forecast purposes, the RMIB maintains a network of automatic weather stations (AWS) in Belgium. These stations provide rainfall measurements at 10 min temporal resolution. The tipping-bucket gauges are progressively replaced by weighted gauges (the first one was installed in Uccle on 10 February 2009). The data are available since 2002-2004 and have been quality controlled.

SPW maintains a dense network of hourly (every 5 min since 2012) rainfall measurements. The tipping bucket gauges are progressively replaced by weighting gauges since 2015. The data have been quality controlled by RMIB since April 2004.

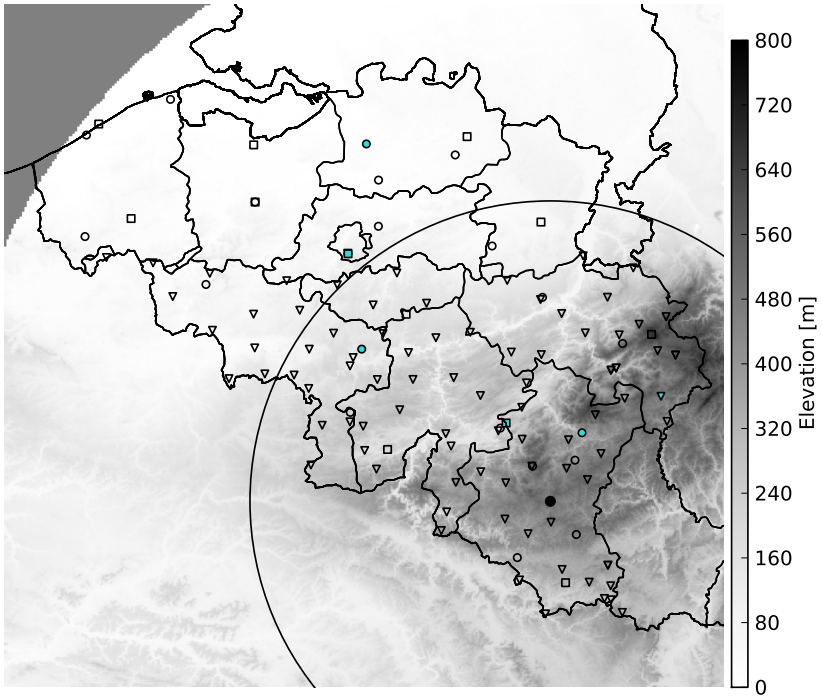

Figure 5.1: Elevation map centered on Belgium with the Wideumont radar (black dot) covering 240 km range (the black circle denotes the 120 km range) with AWS (square), SPW (triangle) and BUL (circle) rain gauge networks. The gauge locations selected in this study are in cyan. Country borders with France, Luxembourg, Germany and the Netherlands are also displayed.

It is important to know the limitations of the respective rain gauges in case of extreme rainfall. It is known (Nystuen, 1999; Duchon and Biddle, 2010) that tipping buckets underestimate high rainfall rates. The use of weighting gauges for extreme rainfall is discussed in Colli et al. (2012). Every 10 mm, the pluviograph has to be emptied which results in an underestimation in case of extreme rainfall. The calibration of the pluviograph is probably not sufficient for sub-daily extremes. Finally, the quality controls, albeit conscientious, can never be considered as perfect.

5.2.2 Radar estimation

The QPE available on a 1 km grid every 5 min is made using an elaborated processing chain from the radar volumetric reflectivity measurements. The quality of the radar volume is controlled using several algorithms :

- a static clutter map : pixels with unrealistic high probability of rainfall are identified as clutter
- a beam blockage map : the percentage of the beam blocked by topography is computed using a simple propagation model
- a first clutter identification based on reflectivity differences between radar beam elevations
- a second clutter identification based on strong deviations of a pixel from its neighborhood and unrealistic lines
- a third clutter identification for radar echoes in cloud free areas determined by satellite observations

A maximum threshold for reflectivity is set to 55 dBZ to mitigate higher reflectivity values due to hail. The rainfall rate estimates are obtained using stratiform-convective classification, a 40 min averaged vertical profile of reflectivity (VPR), a bright band identification and a specific transformation to rain rates for the two precipitation regimes. The detailed procedure is described in chapter 4. As a reference for the QPE product, the CAP product is defined as the interpolation at 800 m above the radar level. It makes use of a standard Z R relationship, which comes from the hypothesis that the drop size distribution follows the distribution of Marshall-Palmer, as discussed in (Uijlenhoet and Pomeroy, 2001).

Consecutive rainrate estimates are integrated to obtain 10 min accumulations (5 min gaps are tolerated) to match the lowest resolution of the rain gauge data. Hourly accumulations are combined with the SPW gauges using a mean field bias correction. This method applied to the QPE product is referred to as the mean field bias (MFB) product from now on. A more complex merging method (i.e. external drift Kriging) was tested but found to be unstable for some time moments.

It is important to mention the limitations of the radar products in case of extreme precipitation. The most important impact of the QPE processing on extreme values is the 55 dBZ reflectivity threshold used to mitigate hail. Using the convective Z R relationship, this corresponds to a maximum rainfall rate

Table 5.1: Rain gauge stations used for comparison and availability of the extreme rainfall datasets. The last column is the percentage of time when both radar and gauge data are available

Station	Altitude (DNG)	Distance to radar (km)	Duration	Avail. Gauge (%)	Avail. Radar (%)	Avail. Both (%)
Humain (AWS)	296	36	1h	98.5	94.8	93.5
Uccle (AWS)	100	128	1h	99.9	94.8	94.7
Uccle (SPW)	100	128	24h	90.6	86.0	78.2
St-Vith (SPW)	456	61	24h	89.2	86.0	76.7
Deurne (BUL)	12	161	1h	86.0	–	–
Uccle (BUL)	100	128	1h	96.3	–	–
Gosselies (BUL)	187	97	1h	85.7	–	–
Nadrin (BUL)	403	30	1h	59.3	–	–

of 80 mm/hour. Higher values of about 100 mm/hour are possible when the standard Z R relationship is used for stratiform areas. This can only happen close to the radar where convective precipitation can not be identified. Slightly higher thresholds of 100 mm/hour and 105 mm/hour have been used by Overeem et al. (2009a) and Wright et al. (2014b), respectively. A higher threshold of 150 mm/hour is used by Marra and Morin (2015) but for a Mediterranean climate. Only half of the AWS gauges recorded up to 3 times more than 100 mm/hour in 10 minutes. Given the sub-pixel spatial variability, one can assume that this threshold will never be exceeded for the pixel average. This threshold can only partly correct for the overestimation due to hail. The second most important error is related to signal attenuation especially in case of well organised convective systems. This is why extremes might be underestimated the further the distance from the radar. In addition, the increasing radar sample volume will produce an underestimation of small scale extremes. The uncertainty in the Z-R relation is another important source of error.

5.2.3 Comparison framework

In this study, we will only consider validated rain gauge data. Given that the SPW network is used for merging, the radar dataset for 2005-2016 is used. To perform a direct comparison, the gauge data of AWS and SPW for the same period are used. For comparison against the reference BUL network, the gauge data for the period 1965-2010 are used. The timeseries of the BUL and CLIM networks have been tested for homogeneity by Van de Vyver (2012) and a

selection of useful stations has been made. Gellens (2000) and Vannitsem and Naveau (2007) found that the vast majority of the CLIM and BUL time series are stationary for summer rainfall. However, the existence of a multi-decadal oscillation in rainfall extremes has been found in the Uccle time series (Ntegeka and Willems, 2008; Willems, 2013).

The 10 min rainfall accumulation from the gauge networks (AWS, BUL) and radar products (CAP, QPE) are summed to obtain sliding 1 h rainfall accumulations. Such duration is associated with convective storms, which can only be properly seen on radar images. The hourly bias obtained by the MFB method could be applied to the 10 min accumulations. However, it will not be used due to the possible risk of representativity errors related to convective storms and the small benefits expected.

The hourly rainfall from the SPW network and the radar products (CAP, QPE, MFB) are summed to obtain sliding 24 h rainfall accumulations. The SPW network is preferred to the AWS network because it is denser and more homogeneous. Such duration is mainly associated with widespread precipitation for which the benefit of merging methods is clear. The risk of instability with MFB (e.g., in case of strong spatial variation of the bias) is tolerated given the significant expected benefit for widespread precipitation events.

It should be noted that using the lowest available duration for each network would result in an underestimation of the extremes due to the discrete time sampling (Marra and Morin, 2015). Additionally, random errors and time sampling difference can be compensated by performing the sum. For both the radar and the gauge, no missing data is tolerated in the sum to avoid underestimation. Furthermore, only timestamps with both radar and gauge data are kept.

Due to the amount of stations, it is not possible to analyse in details the results at each station. Therefore a few stations are picked at different distances from the radar (see Tab. 5.1 and Fig. 5.1). The Uccle station is chosen because it is included in the 3 networks, which makes inter comparison possible. The availability of the 1 h accumulation data is about 95 % for the radar products and close to 100 % for the AWS gauges. The radar availability of the 24h accumulation is lower than the 1 h accumulation because a significant part of the intervals without data are short. The availability of the SPW gauges is around 90 % but this is mainly due to the removal of snow events, when no extreme precipitation is expected. The availability of the BUL stations for the period 1965-2010 is highest at Uccle with 96.3 %, then about 86 % at Deurne and Gosselies. The station of Nadrin has only 60 % of availability (for the period 1965-2010) because it was started in 1978.

5.3 At-site frequency analysis

5.3.1 Methodology

It has been shown by Pickands III (1975) that the extreme values converge asymptotically to a generalized Pareto Distribution (GPD) :

$$F_{(\xi,\mu,\sigma)}(x) = \begin{cases} 1 - \left(1 + \frac{\xi(x-\mu)}{\sigma}\right)^{-1/\xi} & \text{for } \xi \neq 0, \\ 1 - \exp\left(-\frac{x-\mu}{\sigma}\right) & \text{for } \xi = 0. \end{cases} \tag{5.1}$$

with ξ, μ and σ commonly defined as the shape, location and scale parameters. The special case when the shape parameter is equal to zero is defined as the Exponential distribution (EXP).

The choice of the threshold has an important impact on the estimation of the distribution parameters. When the number of selected values increases, the variance naturally decreases but the bias increases (due to the deviation from the theoretical distribution). It is more practical to use a threshold rank instead of a threshold value to control the sample size.

To apply the theory, the extreme values have to be independent but successive peaks within the same time window can be observed due to the nature of precipitation. For 1 h duration, two peaks are considered dependent if the time interval is less than 12 h as proposed by Ntegeka and Willems (2008). This choice is consistent with the characteristics of convective storms analysed in chapter 3. Jakob et al. (2011) used a separation time of 24 h but found little sensitivity when taking lower or higher values. We also found that using 3 days hardly affects the selection of the 1 h extremes. For 24 h duration, we use a time interval of 3 days which is the typical scale of synoptic regimes. These choices are consistent with Roth et al. (2014) who found empirically a temporal dependence of 1 day and 2 days for winter and summer precipitation, respectively. In practice, a peak is kept if it is the maximum compared to its dependent peaks (if any).

The type of the distribution can be derived by looking for the QQ-plot where the extremes behave in an asymptotic linear way. (Willems, 2000) found for the Uccle series that the tail of the distribution has an exponential behavior for all durations. In the gauge datasets used in this study, we also found a tendency for the EXP distribution. The EXP distribution is preferred for short period since estimating the shape parameter is very uncertain. Blanchet et al. (2015) found that GPD fails to robustly estimate the tail of the distribution because of lack of data and unrealistic return levels for very long return periods (when

the shape parameter is positive). An additional argument for the EXP model is that it is less affected by observational errors, which plays an important role here.

In this study we use the QQR fitting method. The Exponential Q–Q plot is the extremes x versus minus the logarithmically transformed exceedance probability $1 - G(x)$. The EXP distribution appears as a line in this plot, with slope equal to the scale parameter σ:

$$x = x_t - \sigma ln(1 - G(x)) \tag{5.2}$$

where x_t is the threshold level. The same properties hold for the plot of the return level x_T against the return period T when the latter is plotted on a logarithmic scale :

$$x_T = x_t + \sigma ln(T * M/n) \tag{5.3}$$

where M is the number of extremes and n the length of the timeseries.

The estimators for the slope are based on linear regression in the Q–Q plot above the specific threshold level x_t. Amongst the available estimators for σ we used an unconstrained and unweighted linear regression.

The optimal threshold rank t is found by minimization of the mean squared error (MSE) of the calibration. With our datasets, this rank is chosen between 18 and 30 considering the uncertainties and the relatively short period, respectively. Confidence intervals for the scale parameter are computed using a parametric bootstrap technique. The fitted distribution is used to generate 1000 extreme values series with a size corresponding to the optimal rank. The fitting procedure is applied to each of the 1000 series to obtain 1000 simulated scale parameters. The 10 and 90 percentiles of the simulated parameters are taken as the 10 % and 90 % confidence interval bounds for the true scale parameter.

5.3.2 Comparison of 1h extremes

The extreme events as seen by both the radar and the gauge are compared in table 5.2. Since the focus is on the tail of the distribution, only the 10 highest values from either the gauge or the radar data are selected. The events for which the probability of hail is high (i.e. when the threshold was applied) are highlighted. An event is considered as problematic if the corresponding radar or gauge extreme rank is below 30. For these events, the underlying precipitation patterns are analysed using the radar images. This comparison allows identifying the weaknesses of the gauge and radar datasets.

The maximum at Humain has been observed by both the radar and the gauge on 7 June 2016. This relatively high value can be due to randomness and the

Table 5.2: Comparison of the 10 highest 1-hour rainfall extremes from the gauge (AWS) and radar (QPE) at Humain and Uccle stations. The events with a high probability of hail have their number in bold. The events are ordered by the maximum of the gauge and radar values.

Humain

Event	Date	Time	Gauge [mm/h]	Radar [mm/h]
1	2016-06-07	18:50	57.65	45.25
2	2005-07-30	00:40	28.60	11.62
3	2014-04-24	15:40	27.00	20.35
4	2014-06-10	21:40	15.60	26.40
5	2007-06-14	01:20	25.80	16.32
6	2009-05-25	13:10	24.10	25.17
7	2008-05-14	17:40	13.10	24.35
8	2015-07-19	01:00	22.87	15.47
9	2009-06-27	14:30	20.40	19.83
10	2009-07-22	21:20	19.80	12.08
11	2010-07-14	15:40	19.80	—
12	2012-06-12	22:20	18.30	15.61
13	2013-03-23	07:40	—	17.30
14	2005-06-28	22:20	—	16.74

Uccle

Event	Date	Time	Gauge [mm/h]	Radar [mm/h]
1	2016-06-07	15:20	18.08	38.21
2	2011-08-23	08:40	35.50	23.22
3	2009-10-07	18:40	30.79	33.32
4	2012-05-20	16:30	12.37	29.79
5	2005-09-10	19:40	29.10	17.54
6	2011-08-18	15:50	28.98	14.77
7	2007-06-14	14:50	21.90	25.88
8	2011-09-03	22:40	25.34	18.46
9	2016-06-11	18:50	—	24.88
10	2005-07-29	19:10	24.29	—
11	2010-07-14	15:20	24.15	—
12	2014-07-29	16:10	20.10	18.17
13	2013-07-27	22:20	20.07	—
14	2008-07-26	10:40	16.60	18.30

Table 5.3: Results of the extreme value distribution fitting at two locations of the AWS network. The tables shows successively the temporal independence, optimal rank, the location parameter and the scale parameter. A value is indicated as missing when its extreme rank is below 30

temporal independence [%]

Station	Gauge	CAP	QPE	MFB
Humain	25.6	20.7	22.6	–
Uccle	20.8	19.4	21.0	–

optimal rank

Station	Gauge	CAP	QPE	MFB
Humain	30	30	28	–
Uccle	29	23	30	–

location parameter [mm/hour]

Station	Gauge	CAP	QPE	MFB
Humain	12.2	11.0	10.7	–
Uccle	12.3	13.9	12.3	–

scale parameter

Station	Gauge	CAP	QPE	MFB
Humain	7.5	8.9	6.6	–
Uccle	6.8	10.8	6.4	–

short period of records. But it is also possible that the other quantiles are underestimated (the maximum was recorded by the new weighted gauge). There is generally a good match between the radar and the gauge quantiles except for the following events :

- event 2 : the radar underestimates globally
- event 7 : the gauge is located at the boundary of the convective cell
- event 11 : the radar signal is strongly attenuated by a mesoscale convective system.
- event 13 : there was probably snow in the gauge
- event 14 : the gauge is located at the boundary of a convective cell.

The second highest quantile at Uccle has been observed by both the radar and the gauge on the 7th of October 2009. There is generally a good match between the two datasets. A few events are problematic :

- event 1,4 : the gauge is at the boundary of a cell
- event 9 : there is a stationary storm underestimated by the gauge
- event 10 : the gauge is at the boundary of a cell and the radar is attenuated (same as event 2 in Humain)
- event 11 : the radar signal is strongly attenuated (same as event 11 in Humain)
- event 13 : the radar is attenuated

The problems with cell boundaries are easily explained : the radar estimation is taken at a given height above ground and the rain is subject to wind drift before reaching the ground. This effect increases with the distance to the radar. Due to its randomness, it should not affect the statistics. The other problematic events can be considered as missing data. Since the level of missingness is limited, the impact on the statistics is expected to be small.

Figure 5.2 shows the results of the extreme value analysis for 1 h rainfall accumulation. The return levels are obtained using formulas from Willems et al. (2007) which are based on the Weibull plotting position. Numerical values of the temporal independence, the optimal rank, the location parameter and the scale parameter can be found in table 5.3. The percentage of independent peaks (among peaks exceeding the threshold) is around 20 % for both the radar and the gauges at the two locations. This low value is mainly due to the fact that 5 consecutive values at 10 min resolution are correlated.

The empirical quantiles of the QPE product are systematically slightly lower than those for the AWS gauges. This may be expected as we compare point rainfall observations with rainfall averaged on a 1 km square. However, the underestimation of very high rainfall rate by tipping-bucket gauges can compensate for this effect. One also notes small groups of similar values for both the radar and the gauge, which are mainly associated with hail events. This can be explained by the effect of hail threshold and the rainfall rate limit, respectively. The extremes tend to be heavy tailed but this can be at least partially explained by the observation biases described above.

The fit of the EXP distribution is relatively good for the two locations with a relatively low MSE (not shown). The scale parameter tends to be higher for the gauge data than the radar data. In general, the uncertainty for the scale

parameter remains high and this results in wide confidence intervals for higher return periods.

When using the CAP product, the higher quantiles are overestimated especially for Uccle. This can be mainly attributed to the effect of hail. This results in an overestimation of the scale parameter.

5.3.3 Comparison of 24h extremes

The comparison of the 10 highest extremes from either the radar (MFB) or the gauge (SPW) can be seen in table 5.4. For Uccle, most extreme values occurred during summer and are therefore associated with convective storms. There is a good match between the gauge and the radar except for a few events:

- event 8, 11 : the gauge is at the boundary of a convective cell
- event 13 : strong radar attenuation by a mesoscale convective system
- event 14 : snow episode probably underestimated by the radar

For Saint-Vith, the extreme values occurred either in summer or in winter with therefore a mix of convective and widespread precipitation episodes. The match is very good except for the following events :

- event 2 : at the boundary of a cell (probably with hail)
- event 3 : slight overestimation due to snow melting (QPE) ; overestimation due to non-uniform bias (MFB)
- event 13 : at the boundary of a cell

The problematic events not related to boundary effects can be considered as missing data. Since they are limited it is expected that they only slightly affect the statistics.

Figure 5.3 shows the results of the extreme value analysis for the 24 h rainfall accumulation. Numerical values can be found in table 5.5. The percentage of independent peaks (amongst peaks exceeding the threshold) is between 6 % and 9 % for the two locations and for all datasets. This is what we expect from 24 h accumulation available every hour.

For Uccle there are not many differences between QPE and MFB because most events are associated with convective storms. Compared to the gauge quantiles,

Table 5.4: Comparison of the 10 highest 24-hour rainfall extremes from the gauge (SPW) and radar (MFB) at Uccle and Saint-Vith stations. A value is indicated as missing when its extreme rank is below 30. The events are ordered by the maximum of the gauge and radar values.

Uccle

Event	Date	Time (end)	Gauge [mm/24h]	Radar [mm/24h]
1	2010-08-16	23:00	63.30	48.99
2	2009-10-07	23:00	52.50	61.83
3	2011-08-23	15:00	59.31	61.00
4	2006-08-03	23:00	43.00	58.44
5	2016-05-30	23:00	35.30	53.34
6	2014-08-26	15:00	45.30	48.51
7	2012-10-04	08:00	34.60	45.63
8	2012-06-12	11:00	—	44.87
9	2016-06-12	17:00	31.30	39.45
10	2011-09-04	21:00	38.70	26.10
11	2015-08-16	03:00	—	37.75
12	2007-06-15	11:00	36.99	33.91
13	2014-07-10	04:00	36.90	—
14	2016-01-16	02:00	36.30	—

Saint-Vith

Event	Date	Time (end)	Gauge [mm/24h]	Radar [mm/24h]
1	2007-01-18	16:00	74.60	56.88
2	2009-07-03	16:00	37.90	61.68
3	2011-12-16	23:00	—	56.62
4	2012-07-28	21:00	53.60	46.72
5	2012-10-04	12:00	49.70	39.86
6	2007-08-22	19:00	47.50	48.73
7	2010-08-16	03:00	45.80	55.50
8	2006-08-05	06:00	43.70	41.10
9	2007-12-03	08:00	43.40	46.09
10	2007-09-28	08:00	42.40	38.87
11	2014-09-21	14:00	34.00	40.71
12	2016-05-31	02:00	40.01	33.44
12	2016-07-23	21:00	40.00	—

Table 5.5: Results of the extreme value distribution fitting at two locations of the SPW network. The tables shows successively the temporal independence, optimal rank, the location parameter and the scale parameter.

temporal independence [%]

Station	Gauge	CAP	QPE	MFB
Uccle	7.1	6.0	6.6	6.7
St-Vith	7.4	8.4	9.0	8.4

optimal rank

Station	Gauge	CAP	QPE	MFB
Uccle	30	26	19	23
St-Vith	30	30	30	28

location parameter [mm/24h]

Station	Gauge	CAP	QPE	MFB
Uccle	27.2	25.0	27.2	27.5
St-Vith	30.2	25.8	26.3	31.5

scale parameter [mm/24h]

Station	Gauge	CAP	QPE	MFB
Uccle	9.0	13.5	12.7	12.9
St-Vith	8.9	8.2	6.9	9.1

the radar quantiles are lower below 1-year and higher between 1-year and 5-year return periods. This can be attributed mainly to hail overestimation by the radar and gauge losses. It results in a higher scale for the radar, which is close the upper bound of the gauge confidence interval.

For Saint-Vith, there is a clear effect of the MFB method to remove the underestimation of the QPE product. As for Uccle, the radar quantiles are higher for return periods higher than 2 years but the effect is limited because less convective storms are involved. The final result is a good match of the two distributions for this station.

For the two stations, no significant instability in the MFB values have been found.

For Uccle, the CAP product overestimates the scale parameter and underestimates the location parameter due to hail and VPR errors, respectively. For Saint-Vith, the quantiles (not shown) are similar to QPE except for a very high

unrealistic maximum.

5.4 Regional frequency analysis

5.4.1 Methodology

As in Overeem et al. (2009a) and Wright et al. (2014b) we consider that the extreme statistics are the same within the region. The region should be sufficiently large to have a large sample size (many extremes) and small enough to neglect extreme statistics variability. No strong variability is expected in Belgium because it is a relatively flat country. Therefore we define our region as the radius of 20 km around the target location. A similar size has been used in other radar studies (e.g., Overeem et al., 2009a; Wright et al., 2014b; Eldardiry et al., 2015).

We also consider that the extremes observed within the 20 km radius during a time window of 12 h are dependent. As in Wright et al. (2014b), we keep only the maximum amongst dependent values. We therefore implicitely assume that the regional maximum follows the same distribution as the local extremes. The possible benefit of taking one extreme value at random is an open question. It is important to remind that we are interested in the extreme statistics of any given pixel in the region. This is different from studying the extreme statistics of the maximum rainfall over the region as in Panziera et al. (2016). We also tested the hypothesis that 1 hour extremes are independent after a certain distance which is set to 10 km. This distance corresponds to the maximum expected size of a convective cell (see chapter 3). If this is true it allows to reduce the uncertainty of the analysis. In the text, we will refer to these datasets by the names REG and R10, respectively.

Due to the spatial dependence, the effective length n_{eff} of the pooled time-series is smaller than the total length of the records. The total length is obtained by multiplying the number of years n by the number of pixels N :

$$n_{max} = n \times N. \tag{5.4}$$

In this study n_{eff} is computed by multiplying n_{max} by the fraction of spatially independent peaks, amongst peaks exceeding the threshold. The latter is obtained by dividing the number of independent peaks by the total number of peaks. It can be shown that this is the same as the method based on the averaged exceedence rate found in Wright et al. (2014b) and explained in details by Weiss et al. (2014). The large number of peaks available from the radar data allows us to choose a higher threshold rank. This increase in sample size

Table 5.6: Results of the extreme value distribution fitting for the regional frequency analysis. The tables shows successively the independence (temporal or spatial), the optimal rank, the location parameter and the scale parameter.

independence [%]

Station	QPE	BUL	R50	R10
Deurne	–	27.5	1.4	2.6
Uccle	–	28.0	1.1	2.6
Gosselies	–	22.2	1.7	3.9
Nadrin	–	19.9	2.6	7.0

optimal rank [%]

Station	QPE	BUL	R50	R10
Deurne	28	22	100	99
Uccle	30	30	70	88
Gosselies	29	30	96	90
Nadrin	23	30	100	91

location parameter [mm/hour]

Station	QPE	BUL	R50	R10
Deurne	10.8	16.7	16.5	20.0
Uccle	11.5	17.5	21.1	24.2
Gosselies	11.9	15.2	20.4	26.5
Nadrin	12.2	12.9	21.0	29.0

scale parameter [mm/hour]

Station	QPE	BUL	R50	R10
Deurne	4.7	5.7	8.0	7.3
Uccle	6.4	4.4	11.7	10.7
Gosselies	6.4	8.7	10.1	8.6
Nadrin	6.1	9.3	11.7	9.5

leads to a more reliable extreme value analysis, which is the final goal of this radar-based RFA. Accordingly the QQR method is applied for threshold ranks between 30 and 100 and the optimal rank is found.

5.4.2 Comparison with rain gauges

Figure 5.4 and 5.5 shows the results of the regional frequency analysis for 1 h rainfall accumulation at the 4 locations selected from the BUL network. The results of the at-site frequency analysis for the gauge and collocated radar pixels are showed as reference. Numerical values can be found in table 5.6. The percentage of temporally independent extremes for the gauge is close to 30 % for Deurne and Uccle while it is slightly above 20 % for the two others stations. This suggests that there are larger clusters which might be related to altitude. Above the threshold, the percentage of spatially independent extremes (REG) ranges from 1.1 % (Uccle) to 2.6 % (Nadrin). The effective period length of the pooled dataset is then between 200 and 500 years. Using a decorrelation distance of 10 km results in twice more data, which is more than one expects from randomness. It suggests that convection can be organised at large spatial scales.

The radar images associated with each maximum of the radar-based RFA is analysed :

- Deurne and Uccle (28 July 2006) : several supercells on the whole of Belgium
- Gosselies (22 August 2011) : a squall line moving parallel to the flow
- Nadrin (26 July 2008) : a stationary convective cell

The highest extremes exhibit abrupt variations in the form of steps for both the gauge and radar. This could be explained by the siphonage of the gauge and hail threshold, respectively. Since Nadrin is close to the radar, the standard Z-R relationship is used instead of the convective Z-R relationship. This permits higher rain rates (i.e. 100 mm/hour).

The gauge extremes are relatively low at Deurne and Uccle compared to Nadrin and Gosselies. The radar extremes are lower at Deurne compared to the other stations. This can be at least partially attributed to the large sample volume at this range. The match between the gauge and the radar REG and R10) is good except at Uccle with much higher radar extremes. The REG exhibits higher extremes than R10 suggesting some dependence beyond 10 km. Indeed the results should be similar if the hypothesis of independence after 10 km was valid.

This can be partially attributed to hail but the similar 4 highest extremes suggest a gauge limitation. It is also striking that half of the 20 highest gauge extremes occurred during the period 1999-2008 (not shown). This positive

trend for Uccle is possibly related to the urban heat island effect (Hamdi and Van de Vyver, 2011). The uncertainty of the radar fit is low because of the larger sample size, due to which a higher rank can be chosen. Furthermore, the fit is less impacted by the potentially large errors of the highest extremes. The location parameter (corresponding to the threshold) increases with the sample size of the products.

Except for the Uccle station, the scale parameter is the lowest for the QPE dataset due to the bias as a result of the small sample size. The scale parameter of the pooled radar datasets is slightly higher at Deurne and significantly higher in Uccle. For Gosselies and Nadrin, the R10 and BUL data have similar scales while it is slightly higher for the REG data. The fit to the REG and R10 data is within the uncertainty bound of the fit to the BUL data. For those two stations, the fit to the BUL data is even in the small uncertainty bound of the fit to the REG data.

5.4.3 Spatial maps

We apply the regional frequency analysis described above for 1 hour duration to all pixel locations in Belgium with some modifications. We use a smaller radius of 10 km to reduce the computation cost and consider that all pixels are spatially dependent. This smaller radius improves the resolution of the maps at the expense of a higher uncertainty. Several pixels in the radar dataset are affected by permanent non-meteorological echoes. They can be identified by an unrealistic high frequency of extremes. In practice one looks at the distribution of the number of values exceeding 12 mm/hour. The pixels with more than 50 exceedances have been found as outliers and removed. To make the comparison easier, we choose a fixed threshold rank of 60. No larger ranks have been considered due to computational limitations.

Figure 5.6 shows the results of the regional frequency analysis applied to Belgium. The provinces of Belgium are also displayed to help comparison between the maps. No values are shown beyond the 180 km range because the quality of the radar QPE is significantly reduced. The return periods are computed using equation 5.3 and therefore depends on the scale parameter and the effective length. The higher the scale the higher the difference between the 10-year and 100-year return levels.

Some artifacts due to the radar and the regional approach can be seen on the maps. The effective length decreases significantly beyond 100 km meaning that the spatial dependence increases. This is due to the fact that the actual radar sample is larger than the 1 km pixel at those ranges. Circular patterns appear on the maps due to the influence of the pixels located at their centers. The high

values are caused by pixels contaminated by non-meteorological echoes (e.g. at the German border) and hail. A stronger filter for non-meteorological echoes is not used because it could remove actual precipitation information. The circular effect might be reduced by using a larger radius or a higher threshold rank but this is computationally expensive. Areas with a 10-year return level exceeding 30 mm are mainly located beyond 100 km. This is probably due to an increased contamination by hail with the distance to the radar (and the height of the measurements). The small scale variability in the study area can be explained by uncertainties due to the sample size.

There is some correlation between the 10-year return level and the scale parameter. Therefore the spatial patterns between the two return periods are similar. Within the 100 km radius, the maps are only slightly influenced by the topography and the mean annual rainfall (Journée et al., 2015). This suggests that applying our regional approach is valid, at least for 1 h duration. Van de Vyver (2012) obtained slightly lower values for the 10-year return level but slightly higher 100-year return level due to the positive shape parameter. One notes that the scale is very high around the Brussels region where the Uccle station is located.

5.5 Conclusions

5.5.1 Results

The potential of a radar-based precipitation datasets to study extreme rainfall at a given location is evaluated. The QPE is obtained by a careful processing of the volumetric reflectivity measurements from a single weather radar in Belgium. The radar dataset covers the period 2005-2016, has a resolution of 1 km, and is available every 5 minutes.

The first evaluation is based on a comparison of the extreme statistics between the radar dataset and two automatic raingauge networks with 10 min and 1 h resolution, respectively. For each network, two locations are chosen to study sliding 1 h and 24 h extremes using the collocated radar estimation. A regression method in Q-Q plots is used to fit an exponential distribution to independent peaks. This method has the property to focus on tail of the extreme value distribution, which is of interest when studying extremes. An optimal threshold rank is selected by minimising the MSE of the regression.

The 10 highest 1 h extremes occurred in summer and are well captured by both the radar and the gauge. A few problematic events are caused by wind drift or severe radar signal attenuation and should be considered as missing

data. Differences up to 30 % between the gauge and radar values are observed and can be explained by spatial sampling and estimation errors. The radar extremes tend to be lower than the gauge extremes especially for short return periods. This is consistent with the results of Peleg et al. (2016) on the small scale spatial variability of extreme rainfall. In particular, tipping bucket gauges underestimate heavy rainfall rate and can be blocked by accumulated snow. The radar underestimates due to signal attenuation and overestimates in case of hail. Additional radar uncertainties come from time sampling and the Z-R relationship. Despite the uncertainties in the datasets, the fitting of the exponential distribution to the QPE product is within the large uncertainty bound of the AWS one. This result is in accordance with the fact that the temporal variability (related to the sample size) is higher than the spatial variability (Peleg et al., 2017).

For 24 h accumulation there is a mix of summer and winter events, with more of the latter for stations with higher altitude. There is a clear benefit of bias correction for the highest station, making the distribution fits similar for both stations. For both 1 h and 24 h accumulations, the basic radar product exhibits unrealistic high extremes, which results in an overestimated scale parameter. Such product is therefore not suitable for an extreme value analysis.

In the second evaluation a regional frequency analysis is applied to 1 h radar data at the location of 4 pluviographs with recordings from 1965 to 2010. Spatially independent extremes within a circle of 20 km are selected using a novel approach. They are fitted with a maximum threshold rank extended from 30 to 100 thanks to the increased sample size. There is a good agreement between the radar and the gauge for the two closest stations. The most important result is that the uncertainty is significantly lower using the available radar data. The extremes are lower when a decorrelation distance of 10 km is assumed suggesting that this hypothesis is not valid. In Brussels, the radar extremes are significantly higher than the gauge rainfall extremes; but similar to these observed by an automatic gauge during the same period. This can be attributed partially to radar overestimation due to hail and gauge underestimations, but the increasing urban heat island effect and iis possible impact on convective precipitation should not be ruled out. The decreasing tail of the radar extremes is at least partially caused by hail threshold but a physical limit for the Belgium climate could play a role.

For each of the rain gauge networks, only a few stations have been selected and presented in this study. The results from these stations are representative of the variability of the results obtained from the other stations.

The regional approach has been applied all over the study area using a 10 km radius and a fixed threshold rank of 60. The extreme statistics for 1 h duration

are slightly influenced by the topography. The reliability of the radar results beyond the 100 km range is questionable.

5.5.2 Prospects

There is still some room to improve the quality of the radar and gauge datasets. The recently installed weighting gauges are able to cope with intense rainfall and snowfall. One will have to wait a few decades before it can produce reliable statistics. Radar calibration errors can be mitigated by computing a monthly bias using rain gauges. The attenuation can be solved easily by using other radars when available. To avoid overestimation of the extremes, an advection correction can be used for the time sampling error. Dual-polarization radars can potentially provide better estimation for high rainfall rates (Figueras-Ventura and Tabary, 2013). However uncertainties related to relation between the radar measurements and the rainfall rate remain, especially in case of hail. In this study we considered all data as the amount of liquid water at the ground. For some applications it could be necessary to take the melting of snow and hail into account. Identification of hail at ground level is a challenging problem using radar and ground station networks (Lukach et al., 2017).

Since the study focuses on comparison between radar and rain gauges, the extreme value analysis has been kept simple. While the EXP distribution was found to fit generally well with the empirical data, the generalised Pareto distribution should be considered as well for the regional frequency analysis. The analysis of longer durations can be refined by taking into consideration the effect of the type of rainfall (e.g., Rulfova et al., 2014; Panziera et al., 2016). A bias correction should also be considered for a proper handling of the asymptotic behavior of the distribution (Willems et al., 2007).

The extreme value theory was applied to the radar datasets by removing the spatially dependent extremes in the region of analysis. This is performed using a simple technique based on a decorellation distance. Evin et al. (2016) decided not to use such method because it reduces the sample size. Better performance are expected using recently proposed statistical models (Buishand et al., 2008; Davison et al., 2012).

The radar-based regional frequency analysis can be extended to other durations to derive IDF curves. Note that the hypothesis of constant parameter over the region might not be valid for longer durations. In many applications in hydrology, it is the averaged rainfall over a given area which is relevant. A popular technique is to apply areal reduction factors to point-based statistics. The radar dataset can be used directly to derive areal rainfall statistics (e.g., Durrans et al., 2002; Overeem et al., 2010; Wright et al., 2014a).

Acknowledgements

The authors would like to thank Francesco Marra, Luca Panziera and Referee #3 for their very constructive comments which allowed us to significantly improve the quality of the text. We thank the hydrological service of the Walloon region for providing their rain gauge data. The comments of Michel Journee and Hans Van de Vyver are highly appreciated.

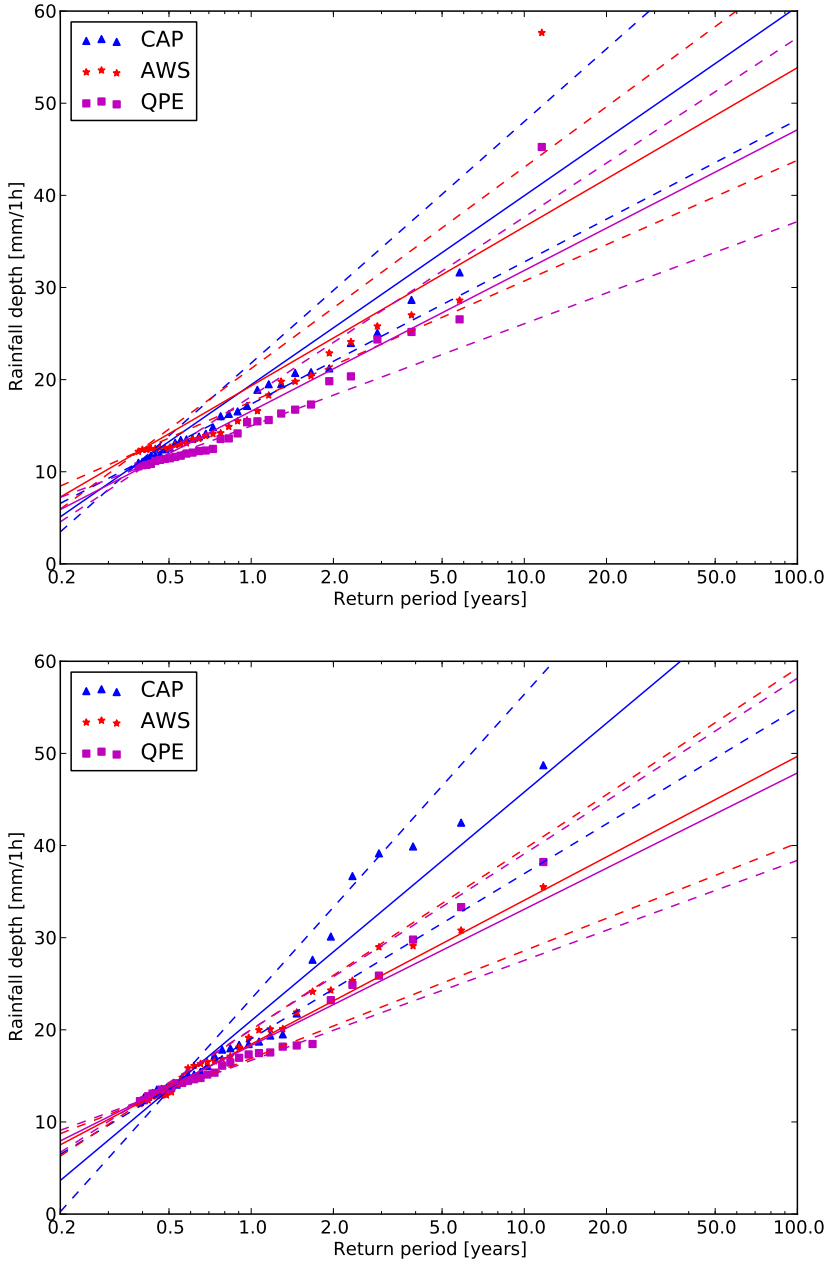

Figure 5.2: Return levels for 1-hour duration at location Humain (top) and Uccle (bottom) of the AWS gauge (red stars) compared to CAP (blue triangles) and QPE (magenta squares) radar products. The extreme value distribution (solid line) fitted to the extremes and its confidence intervals (dashed line) are also displayed.

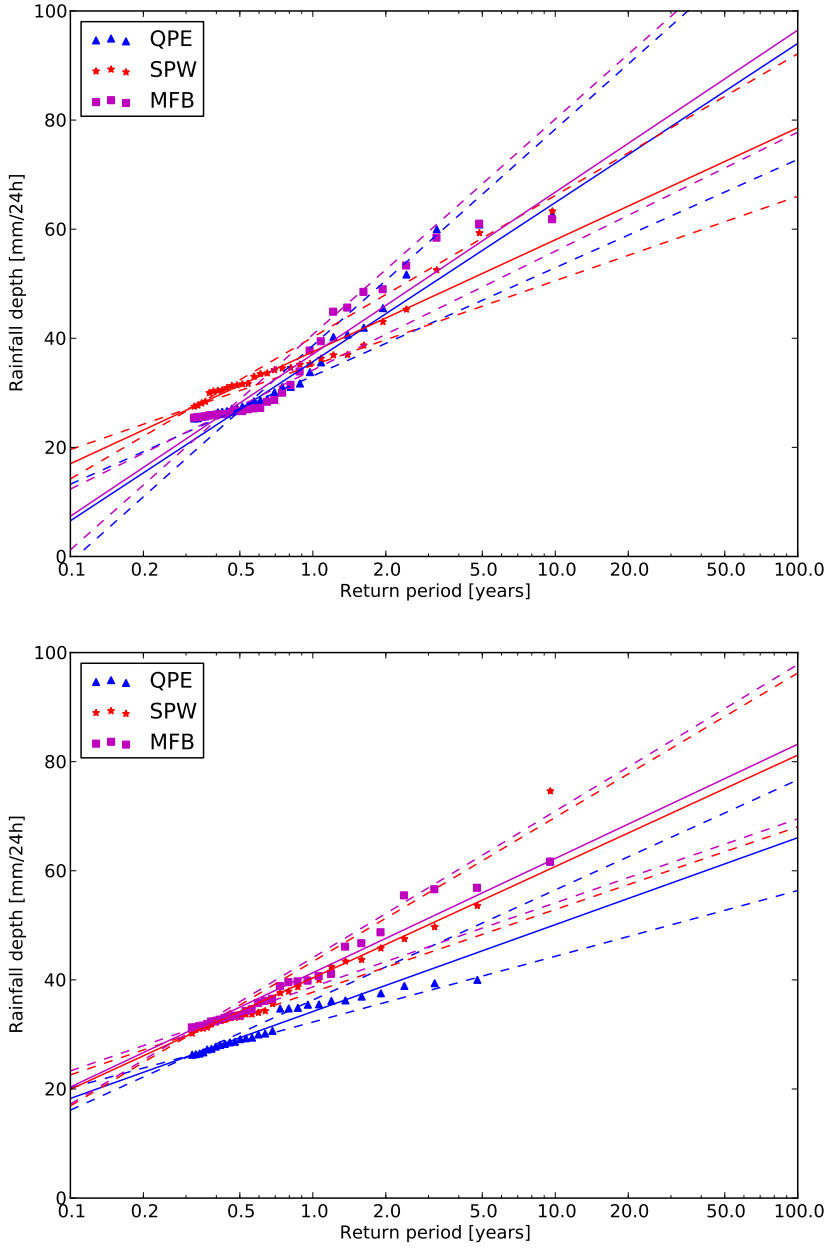

Figure 5.3: Return levels for 24-hour duration at location Uccle (top) and Saint-Vith (bottom) of the SPW gauge (red stars) compared to QPE (blue triangles) and MFB (magenta squares) radar products. The extreme value distribution (solid line) fitted to the extremes and its confidence intervals (dashed line) are also displayed.

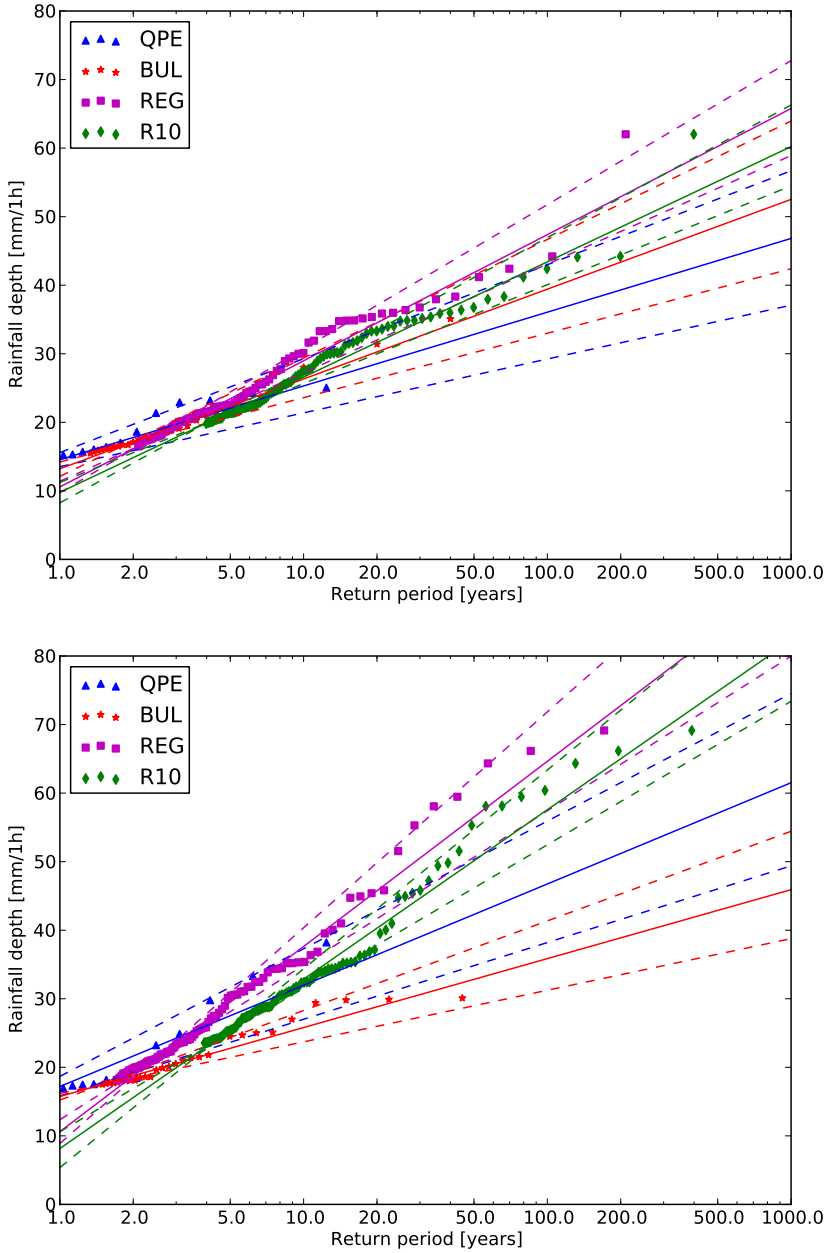

Figure 5.4: Return levels for 1 hour duration at location Deurne (top) and Uccle (bottom) from the BUL gauge data (red stars) compared to the at-site QPE (blue triangle), REG (purple square) and R10 (green diamond) radar data. The extreme value distribution (solid line) fitted to the extremes and its confidence intervals (dashed line) are also displayed.

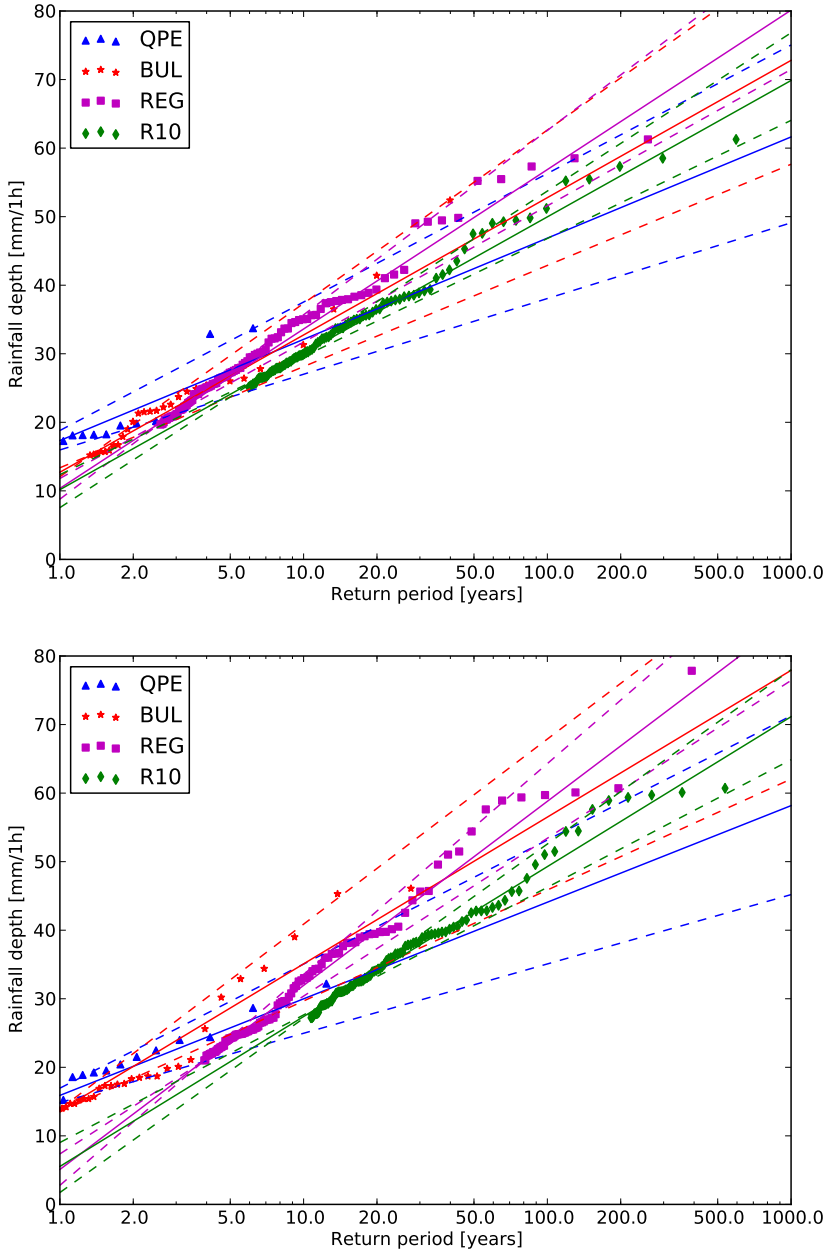

Figure 5.5: Return levels for 1 hour duration at location Gosselies (top) and Nadrin (bottom) from the BUL gauge data (red stars) compared to the QPE (blue triangle), REG (purple square) and R10 (green diamond) radar data. The extreme value distribution (solid line) fitted to the extremes and its confidence intervals (dashed line) are also displayed.

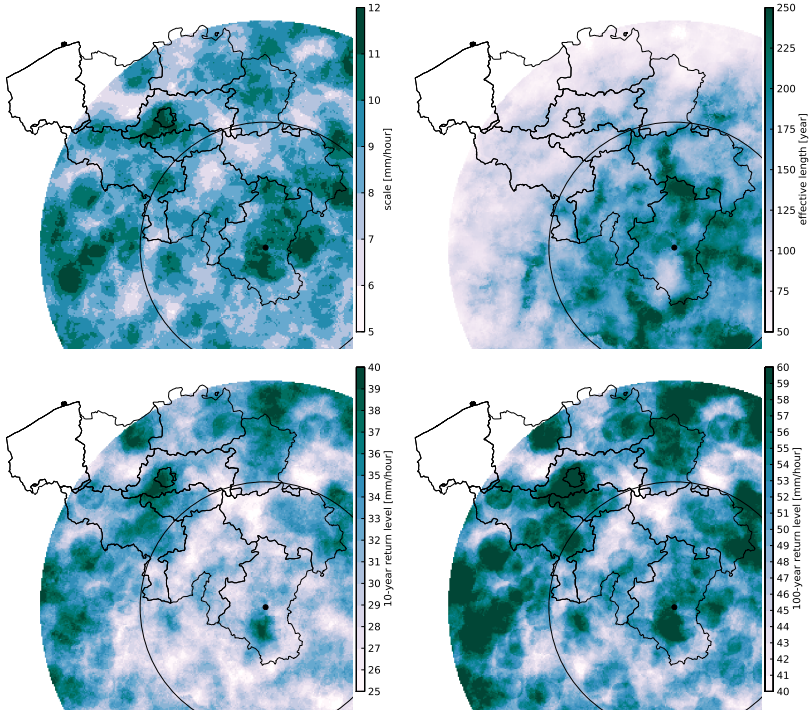

Figure 5.6: Results of the regional frequency analysis for 1 hour duration applied over Belgium up to 180 km from the radar. The scale parameter and the effective length are showned in the top panel. The levels coresponding to a 10-year and 100-year return periods are shown in the bottom panel. A circle with a radius of 100 km centred at the radar is also drawn.

Chapter 6

Conclusions

6.1 Results

6.1.1 How best to combine radar and rain gauge observations?

Several methods combining 24 h gauge measurements and basic radar estimates have been evaluated against an independent gauge network. For the period 2005-2008, a simple bias correction significantly reduces the mean absolute difference. The spatial methods further improve the performance if the rain gauge network density is sufficiently high. The kriging with external drift (KED) method is the best for all months of the year and the added value of the radar is clear in summer. For the sake of simplicity a linear variogram is used for the KED method in chapter 2. In chapter 4, the merging is performed on 1 hour accumulation using the mean field bias (MFB) and KED methods. The latter uses a square root transformation and a spherical variogram. While these two methods are compared, it would have been interesting to test the other methods as well.

In recent studies variants of the KED method have been proposed and compared (e.g., Sideris et al., 2013; Berndt et al., 2014; Jewell and Gaussiat, 2015). While Kriging methods perform well in general, they could suffer from conditional bias in case of heavy rainfall and special methods have been proposed by Kim et al. (2016). The main limitation of merging radar and gauge data remains their uncertainties and the large sampling difference. Solutions for these problems have been proposed recently (e.g., Delrieu et al., 2014; Pulkkinen et al., 2016).

6.1.2 What are the characteristics of convective storms in Belgium ?

Convective storm tracks from a 10-year radar volumetric dataset have been analysed in a comprehensive and unprecedented manner. Most convective storms are organised in clusters of convective cells while mesoscale convective systems (MCSs) are rare. At a given location there is a convective storm 6 hours per year on average. The convective activity, which exhibits large interannual variability, has a higher probability in summer and in the afternoon. There are small spatial variations of the convective activity related to topography. The convective activity is generally weak in the study area. For a reference area of $1 \times 10^4\,\mathrm{km}^2$, it is characterised by :

- more than 3 cells, preferably in June and in the early afternoon
- an area coverage exceeding 3 percents, preferably in July and in the evening
- a total water mass higher than 1 Tg, preferably in July and in the late afternoon.

during 20 hours per year (not simultaneously for the three characteristics). The individual convective cells are mostly small and weak. The extreme convective cells, with a total cumulative duration of 40 hours per year in an area of $1 \times 10^4\,\mathrm{km}^2$, have the following characteristics :

- a volume exceeding $2000\,\mathrm{km}^3$, preferably in June-July and in the late afternoon
- an echo-top above 10 km, preferably in June-July and in the late afternoon
- a mass above 3 Tg, preferably in July and in the late afternoon.

Convective cells last 25 min on average with a median speed of $30\,\mathrm{kmh}^{-1}$ and preferably towards northeast.

A shift of frequency for MCS's towards evening related to strong deep-layer shear has been found by Kaltenboeck and Steinheimer (2015) in Austria. This is consistent with our results on extreme area and water mass which are caused by MCS's. Puskeiler et al. (2016) show the distribution of 2631 storm tracks from hail days during 2005-2011 in Germany. They found patterns relatively similar to the ones of our probability of convective activity but with higher gradients. The maximum convective activity (caused by MCS's) in summer is consistent

with other studies in Europe (e.g., Lewis and Gray, 2010; Punkka and Bister, 2015). The statistics are presented for all storms because a classification into weather regimes like in Peter et al. (2015) is rather subjective.

6.1.3 How to obtain the best rainfall estimation from volumetric radar measurements?

Radar rainfall estimation has been generated for 10 years and verified against independent rain gauges using various statistics. A selection of cases with different weather regimes has been useful to tune the algorithms. Significant improvements in robustness and performance compared to a basic estimation is obtained up to 150 km from the radar. The benefits are mainly due to the vertical profile of reflectivity (VPR) correction and the radar-gauge merging methods. They are slightly higher when considering higher rainfall amounts. Most radar artifacts appearing on statistical maps are mitigated by the removal of non-meteorological echoes and the hail threshold.

To the author's knowledge, there are no similar verification studies of high resolution precipitation estimates available for comparison. Nelson et al. (2016) found for the period 2002-12 that the US hourly quantitative precipitation estimation (QPE) datasets are useful for moderate-high precipitation amounts and benefit from mean field bias but they suffer from bad gauge reports. The US operational QPE has characteristics similar to the ones of the QPE developed in this thesis with a robust VPR correction and different merging methods (Zhang et al., 2016). A local bias correction using a dense network, as done in this thesis, is needed to capture the orographic enhancement of precipitation (Meersmans et al., 2016).

6.1.4 What is the potential of radar rainfall estimates for extreme value analysis?

A 12-year radar-based rainfall dataset has been tested for the study of extreme values at a given location. New insights have been obtained thanks to the quality of the rainfall datasets and the detailed comparative analysis. At the location of automatic gauges, a few discrepancies for 1 h and 24 h extremes are attributed to observation errors and sub-pixel variability. An exponential distribution is fitted to gauge or radar extremes using a quantile-quantile regression method. The results are consistent given the high uncertainty associated with the short record length. A new regional method is applied to 1 h radar extremes using independent values within 20 km distance from the target

location. The uncertainty of the model is very small due to the significantly higher sample size of the radar data. Within 100 km of the radar, the results are similar at the location of rain gauge with more than 40 years of records. Slight spatial variations of the extremes related to topography are found in Belgium.

The results can be compared with the ones of gauge-based studies for Belgium. Mohymont and Demarée (2006) provided return level maps by interpolation of the station distribution parameters. They obtained significant spatial variations which can be attributed to the sample size. The spatial model of Van de Vyver (2012) based on topography gives a smoother result with smaller errors. For 1 hour extremes the model is not consistent for 3 out of 18 gauge stations. Radar studies of rainfall extremes are still very limited in Europe. For the Netherlands, Overeem et al. (2009a) found 20-year return levels ranging mainly from 25 mm to 35 mm but more areas with higher values. This can be explained by the short sample size and probably more radar artifacts. All these studies use a significantly positive (i.e. higher than 1) shape parameter for 1 hour extremes resulting in higher return levels for higher return periods.

6.2 Implications

6.2.1 Availability of precipitation observations

A good spatial coverage is needed to obtain robust results over the region of interest. While Belgium is relatively well covered by dense rain gauge networks, the effective range of the Wideumont radar is limited. Other radars need to be considered to obtain reliable results for the whole Belgium. It would be also interesting to verify the rainfall estimation against climatological stations from France, Germany and the Netherlands.

Missing values in our datasets impact our results depending on the amount of missing data, the mechanisms behind missing data and the type of statistical analysis (Molenberghs et al., 2014). The missing data appear independent from the precipitation characteristics and therefore no complex sensitivity analysis is required. Since radar failures appear randomly and for a short period of time, they do not impact the results. However, the 15 consecutive missing days in October 2013 due to an archive problem, can slightly affect the results of chapters 4 and 5. To avoid a selection bias when computing the annual totals, the mean of the monthly means is used in Fig 4.10. To obtain more robust results, one could use multiple imputation techniques. More efforts should be made in preserving archived data than in dealing with missing data.

6.2.2 Quality of the precipitation observations

The robustness of our statistical analysis depends on the quality of the precipitation observations. One can assume that corrupted data are unlikely with the Wideumont radar due to its hardware and software stability. However, the impact of the calibration on the accuracy of the radar measurements should not be neglected. Besides, a few problems with the quality control of recent rain gauge data have been discovered. It is important for further studies to always check the validity of the quality control. The quality control of the volumetric radar measurements developed in chapter 4 could be considered to enhance the statistical analysis of convective storms (chapter 3).

The uncertainty associated with our results is directly related to the length of the records and the amount of data with good quality. The length of our datasets has been increased to 12 years in chapter 5. It is possible to refine the results obtained in chapters 2, 3, 4, 5 by using the data available every new year. Of course, one should ensure that the quality of the measurements remains stable. The results associated with extreme events or phenomena spanning over a large time scale require several decades of data to be validated.

6.2.3 Radar rainfall estimation

While significant efforts have been made in this thesis to obtain the best rainfall estimation, there is some room for improvements. Calibration errors could be removed by using monthly bias corrections. In particular extreme rainfall estimation could benefit from a temporal sampling correction and refined hail scheme (Lukach et al., 2017). Applying a detailed error correction for specific events like in Hazenberg et al. (2014) should be considered as well.

The estimation of the water equivalent of snow precipitation remains a big challenge (Saltikoff et al., 2015). The rain gauge values were not used for merging if snow was identified during the quality control. If the bright band (BB) can be identified in the radar data, typically in case of melting snow, the water equivalent is estimated. If no BB can be estimated, the lowest value of the profile is used as reference. This means that underestimation, in case of dry snow, or overestimation, in case of melting snow, can occur.

Precipitation can be highly variable in time and space at all scales. For water management, the requirements depend on the space-time dynamics of the hydrological or hydraulic system. The rainfall dataset has a resolution of 5 minutes and 1 km, which is sufficient for most river catchments. For urban water applications, higher spatial and temporal resolutions are needed due to the small

scale of the processes. For a given spatial resolution, the temporal resolution required is related to the dynamic of the rainfall field and the response time of the water system to the rainfall. The characteristics of convective cells have been studied extensively in Chapter 3. With an average speed of $30\,\mathrm{km h^{-1}}$, a cell is already shifted by 2.5 km in 5 minutes. For the 5 % of cell exceeding $60\,\mathrm{km h^{-1}}$, a time resolution of less than 1 minute is required for a spatial resolution of 1 km. With some trade-off regarding the volume coverage, it would be possible to add a low elevation in the scanning strategy of the radar allowing a repetition time of 2.5 minutes. However a more simple solution is to use advection techniques.

6.2.4 Applications

The weather radar reflectivities have been used for the validation of microphysical schemes in numerical weather prediction (NWP) models (Böhme et al., 2011; Van Weverberg et al., 2011; Van Weverberg et al., 2012; Weverberg et al., 2014). The merging products developed in chapter 2 were used as reference rainfall for the validation of new schemes in NWP modelling (Van Weverberg et al., 2010; Böhme et al., 2011; Van Weverberg et al., 2011; Hamdi et al., 2014) and for the verification of regional climate models (Weverberg et al., 2014; Brisson et al., 2016). Applications outside meteorology are found like the study of air pollutants (de Vos and Zhang, 2012), plant diseases (Mahtour et al., 2011) and soil erosivity. The radar-based QPE has been used for the verification of a nowcasting system (Foresti et al., 2016). Other usages include comparisons with lightning datasets or pollutions of swimming waters.

A radar-based rainfall estimation has been implemented operationally in most European countries in the last decade. The estimation developed in chapter 4 was made for climate studies but with an operational application in mind. Since September 2016, rainfall estimates from 4 radars covering Belgium are available in realtime. Only slight modifications of the algorithms were needed due to different scanning strategies and resolutions. An automatic quality control of the gauge measurements has not been implemented yet though.

6.3 Prospects

6.3.1 QPE uncertainty

Information about the rainfall estimation uncertainty is important for many applications including hydrology (Berne and Krajewski, 2013). The analysis of the uncertainty of radar estimates is difficult because of the absence of ground

truth and the various sources of errors. The results of chapter 4 based on gauge comparisons provide only a limited information about this uncertainty. Different approaches have been proposed in the literature to estimate this uncertainty and propagate it (e.g., Germann et al., 2009; Rossa et al., 2011; Hazenberg et al., 2013). In Belgium, the high density of weather radars could be used to provide uncertainty information without the need for complex methods.

6.3.2 Dual-polarization radar

A dual-polarization radar transmits electromagnetic waves with horizontal and vertical polarization. The amplitudes and phases from the back-scattered signals can be used in several ways to obtain new variables. They can be combined to classify the different types of hydrometeors (rain, graupel, hail, dry snow, wet snow) and to identify non-meteorological echoes. While more and more operational services use echo classification schemes, its verification is limited by the availability of ground truth. This type of radar can potentially provide better estimation for high rainfall rates using the differential phase shift (Figueras-Ventura and Tabary, 2013). The useful range can also be extended since the phase is not affected by signal attenuation. The 5 years of measurements from the Jabbeke radar provide material for research in this field.

6.3.3 Areal intensity duration frequency (IDF) curves

The extreme value analysis presented in this thesis is focused on point rainfall. The area-averaged rainfall is more relevant than point rainfall for many hydrological applications. The full potential of the radar data can be unveiled by studying the extremes of areal rainfall. By repeating the analysis for squares of different size, one can derive areal reduction factors. The analysis can also be done on actual catchment and regionalised using storm transposition techniques (Wright et al., 2013a).

6.3.4 Discharge statistics

The research work offers new possibilities to study discharge extreme statistics. The radar rainfall datasets can be used directly as input to hydrological models. This would also constitute an additional verification of the estimation method. Another possibility is to use the radar extreme rainfall statistics to construct design storms. Design storms could also integrate the convective storm characteristics.

6.3.5 Applications

The results obtained in this thesis can be used for numerous practical applications. The radar rainfall datasets can be used as input to nowcasting systems and hydrological models or as reference for NWP and regional climate models. The statistical characteristics of convective storms could be a nice addition to the climate information provided by the Royal Meteorological Institute of Belgium (RMIB). Finally, the extreme rainfall statistics are useful for warning systems and as input for water management and engineering decision making including the design of hydraulic structures.

Bibliography

Allan, R. P. and I. I. Zveryaev (2011). "Variability in the summer season hydrological cycle over the Atlantic-Europe region 1979-2007". In: *International Journal of Climatology* 31.3, p. 337. DOI: 10.1002/joc.2070.

Arnbjerg-Nielsen, K., P. Willems, J. Olsson, S. Beecham, A. Pathirana, I. B. Gregersen, H. Madsen, and V.-T.-V. Nguyen (2013). "Impacts of climate change on rainfall extremes and urban drainage systems: a review". In: *Water Science & Technology* 68.1, p. 16. DOI: 10.2166/wst.2013.251.

Atlas, D. and C. W. Ulbrich (1990). "Early Foundations of the Measurement of Rainfall by Radar". In: *Radar in Meteorology*, p. 86. DOI: 10.1007/978-1-935704-15-7_12.

Bardet, L., C.-M. Duluc, V. Rebour, and J. L'Her (2011). "Regional frequency analysis of extreme storm surges along the French coast". In: *Natural Hazards and Earth System Sciences* 11, p. 1627. DOI: 10.5194/nhess-11-1627-2011.

Bauer, P., A. Thorpe, and G. Brunet (2015). "The quiet revolution of numerical weather prediction". In: *Nature* 525.7567, p. 47. ISSN: 1476-4687. DOI: 10.1038/nature14956.

Bech, J., U. Gjertsen, and G. Haase (2007). "Modelling weather radar beam propagation and topographical blockage at northern high latitudes". In: *Quarterly Journal of the Royal Meteorological Society* 133.626, p. 1191. DOI: 10.1002/qj.98.

Beek, C. van de, H. Leijnse, P. Torfs, and R. Uijlenhoet (2012). "Seasonal semi-variance of Dutch rainfall at hourly to daily scales". In: *Advances in Water Resources* 45, p. 76. ISSN: 0309-1708. DOI: 10.1016/j.advwatres.2012.03.023.

Bellon, A., G. W. Lee, A. Kilambi, and I. Zawadzki (2007). "Real-Time Comparisons of VPR-Corrected Daily Rainfall Estimates with a Gauge Mesonet". In: *Journal of Applied Meteorology and Climatology* 46.6, p. 726. DOI: 10.1175/JAM2502.1.

Bellon, A. and I. Zawadzki (2003). "A 9 year summary of radar characteristics of mesocyclonic storms and of deep convection in southern Quebec". In: *Atmosphere-Ocean* 41.2, p. 99. DOI: 10.3137/ao.410201.

Berenguer, M., D. Sempere-Torres, C. Corral, and R. Sánchez-Diezma (2006). "A fuzzy logic technique for identifying nonprecipitating echoes in radar scans". In: *Journal of Atmospheric and Oceanic Technology* 23.9, p. 1157.

Berndt, C., E. Rabiei, and U. Haberlandt (2014). "Geostatistical merging of rain gauge and radar data for high temporal resolutions and various station density scenarios". In: *Journal of Hydrology* 508, p. 88. DOI: 10.1016/j.jhydrol.2013.10.028.

Berne, A., G. Delrieu, J.-D. Creutin, and C. Obled (2004). "Temporal and spatial resolution of rainfall measurements required for urban hydrology". In: *Journal of Hydrology* 299, p. 166. DOI: 10.1016/j.jhydrol.2004.08.002.

Berne, A., M. ten Heggeler, R. Uijlenhoet, L. Delobbe, P. Dierickx, and M. de Wit (2005). "A preliminary investigation of radar rainfall estimation in the Ardennes region and a first hydrological application for the Ourthe catchment". In: *Natural Hazards and Earth System Science* 5.2, p. 267. ISSN: 1684-9981. DOI: 10.5194/nhess-5-267-2005.

Berne, A. and W. F. Krajewski (2013). "Radar for hydrology: Unfulfilled promise or unrecognized potential?" In: *Advances in Water Resources* 51, p. 357. ISSN: 0309-1708. DOI: 10.1016/j.advwatres.2012.05.005.

Bick, T., C. Simmer, S. Trömel, K. Wapler, H.-J. Hendricks Franssen, K. Stephan, U. Blahak, C. Schraff, H. Reich, Y. Zeng, and R. Potthast (2016). "Assimilation of 3D radar reflectivities with an ensemble Kalman filter on the convective scale". In: *Quarterly Journal of the Royal Meteorological Society* 142, p. 1490. DOI: 10.1002/qj.2751.

Blanchet, J., J. Touati, D. Lawrence, F. Garavaglia, and E. Paquet (2015). "Evaluation of a compound distribution based on weather pattern subsampling for extreme rainfall in Norway". In: *Natural Hazards and Earth System Sciences* 15, p. 2653. DOI: 10.5194/nhess-15-2653-2015.

Böhme, T., N. Van Lipzig, L. Delobbe, E. Goudenhoofdt, and A. Seifert (2011). "Evaluation of microphysical assumptions of the COSMO model using radar and rain gauge observations". In: *Meteorologische Zeitschrift* 20.2, p. 133. ISSN: 0941-2948. DOI: 10.1127/0941-2948/2011/0235.

Borga, M., F. Tonelli, R. J. Moore, and H. Andrieu (2002). "Long-term assessment of bias adjustment in radar rainfall estimation". In: *Water Resources Research* 38.11, p. 8. DOI: 10.1029/2001WR000555.

Brandes, E. A. (1975). "Optimizing Rainfall Estimates with the Aid of Radar". In: *Journal of Applied Meteorology* 14.7, p. 1339. ISSN: 0021-8952. DOI: 10.1175/1520-0450(1975)014<1339:orewta>2.0.co;2.

Brisson, E., M. Demuzere, and N. P. van Lipzig (2016). "Modelling strategies for performing convection-permitting climate simulations". In: *Meteorologische*

Zeitschrift 25.2, p. 149. DOI: 10.1127/metz/2015/0598. URL: http://dx.doi.org/10.1127/metz/2015/0598.

Browning, K. A., C. J. Morcrette, J. Nicol, A. M. Blyth, L. J. Bennett, B. J. Brooks, J. Marsham, S. D. Mobbs, D. J. Parker, F. Perry, P. A. Clark, S. P. Ballard, M. A. Dixon, R. M. Forbes, H. W. Lean, Z. Li, N. M. Roberts, U. Corsmeier, C. Barthlott, B. Deny, N. Kalthoff, S. Khodayar, M. Kohler, C. Kottmeier, S. Kraut, M. Kunz, J. Lenfant, A. Wieser, J. L. Agnew, D. Bamber, J. McGregor, K. M. Beswick, M. D. Gray, E. Norton, H. M. A. Ricketts, A. Russell, G. Vaughan, A. R. Webb, M. Bitter, T. Feuerle, R. Hankers, H. Schulz, K. E. Bozier, C. G. Collier, F. Davies, C. Gaffard, T. J. Hewison, D. N. Ladd, E. C. Slack, J. Waight, M. Ramatschi, D. P. Wareing, and R. J. Watson (2007). "The Convective Storm Initiation Project". In: *Bulletin of the American Meteorological Society* 88.12, p. 1939. DOI: 10.1175/BAMS-88-12-1939.

Buishand, T. A., L. de Haan, and C. Zhou (2008). "On spatial extremes: With application to a rainfall problem". In: *Ann. Appl. Stat.* 2.2, p. 624. DOI: 10.1214/08-AOAS159.

Buishand, T. (1991). "Extreme rainfall estimation by combining data from several sites". In: *Hydrological Sciences Journal* 36.4, p. 345.

Carbone, R. E. and J. D. Tuttle (2008). "Rainfall Occurrence in the U.S. Warm Season: The Diurnal Cycle*". In: *Journal of Climate* 21.16, p. 4132. DOI: 10.1175/2008JCLI2275.1.

Castellarin, A. (2007). "Probabilistic envelope curves for design flood estimation at ungauged sites". In: *Water Resources Research* 43, W04406, W04406. DOI: 10.1029/2005WR004384.

Chumchean, S., A. Sharma, and A. Seed (2006). "An Integrated Approach to Error Correction for Real-Time Radar-Rainfall Estimation". In: *Journal of Atmospheric and Oceanic Technology* 23.1, p. 6779. ISSN: 1520-0426. DOI: 10.1175/jtech1832.1.

Ciach, G. J., W. F. Krajewski, and G. Villarini (2007). "Product-Error-Driven Uncertainty Model for Probabilistic Quantitative Precipitation Estimation with NEXRAD Data". In: *Journal of Hydrometeorology* 8.6, p. 1325. DOI: 10.1175/2007JHM814.1.

Cole, S. J. and R. J. Moore (2008). "Hydrological modelling using raingauge- and radar-based estimators of areal rainfall". In: *Journal of Hydrology* 358.3-4, p. 159. DOI: 10.1016/j.jhydrol.2008.05.025.

Colli, M., L. G. Lanza, and P. La Barbera (2012). "An evaluation of the uncertainty of extreme events statistics at the WMO/CIMO Lead Centre on precipitation intensity". In: *AGU Fall Meeting Abstracts*.

Cooley, D., D. Nychka, and P. Naveau (2007). "Bayesian Spatial Modeling of Extreme Precipitation Return Levels". In: *Journal of the American Statistical Association* 102.479, p. 824. DOI: 10.1198/016214506000000780.

Cristiano, E., M.-C. ten Veldhuis, and N. van de Giesen (2017). "Spatial and temporal variability of rainfall and their effects on hydrological response in urban areas – a review". In: *Hydrology and Earth System Sciences* 21.7, pp. 3859–3878. DOI: 10.5194/hess-21-3859-2017.

Davini, P., R. Bechini, R. Cremonini, and C. Cassardo (2011). "Radar-Based Analysis of Convective Storms over Northwestern Italy". In: *Atmosphere* 3.4, p. 33. DOI: 10.3390/atmos3010033.

Davison, A. C., S. A. Padoan, and M. Ribatet (2012). "Statistical Modeling of Spatial Extremes". In: *Statistical Science* 27.2, p. 161. DOI: 10.1214/11-sts376.

De Troch, R., R. Hamdi, H. Van de Vyver, J.-F. Geleyn, and P. Termonia (2013). "Multiscale Performance of the ALARO-0 Model for Simulating Extreme Summer Precipitation Climatology in Belgium". In: *Journal of Climate* 26.22, p. 8895. ISSN: 1520-0442. DOI: 10.1175/jcli-d-12-00844.1.

de Vos, T. and L. Zhang (2012). "High resolution mapping of total deposition of acidifying pollutants". In: *Atmospheric Environment* 57, p. 80. DOI: 10.1016/j.atmosenv.2012.04.037.

Delobbe, L., D. Dehem, P. Dierickx, E. Roulin, M. Thunus, and C. Tricot (2006). "Combined use of radar and gauge observations for hydrological applications in the Walloon Region of Belgium". In: *Proceedings of ERAD*, p. 418.

Delobbe, L. and I. Holleman (2006). "Uncertainties in radar echo top heights used for hail detection". In: *Meteorological Applications* 13.04, p. 361. DOI: 10.1017/S1350482706002374.

Delrieu, G., I. Braud, A. Berne, M. Borga, B. Boudevillain, F. Fabry, J. Freer, E. Gaume, E. Nakakita, A. Seed, and et al. (2009). "Weather radar and hydrology". In: *Advances in Water Resources* 32.7, p. 969. ISSN: 0309-1708. DOI: 10.1016/j.advwatres.2009.03.006.

Delrieu, G., A. Wijbrans, B. Boudevillain, D. Faure, L. Bonnifait, and P.-E. Kirstetter (2014). "Geostatistical radar–raingauge merging: A novel method for the quantification of rain estimation accuracy". In: *Advances in Water Resources* 71, p. 110. DOI: 10.1016/j.advwatres.2014.06.005.

Demarée, Gaston R. (2003). "Le pluviographe centenaire du plateau d'Uccle: son histoire, ses données et ses applications". In: *La Houille Blanche* 4, p. 95. DOI: 10.1051/lhb/2003082.

Demarée, G. R. (2013). *History of the Royal Meteorological Institute of Belgium*. http://www.meteo.be/meteo/view/fr/6044768-Histoire.html. [Online].

Derrien, M. and H. Le Gléau (2005). "MSG/SEVIRI cloud mask and type from SAFNWC". In: *International Journal of Remote Sensing* 26.21, p. 4707.

Diggle, P. (2003). *Statistical analysis of spatial point patterns*. 2nd edition. Edward Arnold. ISBN: 0340740701.

Dixon, M. and G. Wiener (1993). "TITAN: Thunderstorm Identification, Tracking, Analysis, and Nowcasting - A Radar-based Methodology". In:

Journal of Atmospheric and Oceanic Technology 10, p. 785. DOI: 10.1175/1520-0426(1993)010<0785:TTITAA>2.0.CO;2.

Doviak, R. and D. Zrnić (2006). *Doppler radar and weather observations*. Dover Books on Engineering Series. Dover Publications. ISBN: 9780486450605.

Duchon, C. E. and C. J. Biddle (2010). "Undercatch of tipping-bucket gauges in high rain rate events". In: *Advances in Geosciences* 25, p. 11. DOI: 10.5194/adgeo-25-11-2010.

Durrans, S. R., L. T. Julian, and M. Yekta (2002). "Estimation of depth-area relationships using radar-rainfall data". In: *Journal of hydrologic Engineering* 7.5, p. 356.

Ebert, E., L. Wilson, A. Weigel, M. Mittermaier, P. Nurmi, P. Gill, M. Göber, S. Joslyn, B. Brown, T. Fowler, and A. Watkins (2013). "Progress and challenges in forecast verification". In: *Meteorological Applications* 20, p. 130. DOI: 10.1002/met.1392.

Eldardiry, H., E. Habib, and Y. Zhang (2015). "On the use of radar-based quantitative precipitation estimates for precipitation frequency analysis". In: *Journal of Hydrology* 531, Part 2. Hydrologic Applications of Weather Radar, p. 441. ISSN: 0022-1694. DOI: 10.1016/j.jhydrol.2015.05.016.

Erdin, R., C. Frei, and H. R. Künsch (2012). "Data Transformation and Uncertainty in Geostatistical Combination of Radar and Rain Gauges". In: *Journal of Hydrometeorology* 13.4, p. 1332. DOI: 10.1175/JHM-D-11-096.1.

Evin, G., J. Blanchet, E. Paquet, F. Garavaglia, and D. Penot (2016). "A regional model for extreme rainfall based on weather patterns subsampling". In: *Journal of Hydrology* 541, p. 1185. DOI: 10.1016/j.jhydrol.2016.08.024.

Fabry, F. (2015). "Radar Meteorology". In: DOI: 10.1017/cbo9781107707405.

Fairman, J. G., D. M. Schultz, D. J. Kirshbaum, S. L. Gray, and A. I. Barrett (2015). "A radar-based rainfall climatology of Great Britain and Ireland". In: *Weather* 70.5, p. 153. ISSN: 1477-8696. DOI: 10.1002/wea.2486.

Farr, T. G., P. A. Rosen, E. Caro, R. Crippen, R. Duren, S. Hensley, M. Kobrick, M. Paller, E. Rodriguez, L. Roth, D. Seal, S. Shaffer, J. Shimada, J. Umland, M. Werner, M. Oskin, D. Burbank, and D. Alsdorf (2007). "The Shuttle Radar Topography Mission". In: *Reviews of Geophysics* 45.2. DOI: 10.1029/2005RG000183.

Figueras-Ventura, J. and P. Tabary (2013). "The new French operational polarimetric radar rainfall rate product". In: *Journal of Applied Meteorology and Climatology* 52.8, p. 1817.

Foresti, L., M. Reyniers, A. Seed, and L. Delobbe (2016). "Development and verification of a real-time stochastic precipitation nowcasting system for urban hydrology in Belgium". In: *Hydrology and Earth System Sciences, Volume 20, Issue 1, 2016, pp.505-527* 20, p. 505. DOI: 10.5194/hess-20-505-2016.

Gabella, M. and R. Notarpietro (2002). "Ground clutter characterization and elimination in mountainous terrain". In: *Proceedings of the European Conference on Radar in Meteorology and Hydrology*. Vol. 305. 311.

Gagne, D. J., A. McGovern, and J. Brotzge (2009). "Classification of Convective Areas Using Decision Trees". In: *Journal of Atmospheric and Oceanic Technology* 26.7, p. 1341. DOI: 10.1175/2008JTECHA1205.1.

Gallus, W. A., N. A. Snook, and E. V. Johnson (2008). "Spring and Summer Severe Weather Reports over the Midwest as a Function of Convective Mode: A Preliminary Study". In: *Weather and Forecasting* 23.1, p. 101. DOI: 10.1175/2007WAF2006120.1.

Gellens, D. (2000). "Trend and Correlation Analysis of k-Day Extreme Precipitation over Belgium". In: *Theoretical and Applied Climatology* 66.1, p. 117. ISSN: 1434-4483. DOI: 10.1007/s007040070037.

Germann, U., M. Berenguer, D. Sempere-Torres, and M. Zappa (2009). "REAL-Ensemble radar precipitation estimation for hydrology in a mountainous region". In: *Quarterly Journal of the Royal Meteorological Society* 135.639, p. 445. DOI: 10.1002/qj.375.

Germann, U., G. Galli, M. Boscacci, and M. Bolliger (2006). "Radar precipitation measurement in a mountainous region". In: *Quarterly Journal of the Royal Meteorological Society* 132.618, p. 1669. DOI: 10.1256/qj.05.190.

Germann, U. and J. Joss (2002). "Mesobeta Profiles to Extrapolate Radar Precipitation Measurements above the Alps to the Ground Level". In: *J. Appl. Meteor.* 41.5, p. 542. ISSN: 0894-8763. DOI: 10.1175/1520-0450(2002)041<0542:MPTERP>2.0.CO;2.

Giorgi, F. and W. J. Gutowski (2015). "Regional Dynamical Downscaling and the CORDEX Initiative". In: *Annual Review of Environment and Resources* 40.1, p. 467. ISSN: 1545-2050. DOI: 10.1146/annurev-environ-102014-021217.

Giot, O., P. Termonia, D. Degrauwe, R. De Troch, S. Caluwaerts, G. Smet, J. Berckmans, A. Deckmyn, L. De Cruz, P. De Meutter, A. Duerinckx, L. Gerard, R. Hamdi, J. Van den Bergh, M. Van Ginderachter, and B. Van Schaeybroeck (2016). "Validation of the ALARO-0 model within the EURO-CORDEX framework". In: *Geoscientific Model Development* 9, p. 1143. DOI: 10.5194/gmd-9-1143-2016.

Gjertsen, U., M. Salek, and D. Michelson (2003). "Gauge-adjustment of radar-based precipitation estimates–a review". In: *COST-717 working document No. WDD* 2.200310, p. 1.

Gjertsen, U., M. Salek, and D. Michelson (2004). "Gauge adjustment of radar-based precipitation estimates in Europe". In: *Proceedings of ERAD*. Vol. 7. 11.

Glickman, T. S. and W. Zenk (2000). *Glossary of meteorology*. American Meteorological Society.

Goovaerts, P. (1997). *Geostatistics for natural resources evaluation*. Oxford University Press on Demand.

Goudenhoofdt, E. and L. Delobbe (2009). "Evaluation of radar-gauge merging methods for quantitative precipitation estimates". In: *Hydrology and Earth System Sciences* 13.2, p. 195. DOI: 10.5194/hess-13-195-2009.

Goudenhoofdt, E. and L. Delobbe (2013). "Statistical Characteristics of Convective Storms in Belgium Derived from Volumetric Weather Radar Observations". In: *Journal of Applied Meteorology and Climatology* 52, p. 918. DOI: 10.1175/JAMC-D-12-079.1.

Goudenhoofdt, E. and L. Delobbe (2016). "Generation and Verification of Rainfall Estimates from 10-Yr Volumetric Weather Radar Measurements". In: *Journal of Hydrometeorology* 17, p. 1223. DOI: 10.1175/JHM-D-15-0166.1.

Goudenhoofdt, E., L. Delobbe, and P. Willems (2017). "Regional frequency analysis of extreme rainfall in Belgium based on radar estimates". In: *Hydrology and Earth System Sciences* 21.10, pp. 5385–5399. DOI: 10.5194/hess-2017-150.

Goudenhoofdt, E. and L. Delobbe (2012). "Long-term evaluation of radar QPE using VPR correction and radar-gauge merging". In: *Proceedings of a symposium held in Exeter, UK, April 2011* 351, p. 249.

Haberlandt, U. (2007). "Geostatistical interpolation of hourly precipitation from rain gauges and radar for a large-scale extreme rainfall event". In: *Journal of Hydrology* 332.1-2, p. 144. DOI: 10.1016/j.jhydrol.2006.06.028.

Haberlandt, U. and C. Berndt (2016). "The value of weather radar data for the estimation of design storms - an analysis for the Hannover region". In: *Proceedings of the International Association of Hydrological Sciences, Volume 373, 2016, pp.81-85* 373, p. 81. DOI: 10.5194/piahs-373-81-2016.

Hamdi, R., D. Degrauwe, A. Duerinckx, J. Cedilnik, V. Costa, T. Dalkilic, K. Essaouini, M. Jerczynki, F. Kocaman, L. Kullmann, J.-F. Mahfouf, F. Meier, M. Sassi, S. Schneider, F. Váňa, and P. Termonia (2014). "Evaluating the performance of SURFEXv5 as a new land surface scheme for the ALADINcy36 and ALARO-0 models". In: *Geoscientific Model Development* 7, p. 23. DOI: 10.5194/gmd-7-23-2014.

Hamdi, R. and H. Van de Vyver (2011). "Estimating urban heat island effects on near-surface air temperature records of Uccle (Brussels, Belgium): an observational and modeling study". In: *Advances in Science and Research* 6.1, p. 27. DOI: 10.5194/asr-6-27-2011.

Hamid, K. (2012). "Investigation of the passage of a derecho in Belgium". In: *Atmospheric Research* 107, p. 86. ISSN: 0169-8095. DOI: 10.1016/j.atmosres.2011.12.013.

Han, L., S. Fu, L. Zhao, Y. Zheng, H. Wang, and Y. Lin (2009). "3D Convective Storm Identification, Tracking, and Forecasting–-An Enhanced

TITAN Algorithm". In: *Journal of Atmospheric and Oceanic Technology* 26.4, p. 719. DOI: 10.1175/2008JTECHA1084.1.

Haylock, M. R., N. Hofstra, A. M. G. Klein Tank, E. J. Klok, P. D. Jones, and M. New (2008). "A European daily high-resolution gridded data set of surface temperature and precipitation for 1950–2006". In: *Journal of Geophysical Research* 113.D20. DOI: 10.1029/2008JD010201.

Hazenberg, P., H. Leijnse, and R. Uijlenhoet (2014). "The impact of reflectivity correction and accounting for raindrop size distribution variability to improve precipitation estimation by weather radar for an extreme low-land mesoscale convective system". In: *Journal of Hydrology* 519, p. 3410. DOI: 10.1016/j.jhydrol.2014.09.057.

Hazenberg, P., P. J. J. F. Torfs, H. Leijnse, G. Delrieu, and R. Uijlenhoet (2013). "Identification and uncertainty estimation of vertical reflectivity profiles using a Lagrangian approach to support quantitative precipitation measurements by weather radar". In: *Journal of Geophysical Research: Atmospheres* 118.18, p. 10243. DOI: 10.1002/jgrd.50726.

Heistermann, M., S. Collis, M. J. Dixon, S. Giangrande, J. J. Helmus, B. Kelley, J. Koistinen, D. B. Michelson, M. Peura, T. Pfaff, and D. B. Wolff (2015). "The Emergence of Open-Source Software for the Weather Radar Community". In: *Bulletin of the American Meteorological Society* 96.1, p. 117. DOI: 10.1175/BAMS-D-13-00240.1.

Heistermann, M., U. Ehret, A. Bronstert, and E. Zehe (2008). "Merging radar and ground observations for operational quantitative rainfall estimation in a mountainous head catchment in Germany". In: *International Symposium on Weather Radar and Hydrology, Grenoble, France*, p. 10.

Heistermann, M., S. Jacobi, and T. Pfaff (2013). "Technical Note: An open source library for processing weather radar data (wradlib)". In: *Hydrology and Earth System Sciences* 17.2, pp. 863–871. DOI: 10.5194/hess-17-863-2013. URL: https://www.hydrol-earth-syst-sci.net/17/863/2013/.

Holleman, I. (2007). "Bias adjustment and long-term verification of radar-based precipitation estimates". In: *Meteorological Applications* 14.2, p. 195. DOI: 10.1002/met.22.

Holleman, I., D. Michelson, G. Galli, U. Germann, M. Peura, and H. Hohti (2006). "Quality information for radars and radar data". In: *OPERA workpackage* 1.

Hosking, J. R. M. and J. R. Wallis (1988). "The effect of intersite dependence on regional flood frequency analysis". In: *Water Resources Research* 24, p. 588. DOI: 10.1029/WR024i004p00588.

Hosseinzadehtalaei, P., H. Tabari, and P. Willems (2017). "Uncertainty assessment for climate change impact on intense precipitation: how many model runs do we need?" In: *International Journal of Climatology*. ISSN: 0899-8418. DOI: 10.1002/joc.5069.

Houze, R. A. (2004). "Mesoscale convective systems". In: *Reviews of Geophysics* 42, RG4003, p. 4003. DOI: 10.1029/2004RG000150.

Hubbert, J. C., M. Dixon, S. M. Ellis, and G. Meymaris (2009). "Weather Radar Ground Clutter. Part I: Identification, Modeling, and Simulation". In: *Journal of Atmospheric and Oceanic Technology* 26.7, p. 1165. DOI: 10.1175/2009JTECHA1159.1.

Huuskonen, A., E. Saltikoff, and I. Holleman (2014). "The Operational Weather Radar Network in Europe". In: *Bulletin of the American Meteorological Society* 95, p. 897. DOI: 10.1175/BAMS-D-12-00216.1.

Jakob, D., D. J. Karoly, and A. Seed (2011). "Non-stationarity in daily and sub-daily intense rainfall - Part 1: Sydney, Australia". In: *Natural Hazards and Earth System Sciences* 11, p. 2263. DOI: 10.5194/nhess-11-2263-2011.

Jakubicka, T., F. Vos, R. Phalkey, D. Guha-Sapir, and M. Marx (2010). *Health impacts of floods in Europe: Data gaps and information needs from a spatial perspective*. Tech. rep. Centre for Research on the Epidemiology of Disasters (CRED).

Jewell, S. A. and N. Gaussiat (2015). "An assessment of kriging-based rain-gauge-radar merging techniques". In: *Quarterly Journal of the Royal Meteorological Society* 141.691, p. 2300. DOI: 10.1002/qj.2522.

Johnson, J. T., P. L. Mackeen, A. Witt, E. D. Mitchell, G. J. Stumpf, M. D. Eilts, and K. W. Thomas (1998). "The Storm Cell Identification and Tracking Algorithm: An Enhanced WSR-88D Algorithm". In: *Weather and Forecasting* 13, p. 263. DOI: 10.1175/1520-0434(1998)013<0263:TSCIAT>2.0.CO;2.

Joss, J. and R. Lee (1995). "The Application of Radar*Gauge Comparisons to Operational Precipitation Profile Corrections". In: *J. Appl. Meteor.* 34.12, p. 2612. ISSN: 0894-8763. DOI: 10.1175/1520-0450(1995)034<2612:TAORCT>2.0.CO;2.

Joss, J., A. Waldvogel, and C. G. Collier (1990). "Precipitation Measurement and Hydrology". In: *Radar in Meteorology*, p. 577. DOI: 10.1007/978-1-935704-15-7_39.

Journée, M., C. Delvaux, and C. Bertrand (2015). "Precipitation climate maps of Belgium". In: *Advances in Science and Research, Volume 12, 2015, pp.73-78* 12, p. 73. DOI: 10.5194/asr-12-73-2015.

Kaltenboeck, R. and M. Steinheimer (2015). "Radar-based severe storm climatology for Austrian complex orography related to vertical wind shear and atmospheric instability". In: *Atmospheric Research* 158-159, p. 216. ISSN: 0169-8095. DOI: 10.1016/j.atmosres.2014.08.006.

Kendon, E. J., N. Ban, N. M. Roberts, H. J. Fowler, M. J. Roberts, S. C. Chan, J. P. Evans, G. Fosser, and J. M. Wilkinson (2017). "Do Convection-Permitting Regional Climate Models Improve Projections of Future Precipitation Change?" In: *Bulletin of the American Meteorological Society* 98.1, p. 79. DOI: 10.1175/bams-d-15-0004.1.

Kessinger C., S. E. and J. V. Andel (2003). "The radar echo classifier: A fuzzy logic algorithm for the WSR-88D". In: *3rd Conference on Artificial Applications to the Environmental Science*. AMS Press. Long Beach, California.

Kim, B., D.-J. Seo, S. J. Noh, O. P. Prat, and B. R. Nelson (2016). "Improving multisensor estimation of heavy-to-extreme precipitation via conditional bias-penalized optimal estimation". In: *Journal of Hydrology*. ISSN: 0022-1694. DOI: 10.1016/j.jhydrol.2016.10.052.

Kirstetter, P.-E., H. Andrieu, G. Delrieu, and B. Boudevillain (2010). "Identification of Vertical Profiles of Reflectivity for Correction of Volumetric Radar Data Using Rainfall Classification". In: *Journal of Applied Meteorology and Climatology* 49.10, p. 2167. DOI: 10.1175/2010JAMC2369.1.

Koistinen, J. and H. Pohjola (2014). "Estimation of Ground-Level Reflectivity Factor in Operational Weather Radar Networks Using VPR-Based Correction Ensembles". In: *Journal of Applied Meteorology and Climatology* 53.10, p. 2394. DOI: 10.1175/JAMC-D-13-0343.1.

Krajewski, W. F. (1987). "Cokriging radar-rainfall and rain gage data". In: *Journal of Geophysical Research* 92.D8, p. 9571. DOI: 10.1029/JD092iD08p09571.

Krajewski, W. F., A. Kruger, J. A. Smith, R. Lawrence, C. Gunyon, R. Goska, B.-C. Seo, P. Domaszczynski, M. L. Baeck, M. K. Ramamurthy, J. Weber, A. A. Bradley, S. A. DelGreco, and M. Steiner (2011). "Towards better utilization of NEXRAD data in hydrology: an overview of Hydro-NEXRAD". In: *Journal of Hydroinformatics* 13.2, p. 255. DOI: 10.2166/hydro.2010.056.

Kunz, M., J. Sander, and C. Kottmeier (2009). "Recent trends of thunderstorm and hailstorm frequency and their relation to atmospheric characteristics in southwest Germany". In: *International Journal of Climatology* 29.15, p. 2283. DOI: 10.1002/joc.1865.

Lack, S. A. and N. I. Fox (2007). "An examination of the effect of wind-drift on radar-derived surface rainfall estimations". In: *Atmospheric Research* 85.2, p. 217. ISSN: 0169-8095. DOI: 10.1016/j.atmosres.2006.09.010.

Lakshmanan, V. and T. Smith (2010). "An Objective Method of Evaluating and Devising Storm-Tracking Algorithms". In: *Weather and Forecasting* 25.2, p. 701. DOI: 10.1175/2009WAF2222330.1.

Leclercq, G., G. Bastin, L. Moens, L. Delobbe, P. Dierickx, and M. Thunus (2008). "Using weather radar measurements for real-time river flow forecasting". In: *Proceedings of WraH 2008*.

Leeuw, J. de, J. Methven, and M. Blackburn (2014). "Evaluation of ERA-Interim reanalysis precipitation products using England and Wales observations". In: *Quarterly Journal of the Royal Meteorological Society* 141.688, p. 798. DOI: 10.1002/qj.2395.

Lewis, M. W. and S. L. Gray (2010). "Categorisation of synoptic environments associated with mesoscale convective systems over the UK". In: *Atmospheric Research* 97.1-2, p. 194. ISSN: 0169-8095. DOI: 10.1016/j.atmosres.2010.04.001.

Li, Y., S. Grimaldi, J. Walker, and V. Pauwels (2016). "Application of Remote Sensing Data to Constrain Operational Rainfall-Driven Flood Forecasting: A Review". In: *Remote Sensing* 8.6, p. 456. ISSN: 2072-4292. DOI: 10.3390/rs8060456.

Liu, C. and E. J. Zipser (2009). ""Warm Rain" in the Tropics: Seasonal and Regional Distributions Based on 9 yr of TRMM Data". In: *Journal of Climate* 22.3, p. 767. DOI: 10.1175/2008JCLI2641.1.

Liu, S., G. DiMego, S. Guan, V. K. Kumar, D. Keyser, Q. Xu, K. Nai, P. Zhang, L. Liu, J. Zhang, K. Howard, and J. Ator (2016). "WSR-88D Radar Data Processing at NCEP". In: *Weather and Forecasting* 31, p. 2047. DOI: 10.1175/WAF-D-16-0003.1.

Lobligeois, F., V. Andréassian, C. Perrin, P. Tabary, and C. Loumagne (2014). "When does higher spatial resolution rainfall information improve streamflow simulation?: An evaluation using 3620 flood events". In: *Hydrology and Earth System Sciences* 18.2, p. 575. DOI: 10.5194/hess-18-575-2014.

Lombardo, K. A. and B. A. Colle (2010). "The Spatial and Temporal Distribution of Organized Convective Structures over the Northeast and Their Ambient Conditions". In: *Monthly Weather Review* 138.12, p. 4456. DOI: 10.1175/2010MWR3463.1.

López, R. E., D. O. Blanchard, D. Rosenfeld, W. L. Hiscox, and M. J. Casey (1984). "Population Characteristics, Development Processes and Structure of Radar Echoes in South Florida". In: *Monthly Weather Review* 112, p. 56. DOI: 10.1175/1520-0493(1984)112<0056:PCDPAS>2.0.CO;2.

Lukach, M., L. Foresti, O. Giot, and L. Delobbe (2017). "Estimating the occurrence and severity of hail based on 10 years of observations from weather radar in Belgium". In: *Meteorological Applications*.

Mahtour, A., M. El Jarroudi, L. Delobbe, L. Hoffmann, H. Maraite, and B. Tychon (2011). "Site-specific Septoria leaf blotch risk assessment in winter wheat using weather-radar rainfall estimates". In: *Plant disease* 95.4, p. 384.

Mäkelä, A., P. Rossi, and D. M. Schultz (2011). "The Daily Cloud-to-Ground Lightning Flash Density in the Contiguous United States and Finland". In: *Monthly Weather Review* 139.5, p. 1323. DOI: 10.1175/2010MWR3517.1.

Marra, F. and E. Morin (2015). "Use of radar QPE for the derivation of Intensity-Duration-Frequency curves in a range of climatic regimes". In: *Journal of Hydrology* 531, Part 2. Hydrologic Applications of Weather Radar, p. 427. ISSN: 0022-1694. DOI: 10.1016/j.jhydrol.2015.08.064.

Marra, F., E. Morin, N. Peleg, Y. Mei, and E. N. Anagnostou (2017). "Intensity–duration–frequency curves from remote sensing rainfall estimates: comparing

satellite and weather radar over the eastern Mediterranean". In: *Hydrology and Earth System Sciences* 21.5, p. 2389.

Martins, E. S. and J. R. Stedinger (2000). "Generalized maximum-likelihood generalized extreme-value quantile estimators for hydrologic data". In: *Water Resources Research* 36.3, p. 737. DOI: 10.1029/1999WR900330.

May, P. T. and A. Ballinger (2007). "The Statistical Characteristics of Convective Cells in a Monsoon Regime (Darwin, Northern Australia)". In: *Monthly Weather Review* 135.1, p. 82. DOI: 10.1175/MWR3273.1.

Meersmans, J., K. Van Weverberg, S. De Baets, F. De Ridder, S. Palmer, B. van Wesemael, and T. Quine (2016). "Mapping mean total annual precipitation in Belgium, by investigating the scale of topographic control at the regional scale". In: *Journal of Hydrology* 540, p. 96. ISSN: 0022-1694. DOI: 10.1016/j.jhydrol.2016.06.013.

Metcalf, J. I. (1990). "Technology of Polarization Diversity Radars for Meteorology: Panel Report". In: *Radar in Meteorology*, p. 191. DOI: 10.1007/978-1-935704-15-7_20.

Michelson, D., T. Andersson, J. Koistinen, C. G. Collier, J. Riedl, A. Nielsen, T. Overgaard Persson, et al. (2000). *BALTEX Radar Data Centre products and their methodologies*. SMHI.

Michelson, D., T. Einfalt, I. Holleman, et al. (2005). "Weather radar data quality in Europe: quality control and characterisation". In:

Mohee, F. M. and C. Miller (2010). "Climatology of Thunderstorms for North Dakota, 2002-06". In: *Journal of Applied Meteorology and Climatology* 49, p. 1881. DOI: 10.1175/2010JAMC2400.1.

Mohymont, B. and G. R. Demarée (2006). *Établissement des courbes Intensité-Durée-Fréquence (IDF) des précipitations basées sur les séries temporelles de longue durée des stations hydrométéorologiques situées en Région wallonne pour des durées de 10 minutes (1 heure) jusqu¿a 1 mois*.

Molenberghs, G., G. Fitzmaurice, M. G. Kenward, A. Tsiatis, and G. Verbeke (2014). *Handbook of missing data methodology*. CRC Press.

Murray, J. C. and B. A. Colle (2011). "The Spatial and Temporal Variability of Convective Storms over the Northeast United States during the Warm Season". In: *Monthly Weather Review* 139.3, p. 992. DOI: 10.1175/2010MWR3316.1.

Nelson, B. R., O. P. Prat, D. J. Seo, and E. Habib (2016). "Assessment and Implications of NCEP Stage IV Quantitative Precipitation Estimates for Product Intercomparisons". In: *Weather and Forecasting* 31.2, p. 371. ISSN: 1520-0434. DOI: 10.1175/waf-d-14-00112.1.

Nelson, B. R., D. J. Seo, and D. Kim (2010). "Multisensor Precipitation Reanalysis". In: *Journal of Hydrometeorology* 11.3, p. 666. DOI: 10.1175/2010JHM1210.1.

Ntegeka, V. and P. Willems (2008). "Trends and multidecadal oscillations in rainfall extremes, based on a more than 100-year time series of 10 min

rainfall intensities at Uccle, Belgium". In: *Water Resources Research* 44.7. DOI: 10.1029/2007WR006471.

Nystuen, J. A. (1999). "Relative Performance of Automatic Rain Gauges under Different Rainfall Conditions". In: *Journal of Atmospheric and Oceanic Technology* 16.8, p. 1025. DOI: 10.1175/1520-0426(1999)016<1025:RPOARG>2.0.CO;2.

Ochoa-Rodriguez, S., L.-P. Wang, A. Gires, R. D. Pina, R. Reinoso-Rondinel, G. Bruni, A. Ichiba, S. Gaitan, E. Cristiano, J. van Assel, S. Kroll, D. Murlà-Tuyls, B. Tisserand, D. Schertzer, I. Tchiguirinskaia, C. Onof, P. Willems, and M.-C. ten Veldhuis (2015). "Impact of spatial and temporal resolution of rainfall inputs on urban hydrodynamic modelling outputs: A multi-catchment investigation". In: *Journal of Hydrology* 531, p. 389. DOI: 10.1016/j.jhydrol.2015.05.035.

Ootegem, L. V., K. V. Herck, T. Creten, E. Verhofstadt, L. Foresti, E. Goudenhoofdt, M. Reyniers, L. Delobbe, D. M. Tuyls, and P. Willems (2016). "Exploring the potential of multivariate depth-damage and rainfall-damage models". In: *Journal of Flood Risk Management*. DOI: 10.1111/jfr3.12284.

Overeem, A., T. A. Buishand, and I. Holleman (2009a). "Extreme rainfall analysis and estimation of depth-duration-frequency curves using weather radar". In: *Water Resources Research* 45.10. DOI: 10.1029/2009WR007869.

Overeem, A., T. A. Buishand, I. Holleman, and R. Uijlenhoet (2010). "Extreme value modeling of areal rainfall from weather radar". In: *Water Resources Research* 46.9. DOI: 10.1029/2009WR008517.

Overeem, A., I. Holleman, and A. Buishand (2009b). "Derivation of a 10-Year Radar-Based Climatology of Rainfall". In: *Journal of Applied Meteorology and Climatology* 48.7, p. 1448. DOI: 10.1175/2009JAMC1954.1.

Paixao, E., M. M. Q. Mirza, M. W. Shephard, H. Auld, J. Klaassen, and G. Smith (2015). "An integrated approach for identifying homogeneous regions of extreme rainfall events and estimating IDF curves in Southern Ontario, Canada: Incorporating radar observations". In: *Journal of Hydrology* 528, p. 734. ISSN: 0022-1694. DOI: 10.1016/j.jhydrol.2015.06.015.

Panziera, L., M. Gabella, S. Zanini, A. Hering, U. Germann, and A. Berne (2016). "A radar-based regional extreme rainfall analysis to derive the thresholds for a novel automatic alert system in Switzerland". In: *Hydrology and Earth System Sciences* 20.6, p. 2317. ISSN: 1607-7938. DOI: 10.5194/hess-20-2317-2016.

Parker, M. D. and D. A. Ahijevych (2007). "Convective Episodes in the East-Central United States". In: *Monthly Weather Review* 135, p. 3707. DOI: 10.1175/2007MWR2098.1.

Peleg, N., F. Blumensaat, P. Molnar, S. Fatichi, and P. Burlando (2017). "Partitioning the impacts of spatial and climatological rainfall variability

in urban drainage modeling". In: *Hydrology and Earth System Sciences* 21.3, p. 1559. ISSN: 1607-7938. DOI: 10.5194/hess-21-1559-2017.

Peleg, N., F. Marra, S. Fatichi, A. Paschalis, P. Molnar, and P. Burlando (2016). "Spatial variability of extreme rainfall at radar subpixel scale". In: *Journal of Hydrology*. DOI: 10.1016/j.jhydrol.2016.05.033.

Pereira Fo., A. J., K. C. Crawford, and C. L. Hartzell (1998). "Improving WSR-88D Hourly Rainfall Estimates". In: *Weather and Forecasting* 13.4, p. 1016. ISSN: 1520-0434. DOI: 10.1175/1520-0434(1998)013<1016:iwhre>2.0.co;2.

Peter, J. R., M. J. Manton, R. J. Potts, P. T. May, S. M. Collis, and L. Wilson (2015). "Radar-Derived Statistics of Convective Storms in Southeast Queensland". In: *Journal of Applied Meteorology and Climatology* 54.10, p. 1985. ISSN: 1558-8432. DOI: 10.1175/jamc-d-13-0347.1.

Pickands III, J. (1975). "Statistical inference using extreme order statistics". In: *the Annals of Statistics*, p. 119.

Potts, R. J., T. D. Keenan, and P. T. May (2000). "Radar Characteristics of Storms in the Sydney Area". In: *Monthly Weather Review* 128, p. 3308. DOI: 10.1175/1520-0493(2000)128<3308:RCOSIT>2.0.CO;2.

Prein, A. F., A. Gobiet, M. Suklitsch, H. Truhetz, N. K. Awan, K. Keuler, and G. Georgievski (2013). "Added value of convection permitting seasonal simulations". In: *Climate Dynamics* 41, p. 2655. DOI: 10.1007/s00382-013-1744-6.

Prein, A. F., W. Langhans, G. Fosser, A. Ferrone, N. Ban, K. Goergen, M. Keller, M. Tölle, O. Gutjahr, F. Feser, E. Brisson, S. Kollet, J. Schmidli, N. P. M. van Lipzig, and R. Leung (2015). "A review on regional convection-permitting climate modeling: Demonstrations, prospects, and challenges". In: *Reviews of Geophysics* 53, p. 323. DOI: 10.1002/2014RG000475.

Pulkkinen, S., J. Koistinen, T. Kuitunen, and A.-M. Harri (2016). "Probabilistic radar-gauge merging by multivariate spatiotemporal techniques". In: *Journal of Hydrology* 542, p. 662. ISSN: 0022-1694. DOI: 10.1016/j.jhydrol.2016.09.036.

Punkka, A.-J. and M. Bister (2015). "Mesoscale Convective Systems and Their Synoptic-Scale Environment in Finland". In: *Weather and Forecasting* 30.1, p. 182. ISSN: 1520-0434. DOI: 10.1175/waf-d-13-00146.1.

Puskeiler, M., M. Kunz, and M. Schmidberger (2016). "Hail statistics for Germany derived from single-polarization radar data". In: *Atmospheric Research* 178-179, p. 459. ISSN: 0169-8095. DOI: 10.1016/j.atmosres.2016.04.014.

Rigo, T. and M. C. Llasat (2004). "A methodology for the classification of convective structures using meteorological radar: Application to heavy rainfall events on the Mediterranean coast of the Iberian Peninsula". In: *Natural Hazards and Earth System Sciences* 4, p. 59.

Rinehart, R. E. (1991). *Radar for meteorologists*. University of North Dakota, Office of the President.

Rogers, R. R. (1990). "The Early Years of Doppler Radar in Meteorology". In: *Radar in Meteorology*, p. 122. DOI: 10.1007/978-1-935704-15-7_16.

Rossa, A., K. Liechti, M. Zappa, M. Bruen, U. Germann, G. Haase, C. Keil, and P. Krahe (2011). "The COST 731 Action: A review on uncertainty propagation in advanced hydro-meteorological forecast systems". In: *Atmospheric Research* 100, p. 150. DOI: 10.1016/j.atmosres.2010.11.016.

Roth, M., T. Buishand, G. Jongbloed, A. K. Tank, and J. van Zanten (2014). "Projections of precipitation extremes based on a regional, non-stationary peaks-over-threshold approach: A case study for the Netherlands and north-western Germany". In: *Weather and Climate Extremes* 4, p. 1. DOI: 10.1016/j.wace.2014.01.001.

Roth, M., G. Jongbloed, and T. Buishand (2015). "Threshold selection for regional peaks-over-threshold data". In: *Journal of Applied Statistics* 43.7, p. 1291. DOI: 10.1080/02664763.2015.1100589.

Rulfova, Z., A. Buishand, J. Kysely, and M. Roth (2014). "Two-Component Extreme Value Distributions for Convective and Stratiform Precipitation". In: *AGU Fall Meeting Abstracts*.

Saeed, S., E. Brisson, M. Demuzere, H. Tabari, P. Willems, and N. P. M. van Lipzig (2016). "Multidecadal convection permitting climate simulations over Belgium: sensitivity of future precipitation extremes". In: *Atmospheric Science Letters* 18.1, p. 2936. ISSN: 1530-261X. DOI: 10.1002/asl.720.

Saito, H. and H. Matsuyama (2015). "Probable Hourly Precipitation and Soil Water Index for 50-yr Recurrence Interval over the Japanese Archipelago". In: *SOLA* 11, p. 118. DOI: 10.2151/sola.2015-028.

Salek, M. and P. Novák (2008). "Experience gained by five years of the utilization of the radar-based quantitative precipitation estimation at the Czech Hydrometeorological Institute". In: *Proceedings of ERAD*.

Saltikoff, E., L. P, A. Taskinen, and S. Pulkkinen (2015). "Comparison of quantitative snowfall estimates from weather radar, rain gauges and a numerical weather prediction model". In: 20.

Sapiano, M. R. P. and P. A. Arkin (2009). "An Intercomparison and Validation of High-Resolution Satellite Precipitation Estimates with 3-Hourly Gauge Data". In: *Journal of Hydrometeorology* 10.1, p. 149. DOI: 10.1175/2008JHM1052.1.

Saxen, T. R., C. K. Mueller, T. T. Warner, M. Steiner, E. E. Ellison, E. W. Hatfield, T. L. Betancourt, S. M. Dettling, and N. A. Oien (2008). "The Operational Mesogamma-Scale Analysis and Forecast System of the U.S. Army Test and Evaluation Command. Part IV: The White Sands Missile Range Auto-Nowcast System". In: *Journal of Applied Meteorology and Climatology* 47.4, p. 1123. DOI: 10.1175/2007JAMC1656.1.

Schiemann, R., R. Erdin, M. Willi, C. Frei, M. Berenguer, and D. Sempere-Torres (2011). "Geostatistical radar-raingauge combination with nonparametric correlograms: methodological considerations and application in Switzerland". In: *Hydrology and Earth System Sciences* 15.5, p. 1515. DOI: 10.5194/hess-15-1515-2011.

Schneider, U., A. Becker, P. Finger, A. Meyer-Christoffer, M. Ziese, and B. Rudolf (2014). "GPCC's new land surface precipitation climatology based on quality-controlled in situ data and its role in quantifying the global water cycle". In: *Theoretical and Applied Climatology* 115, p. 15. DOI: 10.1007/s00704-013-0860-x.

Schoen, J. M. and W. S. Ashley (2011). "A Climatology of Fatal Convective Wind Events by Storm Type". In: *Weather and Forecasting* 26, p. 109. DOI: 10.1175/2010WAF2222428.1.

Schumacher, R. S. and R. H. Johnson (2006). "Characteristics of U.S. Extreme Rain Events during 1999-2003". In: *Weather and Forecasting* 21, p. 69. DOI: 10.1175/WAF900.1.

Schuurmans, J. M., M. F. P. Bierkens, E. J. Pebesma, and R. Uijlenhoet (2007). "Automatic Prediction of High-Resolution Daily Rainfall Fields for Multiple Extents: The Potential of Operational Radar". In: *Journal of Hydrometeorology* 8.6, p. 1204. DOI: 10.1175/2007JHM792.1.

Seo, D.-J. and J. P. Breidenbach (2002). "Real-Time Correction of Spatially Nonuniform Bias in Radar Rainfall Data Using Rain Gauge Measurements". In: *Journal of Hydrometeorology* 3.2, p. 93. ISSN: 1525-7541. DOI: 10.1175/1525-7541(2002)003<0093:rtcosn>2.0.co;2.

Sideris, I. V., M. Gabella, R. Erdin, and U. Germann (2013). "Real-time radar-rain-gauge merging using spatio-temporal co-kriging with external drift in the alpine terrain of Switzerland". In: *Quarterly Journal of the Royal Meteorological Society*. DOI: 10.1002/qj.2188.

Sinclair, S. and G. Pegram (2005). "Combining radar and rain gauge rainfall estimates using conditional merging". In: *Atmospheric Science Letters* 6.1, p. 19. DOI: 10.1002/asl.85.

Smith, J. A., M. L. Baeck, G. Villarini, C. Welty, A. J. Miller, and W. F. Krajewski (2012). "Analyses of a long-term, high-resolution radar rainfall data set for the Baltimore metropolitan region". In: *Water Resources Research* 48.4, n/a–n/a. ISSN: 1944-7973. DOI: 10.1029/2011WR010641.

Sokol, Z. (2003). "Utilization of regression models for rainfall estimates using radar-derived rainfall data and rain gauge data". In: *Journal of Hydrology* 278.1-4, p. 144. ISSN: 0022-1694. DOI: 10.1016/s0022-1694(03)00139-2.

Steiner, M., R. A. Houze Jr., and S. E. Yuter (1995). "Climatological Characterization of Three-Dimensional Storm Structure from Operational Radar and Rain Gauge Data." In: *Journal of Applied Meteorology* 34, p. 1978. DOI: 10.1175/1520-0450(1995)034<1978:CCOTDS>2.0.CO;2.

Steiner, M. and J. A. Smith (2002). "Use of three-dimensional reflectivity structure for automated detection and removal of nonprecipitating echoes in radar data". In: *Journal of Atmospheric and Oceanic Technology* 19.5, p. 673.

Stocker, T. F., D. Qin, G.-K. Plattner, M. Tignor, S. K. Allen, J. Boschung, A. Nauels, Y. Xia, V. Bex, P. M. Midgley, et al. (2013). "Climate change 2013: The physical science basis". In: *Intergovernmental Panel on Climate Change, Working Group I Contribution to the IPCC Fifth Assessment Report (AR5)(Cambridge Univ Press, New York)*.

Sun, X., R. Mein, T. Keenan, and J. Elliott (2000). "Flood estimation using radar and raingauge data". In: *Journal of Hydrology* 239.1-4, p. 418. ISSN: 0022-1694. DOI: 10.1016/s0022-1694(00)00350-4.

Sveinsson, O. G. B., D. C. Boes, and J. D. Salas (2001). "Population index flood method for regional frequency analysis". In: *Water Resources Research* 37.11, p. 2733. DOI: 10.1029/2001wr000321.

Svensson, C. and D. A. Jones (2010). "Review of rainfall frequency estimation methods". In: *Journal of Flood Risk Management* 3.4, p. 296. DOI: 10.1111/j.1753-318X.2010.01079.x.

Tabari, H., R. De Troch, O. Giot, R. Hamdi, P. Termonia, S. Saeed, E. Brisson, N. Van Lipzig, and P. Willems (2016). "Local impact analysis of climate change on precipitation extremes: are high-resolution climate models needed for realistic simulations?" In: *Hydrology and Earth System Sciences, Volume 20, Issue 9, 2016, pp.3843-3857* 20, p. 3843. DOI: 10.5194/hess-20-3843-2016.

Tabary, P. (2007). "The New French Operational Radar Rainfall Product. Part I: Methodology". In: *Weather and Forecasting* 22.3, p. 393. DOI: 10.1175/WAF1004.1.

Tang, L., Y. Tian, and X. Lin (2014). "Validation of precipitation retrievals over land from satellite-based passive microwave sensors". In: *Journal of Geophysical Research: Atmospheres* 119.8, p. 4546. DOI: 10.1002/2013JD020933.

Testik, F. Y. and M. Gebremichael (2013). *Rainfall: state of the science*. Vol. 191. John Wiley & Sons.

Thorndahl, S., T. Einfalt, P. Willems, J. E. Nielsen, M.-C. ten Veldhuis, K. Arnbjerg-Nielsen, M. R. Rasmussen, and P. Molnar (2017). "Weather radar rainfall data in urban hydrology". In: *Hydrology and Earth System Sciences* 21.3, p. 1359. ISSN: 1607-7938. DOI: 10.5194/hess-21-1359-2017.

Thorndahl, S., J. E. Nielsen, and M. R. Rasmussen (2014). "Bias adjustment and advection interpolation of long-term high resolution radar rainfall series". In: *Journal of Hydrology* 508, p. 214. DOI: 10.1016/j.jhydrol.2013.10.056.

Todini, E. (2001). "A Bayesian technique for conditioning radar precipitation estimates to rain-gauge measurements". In: *Hydrology and Earth System Sciences* 5.2, p. 187. ISSN: 1607-7938. DOI: 10.5194/hess-5-187-2001.

Tuttle, J. D., R. E. Carbone, and P. A. Arkin (2008). "Comparison of Ground-Based Radar and Geosynchronous Satellite Climatologies of Warm-Season Precipitation over the United States". In: *Journal of Applied Meteorology and Climatology* 47.12, p. 3264. DOI: 10.1175/2008JAMC2000.1.

Uboldi, F., A. N. Sulis, C. Lussana, M. Cislaghi, and M. Russo (2014). "A spatial bootstrap technique for parameter estimation of rainfall annual maxima distribution". In: *Hydrology and Earth System Sciences, Volume 18, Issue 3, 2014, pp.981-995* 18, p. 981. DOI: 10.5194/hess-18-981-2014.

Uijlenhoet, R. and A. Berne (2008). "Stochastic simulation experiment to assess radar rainfall retrieval uncertainties associated with attenuation and its correction". In: *Hydrology and Earth System Sciences* 12.2, p. 587. DOI: 10.5194/hess-12-587-2008.

Uijlenhoet, R. and J. H. Pomeroy (2001). "Raindrop size distributions and radar reflectivity-rain rate relationships for radar hydrology". In: *Hydrology and Earth System Sciences* 5, p. 615.

Van de Vyver, H. (2012). "Spatial regression models for extreme precipitation in Belgium". In: *Water Resources Research* 48.9. DOI: 10.1029/2011WR011707.

Van Weverberg, K., E. Goudenhoofdt, U. Blahak, E. Brisson, M. Demuzere, P. Marbaix, and J.-P. van Ypersele (2014). "Comparison of one-moment and two-moment bulk microphysics for high-resolution climate simulations of intense precipitation". In: *Atmospheric Research* 147, p. 145. DOI: 10.1016/j.atmosres.2014.05.012.

Van Weverberg, K., N. P. M. van Lipzig, L. Delobbe, and D. Lauwaet (2010). "Sensitivity of quantitative precipitation forecast to soil moisture initialization and microphysics parametrization". In: *Quarterly Journal of the Royal Meteorological Society* 136, p. 978. DOI: 10.1002/qj.611.

Van Weverberg, K., N. P. van Lipzig, and L. Delobbe (2011). "Evaluation of moist processes during intense precipitation in km-scale NWP models using remote sensing and in-situ data: Impact of microphysics size distribution assumptions". In: *Atmospheric Research* 99.1, p. 15.

Van Weverberg, K., N. P. van Lipzig, L. Delobbe, and A. M. Vogelmann (2012). "The role of precipitation size distributions in km-scale NWP simulations of intense precipitation: evaluation of cloud properties and surface precipitation". In: *Quarterly Journal of the Royal Meteorological Society* 138.669, p. 2163. ISSN: 0035-9009. DOI: 10.1002/qj.1933.

Vannitsem, S. and P. Naveau (2007). "Spatial dependences among precipitation maxima over Belgium". In: *Nonlinear Processes in Geophysics* 14.5, p. 621.

Velasco-Forero, C. A., D. Sempere-Torres, E. F. Cassiraga, and J. Jaime Gómez-Hernández (2009). "A non-parametric automatic blending methodology to estimate rainfall fields from rain gauge and radar data". In: *Advances in Water Resources* 32.7, p. 986. DOI: 10.1016/j.advwatres.2008.10.004.

Verrier, S., C. Mallet, and L. Barthès (2011). "Multiscaling properties of rain in the time domain, taking into account rain support biases". In: *Journal of Geophysical Research* 116.D20. DOI: 10.1029/2011JD015719.

Vignal, B., H. Andrieu, G. Delrieu, and J. D. Creutin (2003). "Identification of Rain-Rate Profiles from Radar Returns at Attenuating Wavelengths Using an Inverse Method: A Feasibility Study". In: *Journal of Applied Meteorology* 42.7, p. 1014. ISSN: 1520-0450. DOI: 10.1175/1520-0450(2003)042<1014:iorpfr>2.0.co;2.

Villarini, G. and W. F. Krajewski (2010). "Review of the Different Sources of Uncertainty in Single Polarization Radar-Based Estimates of Rainfall". In: *Surveys in Geophysics* 31.1, p. 107. DOI: 10.1007/s10712-009-9079-x.

Villarini, G., P. V. Mandapaka, W. F. Krajewski, and R. J. Moore (2008). "Rainfall and sampling uncertainties: A rain gauge perspective". In: *Journal of Geophysical Research* 113.D11. ISSN: 0148-0227. DOI: 10.1029/2007jd009214.

Vos, L. de, H. Leijnse, A. Overeem, and R. Uijlenhoet (2017). "The potential of urban rainfall monitoring with crowdsourced automatic weather stations in Amsterdam". In: *Hydrology and Earth System Sciences* 21.2, p. 765. ISSN: 1607-7938. DOI: 10.5194/hess-21-765-2017.

Wackernagel, H. (2003). *Multivariate Geostatistics: An Introduction with Applications*. Springer Science & Business Media.

Wagner, A., J. Seltmann, and H. Kunstmann (2012). "Joint statistical correction of clutters, spokes and beam height for a radar derived precipitation climatology in southern Germany". In: *Hydrology and Earth System Sciences* 16.11, p. 4101. DOI: 10.5194/hess-16-4101-2012.

Wattrelot, E., O. Caumont, and J.-F. Mahfouf (2014). "Operational Implementation of the 1D+3D-Var Assimilation Method of Radar Reflectivity Data in the AROME Model". In: *Monthly Weather Review* 142, p. 1852. DOI: 10.1175/MWR-D-13-00230.1.

Weckwerth, T. M., J. W. Wilson, M. Hagen, T. J. Emerson, J. O. Pinto, D. L. Rife, and L. Grebe (2011). "Radar climatology of the COPS region". In: *Quarterly Journal of the Royal Meteorological Society* 137, p. 31. DOI: 10.1002/qj.747.

Weiss, J., P. Bernardara, and M. Benoit (2014). "Modeling intersite dependence for regional frequency analysis of extreme marine events". In: *Water Resources Research* 50, p. 5926. DOI: 10.1002/2014WR015391.

Weusthoff, T. and T. Hauf (2008). "The life cycle of convective-shower cells under post-frontal conditions". In: *Quarterly Journal of the Royal Meteorological Society* 134.633, p. 841. DOI: 10.1002/qj.260.

Weverberg, K. V., E. Goudenhoofdt, U. Blahak, E. Brisson, M. Demuzere, P. Marbaix, and J.-P. van Ypersele (2014). "Comparison of one-moment and two-moment bulk microphysics for high-resolution climate simulations

of intense precipitation". In: *Atmospheric Research* 147-148, p. 145. DOI: 10.1016/j.atmosres.2014.05.012.

Wilks, D. (1995). *Statistical Methods in the Atmospheric Sciences: An Introduction*. International Geophysics. Elsevier Science. ISBN: 9780080541723.

Willems, P. (2000). "Compound intensity/duration/frequency-relationships of extreme precipitation for two seasons and two storm types". In: *Journal of Hydrology* 233.1-4, p. 189. DOI: 10.1016/S0022-1694(00)00233-X.

Willems, P. (2011). *Evaluatie en actualisatie van de IDF-neerslagstatistieken te Ukkel, Aanvulling bij de studie Actualisatie en extrapolatie van hydrologische parameters in de nieuwe Code van Goede Praktijk voor het Ontwerp van Rioleringssystemen (KU Leuven voor VMM, sept. 2009)*.

Willems, P. (2013). "Multidecadal oscillatory behaviour of rainfall extremes in Europe". In: *Climatic Change* 120.4, p. 931. DOI: 10.1007/s10584-013-0837-x.

Willems, P., A. Guillou, and J. Beirlant (2007). "Bias correction in hydrologic GPD based extreme value analysis by means of a slowly varying function". In: *Journal of Hydrology* 338.3-4, p. 221. DOI: 10.1016/j.jhydrol.2007.02.035.

Wilson, J. W. and R. D. Roberts (2006). "Summary of Convective Storm Initiation and Evolution during IHOP: Observational and Modeling Perspective". In: *Monthly Weather Review* 134, p. 23. DOI: 10.1175/MWR3069.1.

Wilson, J. W. and E. A. Brandes (1979). "Radar Measurement of Rainfall?A Summary". In: *Bulletin of the American Meteorological Society* 60.9, p. 1048. ISSN: 1520-0477. DOI: 10.1175/1520-0477(1979)060<1048:rmors>2.0.co;2.

Wilson, J. W., Y. Feng, M. Chen, and R. D. Roberts (2010). "Nowcasting Challenges during the Beijing Olympics: Successes, Failures, and Implications for Future Nowcasting Systems". In: *Weather and Forecasting* 25.6, p. 1691. DOI: 10.1175/2010WAF2222417.1.

Wright, D. B., J. A. Smith, and M. L. Baeck (2014a). "Critical Examination of Area Reduction Factors". In: *Journal of Hydrologic Engineering* 19.4, p. 769. DOI: 10.1061/(ASCE)HE.1943-5584.0000855.

Wright, D. B., J. A. Smith, and M. L. Baeck (2014b). "Flood frequency analysis using radar rainfall fields and stochastic storm transposition". In: *Water Resources Research* 50.2, p. 1592. DOI: 10.1002/2013WR014224.

Wright, D. B., J. A. Smith, G. Villarini, and M. L. Baeck (2013a). "Estimating the frequency of extreme rainfall using weather radar and stochastic storm transposition". In: *Journal of Hydrology* 488, p. 150. DOI: 10.1016/j.jhydrol.2013.03.003.

Wright, D. B., J. A. Smith, G. Villarini, and M. L. Baeck (2013b). "Long-Term High-Resolution Radar Rainfall Fields for Urban Hydrology". In: *JAWRA Journal of the American Water Resources Association* 50.3, p. 713. DOI: 10.1111/jawr.12139.

Wulfmeyer, V., A. Behrendt, C. Kottmeier, U. Corsmeier, C. Barthlott, G. C. Craig, M. Hagen, D. Althausen, F. Aoshima, M. Arpagaus, H.-S. Bauer, L. Bennett, A. Blyth, C. Brandau, C. Champollion, S. Crewell, G. Dick, P. Di Girolamo, M. Dorninger, Y. Dufournet, R. Eigenmann, R. Engelmann, C. Flamant, T. Foken, T. Gorgas, M. Grzeschik, J. Handwerker, C. Hauck, H. Höller, W. Junkermann, N. Kalthoff, C. Kiemle, S. Klink, M. König, L. Krauss, C. N. Long, F. Madonna, S. Mobbs, B. Neininger, S. Pal, G. Peters, G. Pigeon, E. Richard, M. W. Rotach, H. Russchenberg, T. Schwitalla, V. Smith, R. Steinacker, J. Trentmann, D. D. Turner, J. van Baelen, S. Vogt, H. Volkert, T. Weckwerth, H. Wernli, A. Wieser, and M. Wirth (2011). "The Convective and Orographically-induced Precipitation Study (COPS): the scientific strategy, the field phase, and research highlights". In: *Quarterly Journal of the Royal Meteorological Society* 137.S1, p. 3. DOI: 10.1002/qj.752.

Wyard, C., C. Scholzen, X. Fettweis, J. Van Campenhout, and L. François (2017). "Decrease in climatic conditions favouring floods in the south-east of Belgium over 1959-2010 using the regional climate model MAR". In: *International Journal of Climatology, vol. 37, issue 5, pp. 2782-2796* 37, p. 2782. DOI: 10.1002/joc.4879.

Yang, S. and S. W. Nesbitt (2014). "Statistical properties of precipitation as observed by the TRMM precipitation radar". In: *Geophysical Research Letters* 41.15, p. 5636. DOI: 10.1002/2014GL060683.

Young, C. B., A. A. Bradley, W. F. Krajewski, A. Kruger, and M. L. Morrissey (2000). "Evaluating NEXRAD Multisensor Precipitation Estimates for Operational Hydrologic Forecasting". In: *Journal of Hydrometeorology* 1.3, p. 241. DOI: 10.1175/1525-7541(2000)001<0241:ENMPEF>2.0.CO;2. eprint: https://doi.org/10.1175/1525-7541(2000)001<0241:ENMPEF>2.0.CO;2.

Zhang, J., K. Howard, C. Langston, B. Kaney, Y. Qi, L. Tang, H. Grams, Y. Wang, S. Cocks, S. Martinaitis, and et al. (2016). "Multi-Radar Multi-Sensor (MRMS) Quantitative Precipitation Estimation: Initial Operating Capabilities". In: *Bulletin of the American Meteorological Society* 97.4, p. 621. ISSN: 1520-0477. DOI: 10.1175/bams-d-14-00174.1.

Zhang, J. and Y. Qi (2010). "A Real-Time Algorithm for the Correction of Brightband Effects in Radar-Derived QPE". In: *Journal of Hydrometeorology* 11.5, p. 1157. DOI: 10.1175/2010JHM1201.1.

Curriculum vitae

Edouard Goudenhoofdt was born on April 26, 1984 in Mouscron, Belgium. He finished his secondary school in Math-Science at the College Sainte-Marie of Mouscron in 2002. In June 2007, he receives the Master degree in Applied Mathematics from the Louvain School of Engineering of the Université catholique de Louvain. His Master thesis was entitled "Analyse de méthodes de recherche directe et du filtre de Kalman d'ensemble pour l'optimisation des paramètres d'un modèle climatique". Since November 2007 he is working as a scientist in the radar, lightning and nowcasting group of dr. Laurent Delobbe at the Royal Meteorological Institute of Belgium. From 2007 to 2016 he worked on 3 successive research projects founded by the Belgian Science Policy. In April 2015, he enrolled for a PhD based on a research career at the Hydraulics Section of the Department of Civil Engineering at the KU Leuven under the supervision of prof. Patrick Willems. He presented his findings at conferences and workshops in various European countries, Canada, South-Korea and the United States. He served as reviewer for the Journal of Applied Meteorology and Climatology, the Journal of Atmospheric and Oceanic Technology, the Journal of Hydrologic Engineering and the journal of Hydrology and Earth System Sciences. Since March 2016 he is the coordinator of the cooperation between the Royal Meteorological Institute of Belgium and the hydrological service of the Walloon region of Belgium.

FACULTY OF ENGINEERING SCIENCE
DEPARTMENT OF CIVIL ENGINEERING
HYDRAULICS SECTION
Kasteelpark Arenberg 40 - box 2448
B-3001 Leuven
edouard.goudenhooofdt@meteo.be
https://bwk.kuleuven.be/hydr/